

The Kuramoto model on ring networks.

Cluster synchronization and the size of
the Basin of Attraction.

Terry Ringlever

Delft University of Technology
Applied Mathematics

November 2018

The Kuramoto model on ring networks.

Cluster synchronization and the size of
the Basin of Attraction.

by

Terry Ringlever

to obtain the degree of Master of Science
at the Delft University of Technology,
to be defended publicly on Thursday November 29, 2018 at 2:00 PM.

Student number: 4166256
Project duration: March 1, 2017 – November 29, 2018
Thesis committee: Dr. J.L.A. Dubbeldam, TU Delft, supervisor
Dr. J.W. van der Woude, TU Delft
Dr. ir. D.R. van der Heul, TU Delft

This thesis is confidential and cannot be made public until November 29, 2018.

An electronic version of this thesis is available at <http://repository.tudelft.nl/>.

Preface

The focus of this thesis will be on the exploration of cluster synchronization and the calculation of an attractor's basin of attraction in Kuramoto models on ring networks. This topic arose from my interest in dynamical systems on networks and applications of abstract algebra. The combination of these two fields is especially found in the first part of cluster synchronization in dynamical networks. It is for that reason that I studied this topic extensively. The second part is about the determination of an attractor's basin of attraction which I found to be a difficult problem. Nonetheless, I was able to provide a conjecture about the size of this basin that I could verify for all n -node ring networks with n an odd number smaller than nineteen.

I would like to thank my supervisor Johan Dubbeldam for his guidance, support and advice not only during this process but also during my entire bachelor and master studies. In truth, this work would not have been possible without his contributions of time and ideas. Lastly, I would also like to thank my friends and family for their support.

Terry Ringlever
Delft, November 2018

Contents

1	Introduction	1
1.1	Background	3
1.2	Outline	3
2	Representations of Finite Groups	5
2.1	Introduction to Representation Theory	5
2.2	The Algorithm	11
2.3	Decoupling of ordinary differential equations.	15
3	Cluster Synchronization	19
3.1	Symmetry groups for network clusters	20
3.2	Linearization of Kuramoto dynamics on a ring network.	23
3.3	Merging clusters in a ring network.	25
4	Basin of Attraction	29
4.1	Motivation	29
4.2	A Complete Network	31
4.3	Ring networks of odd-dimension	35
5	Results	39
5.1	Cluster synchronization in a ring network.	39
5.2	Size of the Basin of Attraction..	43
6	Conclusion	45
6.1	Recommendation.	46
6.2	Future Research.	46
A	Appendix	47
B	Appendix	49
C	Appendix	55
	Bibliography	59



Introduction

Networks play an important role in many aspects of modern day society. The general concept of a network in which a system consisting of elements or nodes interact with one another is present across a vast range of areas such as biological systems, neuronal networks, social networks and power grids. For instance a foodweb can be thought of as being a biological network where predators and prey form the network nodes whereas the relations between them are represented by network links. This relation between predator and prey indicates the feeding relationship in a certain habitat and is therefore often a directional relationship. This is in contrast to many social networks where there are interactions in both directions, so called undirected networks. Besides this structural difference there may be more, among of which, the number of incoming and outgoing links at a node and the coupling strengths between nodes as well as the type of coupling between the network nodes. These aspects are instrumental in the way that networks operate. Besides the fact that these aspects differ among the various networks there is also the observation that many networks tend to change over time. For instance a growing demand for electricity tends to enlarge the structure of a power grid. This structural growth may have effects on factors such as the reliability of power supply to consumers and the robustness of the power grid. In order to maintain a reliable and stable network and to prevent power outages from happening it is of importance to gain an understanding about the phenomena occurring in dynamical networks. Among the many phenomena that may occur in a general network, synchronization of the network nodes and stability of the network dynamics, are of primary interest in this report. In regard to synchronization of the network nodes we view a synchronized network as a system in which all elements have the same behaviour whereas in stability of the network dynamics one focusses upon a state where the system returns to its original state after a perturbation. In man-made networks it is often desirable to have a combination of both aspects, i.e. a stable synchronous state. This stable synchronous state provides reliable network dynamics and plays a major role in for instance power grids. In a power grid one encounters generators and consumers. A power grid which is in synchrony has generators of which their rotors move in synchrony. This provides the consumers with a steady power supply. However, heavy fluctuations in demand on the side of the consumers may break such a synchronous state. Therefore it is of practical importance to also have stability in such a network. This stable synchronous state could also present itself in a more natural way. For instance it also occurs in a swarm of fireflies which light up the night sky. At first, they light up in an irregular pattern. However, after a while they tend to light up in synchrony for a longer period of time.

These similarities in states among the various networks makes the fascinating phenomenon of synchrony a popular topic of research. At first glance it might not be clear how one could investigate such a phenomenon as it appears in such a broad context. There might be various possibilities since networks are distinctive in structure and dynamics. However, it is convenient to describe them by means of a model. A model that rised in popularity among the past years and which will play a central role throughout this report is the so-called Kuramoto model. This model originates from behaviour presented in networks of chemical and biological oscillators [15][16]. Throughout the years it became apparent that it arises in many more natural but also engineered systems. This model forms the basis in the research of many different systems and is regularly adjusted to incorporate specific features of networks [3]. In this report we will restrict ourselves to basic models which capture nonlinear interactions, the coupling strength between network nodes and the topological structure of a network. Moreover, it allows us to study synchrony for a broad spectrum of networks.

In the Kuramoto model, the network nodes are treated as oscillators which are able to emit and receive signals with a certain frequency. The state in which a particular subset of oscillators pulse at the same frequency is known as cluster synchronization. In the particular case in which all oscillators in the network pulse at the same frequency it is called global synchronization. Often a state of global synchronization is chosen over a state in which there are different synchronized clusters. This state of global synchronization does not only benefit consumers in man-made networks but also individuals in natural systems such as a swarm of fireflies or a school of fish.

However, when a loss of synchrony occurs in these systems a transition is made to a state of asynchrony or a state in which there are still some synchronized clusters. This last phenomenon of synchronized clusters is what we intend to discuss in the coming chapters. In particular we will work towards a stability analysis of such a cluster synchronized state. The approach which is taken in a stability analysis of synchronized clusters is often different from a stability analysis for a global synchronized system. In a typical stability analysis for global synchronization one linearizes a system of nonlinear coupled ordinary differential equations and obtains a linear system which can be written by means of a coupling matrix [18]. Afterwards, one decouples the system, often partially, by means of diagonalization of the coupling matrix. Finally the resulting eigenvalues in the coupling matrices of the untangled systems are determined and checked for having a negative sign. The sign of these eigenvalues often depend on some parameters that are considered to be of practical importance such as a coupling strength or a damping coefficient. By using this eigenvalue analysis it is possible to adjust networks such that they retain in a stable state which is less vulnerable for disruptions. This approach is very convenient as it can be applied in many situations. However, when it comes down to the investigation of the phenomenon of stable synchronized clusters it is too restrictive. The trouble occurs where one diagonalizes the entire system of equations. This operation does not provide us with a relation between the resulting eigenvalues and the clusters appearing in the network dynamics. Luckily, there is an alternative approach in which the linearized system is partially decoupled depending on the symmetries provided by the networks dynamics [22]. In this way, it is possible to relate the network symmetries with the resulting eigenvalues and determine the stability of the clusters. However, the theory is not yet fully developed and faces some basic problems. One of these problems occurs when confronted with a network and all possible cluster configurations have to be determined. Since networks tend to become large in size with many mutual interactions, it is often not sufficient to achieve this goal solely by inspection. Moreover, methods that are available could become computationally expensive. In the case of symmetric networks there is a promising method available. This method is what we will use in the coming chapter about Cluster Synchronization. In essence it uses the symmetry group given by the topological structure of the network. This group is then written as a direct product of subgroups. These subgroups are then decomposed further until one reaches the trivial group. All these instances within the direct products describe a state of a certain cluster within the network.

Most of the tools that are used to achieve the goal of a stability analysis of clusters are well known and used in many areas such as spectroscopy and quantum chemistry [24][10]. These techniques rely heavily on what is called Representation Theory. We will only look at so-called linear representations of finite groups. This theory combines the abstract notion of Groups with Linear Algebra. Since group structures or symmetry groups are often difficult to grasp it is beneficial to write them in terms of matrices. These matrices or linear maps are studied in Linear Algebra and tend to make the group structure more explicit. This relation between a group and a set of matrices is provided by a structure preserving map which transfers the group structure to a set of matrices. Since we do not expect the reader to be very familiar with representation theory we will devote much attention to the subject in the coming chapters. The theory about linear representations is well developed and we will devote much of our attention to only a tiny part. We recommend the interested reader to take a look at [23] in which the subject is discussed more extensively.

Besides in the study of clusters by means of symmetry groups and their representations we will also use the symmetry which is present in the Kuramoto model to study stability on a global scale. In particular, we will focus upon the basin of attraction of a stable node in phase space. This basin of attraction defines a region in phase space where every trajectory within this region will ultimately find its way to the stable node. The determination of the size of the basin of attraction with respect to a stable node is a difficult task. We study this basin of attraction for only one network structure, namely a ring structure. In order to determine the

size of the basin of attraction there is a theorem that stands out in many illustrative examples. However, for many nonlinear systems it is likely not possible or computationally inefficient to verify the hypotheses of this theorem. One of the problems that arises in the dynamical Kuramoto model is how to calculate all the equilibria. The difficulty of this problem is found in the nonlinear nature of the system of differential equations. Therefore, one tries to verify most of these hypothesis by means of numerical approaches [25][4]. Numerical approaches have succeeded in calculating all equilibria for relatively small networks, see chapter 4 and [2], but fail for large networks. Therefore we try to make steps towards a more theoretical understanding. Although this method still suffers from deficiencies, we do think that it might interest the reader and provide insights in the way one could tackle this problem.

1.1. Background

The Kuramoto model forms the backbone in all dynamical systems we intend to discuss. The network nodes are considered to be the oscillators of our network and provide the dynamics. The oscillators all have their own angle which we will denote by θ_i . These angles change over time and this change is given for each oscillator angle by a first order ordinary differential equation. In particular, the angles of the oscillators follow the dynamics provided by the Kuramoto model which is given mathematically by [15].

$$\frac{d\theta_i}{dt} = \omega_i + \frac{\tilde{K}}{n} \sum_j \sin(\theta_j - \theta_i), \quad 1 \leq i \leq n. \quad (1.1)$$

These dynamics present the change in state of each oscillator i by means of their respective phase angles θ_i . The total number of oscillators in the network is denoted by the parameter n , such that $i \in \{1, \dots, n\}$ holds. The coupling between two angles is given by a sinusoidal function of the phase difference. The coupling strength between the oscillators in the network is assumed to be constant and is denoted by the parameter \tilde{K} . We will often scale the parameter \tilde{K} such that $K := \tilde{K}/n$ is used as coupling strength instead of \tilde{K} . The structure of the network is determined by the sum in each differential equation and this summation will be made explicit later on whenever necessary.

The former Kuramoto model also extends to a model with second-order oscillators [5]. This means that the angles satisfy second-order differential equations. The dynamics of such a model with inertia may be captured by the following system of differential equations,

$$\frac{d^2\theta_i}{dt^2} = \hat{D}_i \frac{d\theta_i}{dt} + \omega_i + \frac{\tilde{K}}{n} \sum_j \sin(\theta_j - \theta_i), \quad 1 \leq i \leq n. \quad (1.2)$$

This models includes parameters \hat{D}_i for each oscillator. We assume $\hat{D}_i \leq 0$ for each oscillator such that it serves as a damping parameter. This second-order differential equation simplifies if there is no damping, i.e. $\hat{D}_i = 0$. In a similar way as in the first-order Kuramoto model we will also scale \tilde{K} such that $K := \tilde{K}/n$ is used.

1.2. Outline

This thesis is organized as follows. We start with an introduction to Representation Theory in Chapter 2. Here we discuss fundamental notions and intend to provide clarity by means of examples. These notions are necessary for a formal treatment of an important algorithm which we will discuss in detail. This algorithm is usually not covered in textbooks, but is often used in practice. At the end of Chapter 2 we apply this algorithm in detail to a small three node network with simple dynamics.

In Chapter 3 we discuss the topic of cluster synchronization in symmetric networks. In particular, we discuss this phenomenon in a symmetric network of moderate size. Here we deal with problems like how one could deal with different cluster configurations and stability properties. After the treatment of clusters in dynamical networks we move on to apply symmetries on a global scale in Chapter 4. In this chapter we consider the basin of attraction of a stable node in ring networks where we make use of symmetries provided by the Kuramoto model. In particular, we are interested in the size of the basin of attraction around a stable node. It turns out that it can be determined theoretically for small networks. Afterwards, we show our findings in chapter 5. We finalize this thesis in Chapter 6 with a conclusion including a recommendation and suggestions for future research. In the appendix we included lengthy computations as well as details that are of less relevance. In addition we provide the used codes that lead up to some of the results.

2

Representations of Finite Groups

Networks often show signs of symmetry. These symmetries may be present around different aspects of a network. For instance a network may possess symmetry in the underlying topology or even symmetry in the underlying dynamics of the network. In this chapter we will devote much of our attention to the mathematical tools that can be used to study these symmetries in networks. In particular, it will revolve around the theory of representations of finite groups called Representation Theory. In Representation Theory, one combines Group Theory and Linear Algebra to study symmetry operations on a certain structure. A structure may be understood as an abstract mathematical structure such as a vector space or module, or less abstract such as the nodes in a network or the structure of a molecule. Here, we will focus solely upon a set with the structure of a finite dimensional vector space. Since representation theory is an area in its own right, we intend to cover only those subjects which enables the reader to understand the applications presented later on.

We start this chapter by introducing some common notions in the field of Representation Theory. We intend to clarify these notions by providing some examples. Hereafter, it tends to become more theoretical as we want to provide some mathematical theory about an algorithm that allows us to study the presence of symmetries in networks. In the end, we discuss an application of this algorithm in detail. Before we move on we want to emphasize that we used for most of the theory in this chapter the resources [23], [11] and [12].

2.1. Introduction to Representation Theory

In mathematics we describe symmetry operations often by means of elements of a group. We assume that these groups are finite as we will only deal with networks that possess finitely many symmetries. Since groups are often abstract in nature it will be useful to make them more explicit. This is achieved by means of a so-called representation of a finite group. The definition can be stated as follows [23].

Definition 1 *Let V be an n -dimensional vector space over the field \mathbb{C} . A representation D of a finite group G is a group homomorphism $D : G \rightarrow GL(V)$, i.e. a map $D : G \rightarrow GL(V)$ satisfying $D(g_1 g_2) = D(g_1) D(g_2)$ for all $g_1, g_2 \in G$. The dimension of the vector space V is also called the degree of the representation D . If V is equipped with an hermitian inner product $\langle \cdot, \cdot \rangle$ and the map D also satisfies $\langle D(g)v, D(g)w \rangle = \langle v, w \rangle$ for all $v, w \in V$ and $g \in G$ then we call D a unitary representation.*

Since we often deal with finite dimensional vector spaces V , we may choose a basis and identify the linear invertible maps $GL(V)$ with invertible $n \times n$ matrices over \mathbb{C} , denoted by $GL_n(\mathbb{C})$. In this way, we may replace the map in the former definition by $D : G \rightarrow GL_n(\mathbb{C})$ and call D a matrix representation. Moreover, such a representation is unitary if for all $g \in G$ it holds that the inverse of $D(g)$ is equal to the conjugate transpose of $D(g)$. To get a better grasp of the definition we provide some examples.

Example 1 *Suppose G is a finite group. The map $D : G \rightarrow GL_1(\mathbb{C})$ given by $D(g) = 1$ for all $g \in G$ is a representation called the trivial representation. It is clearly a unitary representation.*

Example 2 *Suppose H is a subgroup of index 2 of the finite group G , i.e. H has two cosets in G . Let $D : G \rightarrow GL_1(\mathbb{C})$ such that $D(g) = 1$ for all $g \in H$ and $D(g) = -1$ otherwise. This is called the alternating representation.*

Example 3 Consider a finite group G with n elements. Order the elements of G , say g_1, \dots, g_n . Let V denote an n -dimensional vector space with standard basis elements indexed by the group elements. More specifically, denote the i -th standard basis element by e_{g_i} for all $1 \leq i \leq n$. We define an action μ of G on \mathbb{C}^n , i.e. a map $\mu: G \times \mathbb{C}^n \rightarrow \mathbb{C}^n$, by

$$\mu(g, x) := g(x_1 e_{g_1} + x_2 e_{g_2} + \dots + x_n e_{g_n}) = x_1 e_{gg_1} + x_2 e_{gg_2} + \dots + x_n e_{gg_n} \quad (2.1)$$

where $x := (x_1, \dots, x_n) \in \mathbb{C}^n$ and $g \in G$. This group action defines a representation $D: G \rightarrow \text{Sym}(\mathbb{C}^n)$ by setting $D(g)(x) := \mu(g, x)$ which is called the (left) regular representation of G . For a specific group G it is often more convenient to write the regular representation as a matrix representation. For instance, if we set $G = A_3$ we may order the elements as $g_1 := (1)$ followed by $g_2 := (123)$ and $g_3 := (132)$ and use the standard basis on \mathbb{C}^3 with this order such that the i -th standard basis element is denoted by e_{g_i} for $1 \leq i \leq 3$. In this case, the regular representation of A_3 reads,

$$D(g_1) = \begin{bmatrix} 1 & 0 & 0 \\ 0 & 1 & 0 \\ 0 & 0 & 1 \end{bmatrix}, \quad D(g_2) = \begin{bmatrix} 0 & 0 & 1 \\ 1 & 0 & 0 \\ 0 & 1 & 0 \end{bmatrix} \quad \text{and} \quad D(g_3) = \begin{bmatrix} 0 & 1 & 0 \\ 0 & 0 & 1 \\ 1 & 0 & 0 \end{bmatrix}. \quad (2.2)$$

Sometimes two representations provide the same action of the group G on the vector space V . This leads us to a notion of isomorphic or equivalent representations.

Definition 2 A representation $D: G \rightarrow GL(V)$ is called equivalent or isomorphic to another representation $D': G \rightarrow GL(W)$ if there exists an invertible linear transformation $\alpha: V \rightarrow W$ such that $D(g) = \alpha D'(g) \alpha^{-1}$ for all $g \in G$.

The map α is also called a vector space isomorphism. This map preserves the action of the group, so in a natural way we may view equivalent representations as being the same. Moreover, the relation provided in the definition is an equivalence relation so we can partition the set of representations in equivalence classes. In this way, many notions in Representation Theory are studied up to equivalence. In the case where V and W have the same finite dimension, the condition $D(g) = \alpha D'(g) \alpha^{-1}$ for all $g \in G$ says that the matrices $D(g)$ and $D'(g)$ are similar for all $g \in G$.

Example 4 Let $\{e_1, e_2, \dots, e_n\}$ denote the standard basis for \mathbb{C}^n . Define the action μ of S_n on \mathbb{C}^n , i.e. the map $\mu: S_n \times \mathbb{C}^n \rightarrow \mathbb{C}^n$, by

$$\mu(\sigma, x) := \sigma(x_1 e_1 + x_2 e_2 + \dots + x_n e_n) = x_1 e_{\sigma(1)} + x_2 e_{\sigma(2)} + \dots + x_n e_{\sigma(n)} \quad (2.3)$$

where $x := (x_1, \dots, x_n) \in \mathbb{C}^n$ and $\sigma \in S_n$. This group action defines a representation $D: S_n \rightarrow \text{Sym}(\mathbb{C}^n)$ by setting $D(\sigma)(x) = \mu(\sigma, x)$ which is called the permutation representation of S_n as it permutes the coordinates of the standard basis. In particular, for the symmetric group $S_2 := \{\sigma_1, \sigma_2\}$ where $\sigma_1 = (1)(2)$ and $\sigma_2 = (12)$ we may write the permutation representation $D: S_2 \rightarrow GL_2(\mathbb{C})$ explicitly as,

$$D(\sigma_1) = \begin{bmatrix} 1 & 0 \\ 0 & 1 \end{bmatrix} \quad \text{and} \quad D(\sigma_2) = \begin{bmatrix} 0 & 1 \\ 1 & 0 \end{bmatrix}. \quad (2.4)$$

The permutation representation in 3.4 is equivalent to the representation $D': \mathbb{Z}_2 \rightarrow GL_2(\mathbb{C})$ given by,

$$D'(\sigma_1) = \begin{bmatrix} 1 & 0 \\ 0 & 1 \end{bmatrix} \quad \text{and} \quad D'(\sigma_2) = \begin{bmatrix} 1 & 0 \\ 0 & -1 \end{bmatrix}. \quad (2.5)$$

This is easily verified as $D'(\sigma_2)$ is the diagonal matrix in the eigendecomposition of $D(\sigma_2)$.

It turns out that some representations can be viewed as being the building blocks of representations in general. For representations of finite groups we call these building blocks irreducible representations. The formal definition is presented below.

Definition 3 A non-zero representation $D: G \rightarrow GL_n(\mathbb{C})$ is called irreducible if it has no nontrivial invariant subspaces. This means that the only G -invariant subspaces of V are $\{0\}$ and the whole space V , i.e. if for $K \subseteq V$ we have $D(g)(k) \in K$ for all $g \in G$ and $k \in K$ then $K = \{0\}$ or $K = V$.

$D|_{V_1}(\sigma_i) = 1$ where $1 \leq i \leq 2$. The other subrepresentation must be given by $D|_{V_2}(\sigma_1) = 1$ and $D|_{V_2}(\sigma_2) = -1$ since σ_2 is of order 2 and $D|_{V_2}(\sigma_2)$ must have an order which divides the order of σ_2 by the homomorphism property. Hence, for $g \in S_2$ we write

$$D(g) \cong [D|_{V_1} \oplus D|_{V_2}](g) \cong \begin{bmatrix} D|_{V_1}(g) & 0 \\ 0 & D|_{V_2}(g) \end{bmatrix} = \begin{bmatrix} D^{(1)}(g) & 0 \\ 0 & D^{(2)}(g) \end{bmatrix} \quad (2.9)$$

where the last equality is just a matter of notation. Notice that 2.9 coincides with the representation 2.5.

In order to cope with the difficulty of finding the representation on the right-hand side of 2.6 we provide some tools that can be used for this purpose. Many of these, can be found in [23] and [1]. First, we write the block diagonal representation on the right-hand side of 2.6 in a more convenient way. Fix $1 \leq i \leq \hat{n}$. Since it could be the case that there are m_i representations in the right-hand side of 2.6 which are equivalent to an irreducible subrepresentation $D^{(i)}$, we could treat them as if they were all the same. By picking a representative, say $D^{(j)}$, among these m_i equivalent representations we may replace the remaining $m_i - 1$ representations which are equivalent to $D^{(j)}$ by $D^{(j)}$. In this way we find mutually inequivalent representatives, say $D^{(1)}, \dots, D^{(s)}$, such that along with a re-ordering of the summands in 2.6 we may rewrite 2.6 as,

$$D \cong \oplus_{j=1}^s m_j D^{(j)} \quad (2.10)$$

where

$$m_j D^{(j)} := \oplus_{i=1}^{m_j} D^{(j)}. \quad (2.11)$$

The existence of such a complete set of representatives $D^{(1)}, \dots, D^{(s)}$ follows from the fact that representation equivalence as in definition 2 is an equivalence relation. We call each of the positive integers m_j in 2.10, which indicate how many representations in the right-hand side of 2.6 are equivalent to $D^{(j)}$, the multiplicity of $D^{(j)}$ in D . We set the multiplicity of an irreducible representation equal to zero if it is not a subrepresentation of the representation D . It turns out, that it is possible to find these multiplicities for each representation. This is achieved by means of the character of a representation.

Definition 4 Let G be a finite group and $D : G \rightarrow GL(V)$ be a representation. The character of D is a map $\chi_D : G \rightarrow \mathbb{C}$ defined by taking the trace of $D(g)$ with $g \in G$, i.e. $\chi_D(g) = \text{Tr}(D(g))$.

A basic property of characters is that they are constant on conjugacy classes. Indeed, by the homomorphism property and trace property it holds that

$$\chi_D(hgh^{-1}) = \text{Tr}(D(h)D(g)D(h^{-1})) = \text{Tr}(D(h)^{-1}D(h)D(g)) = \text{Tr}(D(g)) = \chi_D(g). \quad (2.12)$$

The character of a representation $D : G \rightarrow GL(V)$ can be viewed as an element of the following set,

$$L(G) := \{f \mid f : G \rightarrow \mathbb{C}\}. \quad (2.13)$$

This is an inner product space with pointwise addition and pointwise multiplication defined in the usual way and an inner product given by,

$$(f_1 \mid f_2) := \frac{1}{|G|} \sum_{g \in G} f_1(g) \overline{f_2(g)}. \quad (2.14)$$

By using this inner product on characters one can easily verify whether two representations are equivalent or not due to the following orthogonality relations.

Theorem 2 Let D and \hat{D} be irreducible representations. Then the following holds,

$$\left(\chi_D \mid \chi_{\hat{D}}\right) = \begin{cases} 1 & \text{if } D \cong \hat{D} \\ 0 & \text{if } D \not\cong \hat{D}. \end{cases} \quad (2.15)$$

A consequence of these orthogonality relations is that it enables us to find the multiplicities m_j of the irreducible representations of a finite group G .

Corollary 3 A representation $D : G \rightarrow GL(V)$ is irreducible if and only if $(\chi_D \mid \chi_D) = 1$. In the case that D is reducible we have a direct sum decomposition as in 2.10 and the multiplicities m_j satisfy,

$$m_j = \left(\chi_D \mid \chi_{D^{(j)}}\right). \quad (2.16)$$

for each $1 \leq j \leq s$.

In order to get an overview of the possible number of irreducible representations of a finite group we will make use of the following result [23].

Corollary 4 *The number of irreducible representations of a finite group G is up to equivalence equal to the number of conjugacy classes of G .*

The next result relates the cardinality of the group to the degrees of the irreducible representations of this group. It is often convenient to use it after one has applied Corollary 4. The Theorem is often called the Dimensionality Theorem and is stated as follows [1].

Theorem 5 *Let G be a finite group with \hat{n} irreducible representations D^i of dimension d_i . Then d_i divides $|G|$ and the following formula holds,*

$$|G| = \sum_{i=1}^{\hat{n}} d_i^2. \quad (2.17)$$

We will clarify many of the aforementioned results in the following example.

Example 6 *Consider the symmetric group S_3 on the 3 vertices $(1, 0)$, $(-\frac{1}{2}, \frac{1}{2}\sqrt{3})$ and $(-\frac{1}{2}, -\frac{1}{2}\sqrt{3})$ of an equilateral triangle. The vertices are labeled by the numbers 1, 2 and 3 as depicted below. This group consists of six distinct elements, so we write $S_3 := \{E, \rho, \rho^2, \sigma_1, \sigma_2, \sigma_3\}$ where E denotes the identity element, ρ a rotation over an angle $\frac{2\pi}{3}$ around the incenter and each σ_i is a reflection in an angle bisector. In cycle notation we end up with $E := (1)$, $\rho := (123)$, $\rho^2 := (132)$, $\sigma_1 := (12)$, $\sigma_2 := (23)$ and $\sigma_3 := (13)$.*

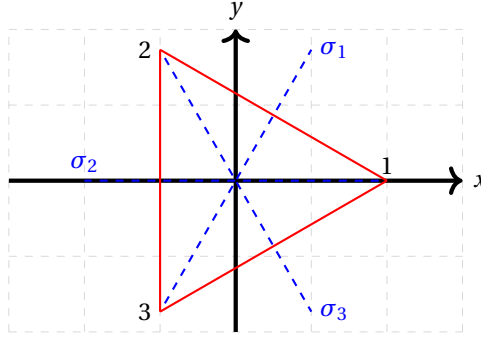


Fig. 2.1: Triangle with angle bisectors.

Let $D : S_3 \rightarrow GL_3(\mathbb{C})$ be the permutation representation of S_3 . Since the group S_3 is generated by a rotation and a reflection, we only write D explicitly for the elements $\rho := (123)$ and $\sigma_1 := (12)$. We have,

$$D(\rho) = \begin{bmatrix} 0 & 1 & 0 \\ 0 & 0 & 1 \\ 1 & 0 & 0 \end{bmatrix} \quad \text{and} \quad D(\sigma_1) = \begin{bmatrix} 0 & 1 & 0 \\ 1 & 0 & 0 \\ 0 & 0 & 1 \end{bmatrix}. \quad (2.18)$$

We intend to clarify the aforementioned results by computing the characters of each irreducible subrepresentation of D . Since we consider a symmetric group, it follows from Group Theory that elements within a conjugacy class have the same cycle type [7]. The symmetric group S_3 has three cycle types, namely the three cycles $\mathcal{C}_1 := \{\rho, \rho^2\}$, the transpositions $\mathcal{C}_2 := \{\sigma_i : 1 \leq i \leq 3\}$ and the one given by the identity element $\mathcal{C}_3 := \{E\}$. From Corollary 4 we deduce that there are 3 irreducible representations of S_3 . The dimensions of these irreducible representations follow from Theorem 5 which tells us that $6 = d_1^2 + d_2^2 + d_3^2$ holds. Hence, we have one irreducible representation of dimension 2 and two irreducible representations of dimension 1. The 2 inequivalent irreducible one-dimensional representations are given by the trivial representation and the alternating representation. The alternating representation is defined as $D^2(g) = 1$ for $g \in A_3$ and $D^2(g) = -1$ for $g \in S_3 \setminus A_3$. In order to determine a two-dimensional representation, we recall that the rotation and reflection matrices from linear algebra rotate points in Euclidean space around the origin over an angle θ in counterclockwise direction and reflect points over a line having an angle θ are given by respectively [1],

$$\begin{bmatrix} \cos(\theta) & -\sin(\theta) \\ \sin(\theta) & \cos(\theta) \end{bmatrix} \quad \text{and} \quad \begin{bmatrix} \cos(2\theta) & \sin(2\theta) \\ \sin(2\theta) & -\cos(2\theta) \end{bmatrix}. \quad (2.19)$$

The angle θ is measured in both cases with respect to the positive axis in figure 2.1. By using the appropriate angles in 2.19 we find

$$D^3(\rho) = \begin{bmatrix} -\frac{1}{2} & -\frac{1}{2}\sqrt{3} \\ \frac{1}{2}\sqrt{3} & -\frac{1}{2} \end{bmatrix} \quad \text{and} \quad D^3(\sigma_1) = \begin{bmatrix} -\frac{1}{2} & \frac{1}{2}\sqrt{3} \\ \frac{1}{2}\sqrt{3} & \frac{1}{2} \end{bmatrix}. \quad (2.20)$$

It remains to be shown that this two-dimensional representation is irreducible. To this end, we compute the inner product $(\chi_{D^3} | \chi_{D^3})$ which depends on the characters $\chi_{D^3}(g)$ where $g \in S_3$. Since characters are constant on conjugacy classes by 2.12, it suffices to know the characters of $D^3(E)$, $D^3(\rho)$ and $D^3(\sigma_1)$. By definition of a character this leads to computing the traces for the two-dimensional identity matrix along with those in 2.20. Consequently,

$$\begin{aligned} (\chi_{D^3} | \chi_{D^3}) &= \frac{1}{6} \left(1 \cdot \chi_{D^3}(E) \overline{\chi_{D^3}(E)} + 2 \cdot \chi_{D^3}(\rho) \overline{\chi_{D^3}(\rho)} + 3 \cdot \chi_{D^3}(\sigma_1) \overline{\chi_{D^3}(\sigma_1)} \right) \\ &= \frac{1}{6} (1 \cdot (2 \cdot 2) + 2 \cdot (-1 \cdot -1) + 3 \cdot (0 \cdot 0)) = 1 \end{aligned} \quad (2.21)$$

where the integers 1, 2 and 3 in the first line indicate the size of each conjugacy class. By Corollary 3 it follows that it is indeed an irreducible two-dimensional representation. In order to determine whether the preceding 3 irreducible representations occur as subrepresentations of D in 2.18, we first determine the characters of these irreducible representations and collect them in a so-called character table. In this character table we write the characters of the irreducible representations of S_3 depending on both the conjugacy class as presented in the first row and the irreducible representation under consideration as presented in the first column. Since the character of a one-dimensional representation equals the one-dimensional matrix representation it is easy to fill up the rows corresponding to trivial D^1 and alternating representation D^2 . The last row presents the characters of D^3 which we already derived in 2.21.

	\mathcal{C}_1	\mathcal{C}_2	\mathcal{C}_3
D^1	1	1	1
D^2	1	-1	1
D^3	2	0	-1

At last, with the formula of Corollary 3 we compute the multiplicities of the irreducible representations D^1 , D^2 and D^3 .

$$m_1 = (\chi_D | \chi_{D^1}) = \frac{1}{6} \left[\chi_D(E) \overline{\chi_{D^1}(E)} + 2 \cdot \chi_D(\rho) \overline{\chi_{D^1}(\rho)} + 3 \cdot \chi_D(\sigma_1) \overline{\chi_{D^1}(\sigma_1)} \right] = \frac{1}{6} [3 \cdot 1 + 2 \cdot (0 \cdot 1) + 3 \cdot (1 \cdot 1)] = 1$$

$$m_2 = (\chi_D | \chi_{D^2}) = \frac{1}{6} \left[\chi_D(E) \overline{\chi_{D^2}(E)} + 2 \cdot \chi_D(\rho) \overline{\chi_{D^2}(\rho)} + 3 \cdot \chi_D(\sigma_1) \overline{\chi_{D^2}(\sigma_1)} \right] = \frac{1}{6} [3 \cdot 1 + 2 \cdot (0 \cdot 1) + 3 \cdot (1 \cdot -1)] = 0$$

$$m_3 = (\chi_D | \chi_{D^3}) = \frac{1}{6} \left[\chi_D(E) \overline{\chi_{D^3}(E)} + 2 \cdot \chi_D(\rho) \overline{\chi_{D^3}(\rho)} + 3 \cdot \chi_D(\sigma_1) \overline{\chi_{D^3}(\sigma_1)} \right] = \frac{1}{6} [3 \cdot 2 + 2 \cdot (0 \cdot -1) + 3 \cdot (1 \cdot 0)] = 1$$

Thus, the alternating representation does not appear in the unique direct sum decomposition of representation D in 2.18. This result can also be derived by taking the direct sum decomposition of \mathbb{C}^3 with $n = 3$ in the preceding example into account. Since V_2 for $n = 3$ in 2.8 is two-dimensional we look solely at V_1 in formula 2.7. Notice $V_1 := \{(a, a, a) \in \mathbb{C}^3\}$. For $x = (x_1, x_2, x_3) \in V_1$ we have $x_1 = x_2 = x_3$ so $D|_{V_1} : S_3 \rightarrow GL_1(V_1)$ satisfies $D|_{V_1}(g)(x) = D(g)(x) = x$ for all $g \in S_3$, i.e. $D|_{V_1}$ is equivalent to the trivial representation $D|_{V_1}(g) = 1$ for all $g \in S_3$ and not equivalent to the alternating representation.

In conclusion we have $D \cong D^1 \oplus D^3$. For convenience, we denote the resulting block diagonal representation by $D' := D^1 \oplus D^3$. It is given explicitly by the following two matrices,

$$D'(\rho) = \begin{bmatrix} 1 & 0 & 0 \\ 0 & -\frac{1}{2} & -\frac{1}{2}\sqrt{3} \\ 0 & \frac{1}{2}\sqrt{3} & -\frac{1}{2} \end{bmatrix} \quad \text{and} \quad D'(\sigma_1) = \begin{bmatrix} 1 & 0 & 0 \\ 0 & -\frac{1}{2} & \frac{1}{2}\sqrt{3} \\ 0 & \frac{1}{2}\sqrt{3} & \frac{1}{2} \end{bmatrix}. \quad (2.22)$$

One can verify that this block-diagonal representation can also be found by writing the elements of the image of D in terms of the basis,

$$\left\{ \begin{bmatrix} \frac{1}{\sqrt{3}} \\ \frac{1}{\sqrt{6}} \\ 0 \end{bmatrix}, \begin{bmatrix} \frac{1}{\sqrt{3}} \\ -\frac{1}{\sqrt{6}} \\ 1 \end{bmatrix}, \begin{bmatrix} \frac{1}{\sqrt{3}} \\ -\frac{1}{\sqrt{6}} \\ -1 \end{bmatrix} \right\}. \quad (2.23)$$

2.2. The Algorithm

In Maschke's Theorem 1, in particular in formula 2.6, we have seen that a representation can equivalently be written by block diagonal matrices for each group element. The block diagonal form is easier to work with and we will determine a single transformation matrix α that transforms each representation matrix $D(g)$ to a block diagonal matrix as in the right-hand side of 2.6. In the following we cover the construction of an important algorithm which enables us to compute the transformation α that provides the equivalence of the two representations in 2.6 of Maschke's Theorem 1. To this end, we assume from here on that $D : G \rightarrow GL(V)$ is a unitary reducible representation of finite degree n . In addition, we assume g to be an element of the finite group G . By Maschke's theorem it follows that the representation is completely reducible and write the representation as

$$D \cong \oplus_{i=1}^{\hat{n}} D^{(i)} \tag{2.24}$$

where $\hat{n} \leq n$ a positive integer. It could be the case that a certain irreducible representations $D^{(i)}$ in the direct sum decomposition of D in 2.24 are equivalent to m_ℓ other irreducible representations in the same direct sum. In that case we collect these equivalent representations by choosing a certain representative among these equivalent representations, say $D^{(\ell)}$, and write

$$m_\ell D^{(\ell)} := \oplus_{j=1}^{m_\ell} D^{(\ell)} = D^{(\ell)} \oplus \dots \oplus D^{(\ell)} \tag{2.25}$$

Suppose we have a complete set of representatives of the equivalence classes of irreducible representations which consists of s members. In that case we may re-enumerate such that the representatives are given by $D^{(1)}, \dots, D^{(s)}$ and simplify 2.24 as follows

$$D \cong \oplus_{j=1}^s m_j D^{(j)} \tag{2.26}$$

where $s \leq \hat{n}$ and each positive integers m_j denotes the multiplicity of $D^{(j)}$ in D . If $D^{(j)}$ appears in 2.26 it is called an irreducible constituent. Notice that in essence we obtain 2.26 from 2.24 by collecting all equivalent irreducible representations. Similarly, we collect the underlying vector spaces $V^{(i)}$ of the irreducible representations $D^{(i)}$ in 2.24 and write

$$V \cong \oplus_{j=1}^s m_j V^{(j)} \quad \text{where} \quad m_\ell V^{(\ell)} := \oplus_{j=1}^{m_\ell} V^{(\ell)} = V^{(\ell)} \oplus \dots \oplus V^{(\ell)} \quad \text{for} \quad \ell \in \{1, \dots, s\}. \tag{2.27}$$

This can be written in full length by introducing $V_j^{(\ell)}$ to be the j -th subspace in $m_\ell V^{(\ell)}$. Hence, 2.27 in full length is given by,

$$V \cong V_1^{(1)} \oplus \dots \oplus V_{m_1}^{(1)} \oplus V_1^{(2)} \oplus \dots \oplus V_{m_2}^{(2)} \oplus V_1^{(3)} \oplus \dots \oplus V_{m_s}^{(s)} \tag{2.28}$$

From here on let d_i denote the degree of the representation $D^{(i)}$, i.e. the dimension of the underlying vector space $V^{(i)}$. Since V is a finite-dimensional vector space it is possible to find a basis for V . We denote the basis elements by $b_d^{i,j}$ where the superscript i indicates that it corresponds to the subspace $V^{(i)}$ and the superscript j indicates that it corresponds to j -th subspace $V_j^{(i)}$ in $m_i V^{(i)}$ and the subscript d indicates that it is the d -th basis element. Below we depicted all basis elements for only one block $m_i V^{(i)}$, but keep in mind that we have s of these blocks as $1 \leq i \leq s$.

	$\mathbf{W}_1^{(i)}$	$\mathbf{W}_2^{(i)}$...	$\mathbf{W}_d^{(i)}$...	$\mathbf{W}_{d_i}^{(i)}$
$\mathbf{V}_1^{(i)}$	$b_1^{i,1}$	$b_2^{i,1}$...	$b_d^{i,1}$...	$b_{d_i}^{i,1}$
$\mathbf{V}_2^{(i)}$	$b_1^{i,2}$	$b_2^{i,2}$...	$b_d^{i,2}$...	$b_{d_i}^{i,2}$
\vdots	\vdots	\vdots		\vdots		\vdots
$\mathbf{V}_j^{(i)}$	$b_1^{i,j}$	$b_2^{i,j}$...	$b_d^{i,j}$...	$b_{d_i}^{i,j}$
\vdots	\vdots	\vdots		\vdots		\vdots
$\mathbf{V}_{m_i}^{(i)}$	b_1^{i,m_i}	b_2^{i,m_i}	...	b_d^{i,m_i}	...	$b_{d_i}^{i,m_i}$

Fig. 2.2: Basis elements of block $m_i V^{(i)}$

The enclosed symbols in figure 2.2 are the basis elements of $m_i V^{(i)}$. Notice that each row in figure 2.2 consist of basis elements of some subspace in the direct sum of $m_i V^{(i)}$ as indicated by the first column outside the enclosed region. For instance, the blue row corresponds to the j -th subspace $V_j^{(i)}$ of $m_i V^{(i)}$. Besides the subspaces $V_j^{(i)}$ we could also consider the subspaces of $m_i V^{(i)}$ corresponding to columns of figure 2.2. The basis elements in a column of figure 2.2 are denoted by $W_d^{(i)}$ for a $d \in \{1, \dots, d_i\}$ as can be seen in the first row outside the enclosed region. In figure 2.2 we highlighted such a typical column in red. It consists of one basis element from each $V_j^{(i)}$ in $m_i V^{(i)}$ and such a subspace for $1 \leq i \leq s$ and $1 \leq d \leq d_i$ can be written as

$$W_d^{(i)} := \left\{ b_d^{i,j} : 1 \leq j \leq m_i \right\} \quad (2.29)$$

Before we move on, we emphasize that our vector space V is of dimension n . Hence, the representation D is of finite degree n and can be written as $D : G \rightarrow GL_n(\mathbb{C})$ by choosing a basis. In this way, $D(g)$ can be viewed as a matrix. Its entries will be denoted in the usual way, i.e. $D_{\ell,\gamma}(g)$ for matrix entry (ℓ, γ) . At this point, we are ready to introduce an important operator which enables us to obtain a special kind of basis of V solely by making use of the representation D . The linear operator $P_{d,j}^i : V \rightarrow V$ is defined for $d, j \in \{1, \dots, d_i\}$ and $i \in \{1, \dots, s\}$ as follows

$$P_{d,j}^i := \frac{d_i}{|G|} \sum_{g \in G} D_{j,d}^{(i)}(g^{-1}) D(g) \quad (2.30)$$

where $|G|$ denotes the cardinality of the group G which is finite by assumption. Notice that the operator in 2.30 depends on three indices d, j and i . All these operators will be referred to as projection operators although we have not yet shown that they are projection operators. Before we dive into the details regarding these projection operators we first discuss the special basis of V . The special kind of basis of V we intend to find is called a symmetry adapted basis for V . It consists of vectors that make up the invertible linear transformation α in $D(g) = \alpha D'(g) \alpha^{-1}$ of definition 2 where $D'(g)$ will be the block diagonal matrix of 2.6 [11]. This type of basis is of interest as it allows us to simplify for instance a system of differential equations. Its definition is given below.

Definition 5 A symmetry adapted basis of V is a basis B of V where B consists of basis elements of V , i.e.

$$B = \left\{ b_d^{i,j} : 1 \leq d \leq d_i, 1 \leq j \leq m_i, 1 \leq i \leq s \right\}, \quad (2.31)$$

such that each of the basis elements $b_d^{i,j}$ satisfy,

$$D(g) b_d^{i,j} = \sum_{d=1}^{d_i} D_{d,i}^{(i)}(g) b_d^{i,j}. \quad (2.32)$$

Notice that formula 2.32 describes the equivalence of the two representations as shown in 2.6, i.e. it describes the formula $D(g)\alpha = \alpha D'(g)$ where $D'(g)$ is the matrix representation in the right-hand side of 2.6 and α the similarity transformation with columns given by elements of the form $b_d^{i,j}$. Before we are able to find a symmetry adapted basis for V we first consider what it is that a projection operator does with such a symmetry adapted basis. By means of these properties it will eventually be clear how we can construct a symmetry adapted basis. The details are provided in the corollary below.

Corollary 6 Let D be a unitary and reducible representation of finite degree. Assume we have a symmetry adapted basis B as stated in the preceding definition. The linear operators $P_{d,j}^i$ as defined in 2.30 satisfy,

1. The elements of a block scheme $m_i V^{(i)}$ as depicted in figure 2.2 are mapped onto zero if $i \neq l$.
2. The j -th column of $m_i V^{(i)}$ is mapped onto the d -th column of $m_i V^{(i)}$, the other columns are mapped onto zero.
3. For fixed $1 \leq d \leq d_i$ and $1 \leq i \leq s$ the linear operator $P_{d,d}^i$ is a projection of V onto the subspace $W_d^{(i)}$.

Proof: Let $b_n^{l,m} \in B$, then

$$P_{d,j}^i b_n^{l,m} = \frac{d_i}{|G|} \sum_{g \in G} D_{j,d}^{(i)}(g^{-1}) D(g) b_n^{l,m} \stackrel{(i)}{=} \frac{d_i}{|G|} \sum_{g \in G} D_{j,d}^{(i)}(g^{-1}) \sum_{p=1}^{d_i} D_{p,n}^{(l)}(g) b_p^{l,m} = \sum_{p=1}^{d_i} \left(\frac{d_i}{|G|} \sum_{g \in G} D_{j,d}^{(i)}(g^{-1}) D_{p,n}^{(l)}(g) \right) b_p^{l,m}$$

In (i) we used the property of a symmetry adapted basis as given in (2.32). Since subrepresentations of a unitary representation are unitary by restriction of the inner product we find for $g \in G$,

$$D_{j,d}^{(i)}(g^{-1}) \stackrel{(ii)}{=} D_{j,d}^{(i)}(g)^{-1} \stackrel{(iii)}{=} \overline{D_{d,j}^{(i)}(g)}$$

where in (ii) we used the homomorphism property of a representation and in (iii) we used the unitary matrix property. This allows us to simplify the penultimate formula,

$$P_{d,j}^i b_n^{l,m} = \sum_{p=1}^{d_i} \left(\frac{d_i}{|G|} \sum_{g \in G} \overline{D_{d,j}^{(i)}(g)} D_{p,n}^{(l)}(g) \right) b_p^{l,m} \stackrel{(iv)}{=} \sum_{d=1}^{d_i} d_i \delta_{i,l} \delta_{d,p} \delta_{j,n} \frac{b_p^{l,m}}{d_i} = \begin{cases} b_d^{i,m} & \text{if } i = l, j = n. \\ 0 & \text{otherwise.} \end{cases}$$

where in (iv) we used Schur's Orthogonality Relations. This shows that statement 1. holds as it corresponds to the situation where $i \neq l$. Also, statement 2. follows as a necessary condition for a nonzero contribution is that $j = n$. Finally, statement 3. holds as

$$P_{d,d}^i b_n^{l,m} = \begin{cases} b_d^{i,m} & \text{if } i = l, d = n. \\ 0 & \text{otherwise.} \end{cases}$$

which shows that for fixed $1 \leq i \leq s$ and $1 \leq d \leq d_i$ we end up with $P_{d,d}^i b_d^{i,m} = b_d^{i,m}$ for $1 \leq m \leq m_i$, i.e. a projection of V onto the subspace $W_d^{(i)}$. \square

The former result makes it possible to find a symmetry adapted basis for each subspace $m_i V^{(i)}$. We will show how this is done by means of the projection operator and the properties of Corollary 2. Fix $1 \leq i \leq s$, i.e. consider one block $m_i V^{(i)}$ as depicted in figure 2.2. Let a basis of $W_1^{(i)}$ be given by

$$\{b_1^{i,1}, \dots, b_1^{i,m_i}\} \quad (2.33)$$

Notice, that we can find such a basis by taking any basis for V and computing $P_{l,1}^i b$ for each basis element $b \in V$. The result consists of vectors which span the subspace $W_1^{(i)}$ as can be seen from statement 3 of Corollary 2. Since D is completely reducible we know that there exists a symmetry adapted basis for V . We denote this symmetry adapted basis for V by

$$\{v_l^{i,j} : 1 \leq i \leq s, 1 \leq j \leq m_i, 1 \leq l \leq d_i\} \quad (2.34)$$

where the subspace $W_1^{(i)}$ consists of elements of the form $v_1^{i,j}$ with $1 \leq j \leq m_i$. Now, that we have two bases for $W_1^{(i)}$ it is possible to write each element of the basis given by 2.30 as a linear combination of the symmetry adapted basis elements of the same subspace $W_1^{(i)}$, i.e. with $z_k \in \mathbb{C}$ for all k we write

$$b_1^{i,j} = \sum_{k=1}^{m_i} z_k^{i,j} v_1^{i,k}. \quad (2.35)$$

The application of a linear projection operator $P_{l,1}^i$ which maps the first column $W_1^{(i)}$ of block $m_i V^{(i)}$ to the l -th column $W_l^{(i)}$ of block $m_i V^{(i)}$ yields,

$$P_{l,1}^i b_1^{i,j} = \sum_{k=1}^{m_i} z_k^{i,j} P_{l,1}^i v_1^{i,k} = \sum_{k=1}^{m_i} z_k^{i,j} v_l^{i,k} \quad (2.36)$$

where the last equality follows from Corollary 2. We give a name to the right-hand side of 2.36,

$$b_l^{i,j} := \sum_{k=1}^{m_i} z_k^{i,j} v_l^{i,k} \quad (2.37)$$

Thus, $P_{l,1}^i b_1^{i,j} = b_l^{i,j}$. Since 2.33 is a basis for $W_1^{(i)}$ and the projection operator $P_{l,1}^i$ maps onto the l -th column $W_l^{(i)}$ for each $1 \leq l \leq d_i$ it follows that all $b_l^{i,j}$ with $1 \leq l \leq d_i$ and $1 \leq j \leq m_i$ form a basis of block $m_i V^{(i)}$. This procedure can be done for each $1 \leq i \leq s$, resulting in a basis for V given by

$$\left\{ b_l^{i,j} : 1 \leq i \leq s, 1 \leq j \leq m_i, 1 \leq l \leq d_i \right\}. \quad (2.38)$$

If we can show that the basis given by 2.38 is also a symmetry adapted basis, then we found an algorithm for finding a symmetry adapted basis by means of the projection operators. It turns out, that it is indeed the case that 2.38 is a symmetry adapted basis. We summarize the algorithm in the following corollary and prove that the basis elements for V in 2.38 satisfy the required property of 2.32.

Corollary 7 *The vectors $b_l^{i,j}$ in 2.38 form a symmetry adapted basis for V . The procedure as presented above for obtaining a symmetry adapted basis can be summarized as follows.*

1. Choose an arbitrary basis for V and evaluate $P_{1,1}^i b$ for all b in the chosen basis for V and for all $1 \leq i \leq s$ where s denotes the number of inequivalent irreducible subrepresentations of the representation.
2. Construct for each $1 \leq i \leq s$ a basis for $W_1^{(i)}$ as in 2.33 by getting rid of the zero vectors and linear dependent vectors obtained in the previous step by application of $P_{1,1}^i$ to all basis vectors $b \in V$. Denote the resulting basis elements by $b_1^{i,j}$ with $1 \leq i \leq s$ and $1 \leq j \leq m_i$
3. Apply the projection operators $P_{l,1}^i$ as in 2.36 to the basis elements $b_1^{i,j}$ obtained in the previous step. Denote the result $b_l^{i,j} := P_{l,1}^i b_1^{i,j}$ in similar way as presented by 2.36 and 2.37. These vectors form a symmetry adapted basis for V .

Proof: It suffices to show that the elements in 2.38 form a symmetry adapted basis for V . This means that it suffices to show that 2.32 holds, i.e.

$$D(g)b_l^{i,j} = \sum_{d=1}^{d_i} D_{d,l}^{(i)}(g)b_d^{i,j}$$

Notice that

$$D(g)b_l^{i,j} \stackrel{(i)}{=} D(g)P_{l,1}^i b_1^{i,j} \stackrel{(ii)}{=} D(g) \frac{d_i}{|G|} \sum_{h \in G} D_{1,l}^i(h^{-1}) D(h)b_1^{i,j} \stackrel{(iii)}{=} \frac{d_i}{|G|} \sum_{h \in G} D_{1,l}^i(h^{-1}) D(gh)b_1^{i,j}$$

where (i) follows from the combination 2.36 with 2.37 and in (ii) we used the definition of the projection operator $P_{l,1}^i$ and in (iii) we used the homomorphism property. Now we take a closer look at the term $D_{1,l}^i(h^{-1})$ appearing in the right-hand side of the former formula. The subscripts in $D_{1,l}^i(h^{-1})$ denote the entry (i, l) of the matrix $D^i(h^{-1})$. Now we use brackets to indicate exactly the same entry, i.e. we write $[D^i(h^{-1})]_{1,l}$ for $D_{1,l}^i(h^{-1})$. In this way we derive for $h, g \in G$,

$$D_{1,l}^i(h^{-1}) = [D^i(h^{-1})]_{1,l} \stackrel{(iv)}{=} [D^i(h^{-1}g^{-1})D^i(g)]_{1,l} = \sum_{d=1}^{d_i} D_{1,d}^i(h^{-1}g^{-1})D_{d,l}^i(g)$$

where in (iv) we used the homomorphism property. A simple substitution of this expression in the penultimate formula yields,

$$\begin{aligned} D(g)b_l^{i,j} &= \frac{d_i}{|G|} \sum_{h \in G} \sum_{d=1}^{d_i} D_{1,d}^i(h^{-1}g^{-1})D_{d,l}^i(g)D(gh)b_1^{i,j} = \sum_{d=1}^{d_i} D_{d,l}^i(g) \frac{d_i}{|G|} \sum_{h \in G} D_{1,d}^i((gh)^{-1})D(gh)b_1^{i,j} \\ &\stackrel{(v)}{=} \sum_{d=1}^{d_i} D_{d,l}^i(g)P_{d,1}^i b_1^{i,j} \stackrel{(vi)}{=} \sum_{d=1}^{d_i} D_{d,l}^i(g)b_d^{i,j} \end{aligned}$$

where in (v) we used the definition of the projection operator $P_{d,1}^i$ and in (vi) the combination of the formulas 2.36 with 2.37. \square

By means of the algorithm discussed in corollary 7 we are able to compute the similarity transformation α in $D(g) = \alpha D'(g) \alpha^{-1}$ where $D'(g)$ is a block diagonal matrix as in 2.6 for each $g \in G$. In the construction described above we assumed D to be a unitary representation. By restriction of the inner product to an appropriate subspace it follows that the subrepresentations $D^{(i)}$ are unitary as well. If one takes a closer look at the proof of Maschke's Theorem 1 as presented in [23] or [14], it follows that the equivalence between D and D' is given by a unitary matrix α . This unitary matrix can be computed by making a small adjustment to the algorithm of Corollary 7. To this end, suppose we have performed steps 1 and 2 of Corollary 7. This means that we have a basis $b_1^{i,j}$ with $1 \leq i \leq s$ and $1 \leq j \leq m_i$ for each $W_1^{(i)}$ with $1 \leq i \leq s$. Since we assume D to be unitary it follows that the direct sum decomposition in 2.26 is orthogonal, see Maschke's Theorem in [14]. This means that all these basis vectors are orthogonal. In order to find the remaining vectors we should apply step 3 of Corollary 7 in which we find a basis for each $V_j^{(i)}$. After applying step 3 of Corollary 7 we apply the Gram Schmidt procedure. In that case we have found for each subspace $V_j^{(i)}$ a basis of pairwise orthonormal vectors which are also orthogonal between the different $V_j^{(i)}$ due to the orthogonal direct sum decomposition as presented in 2.27.

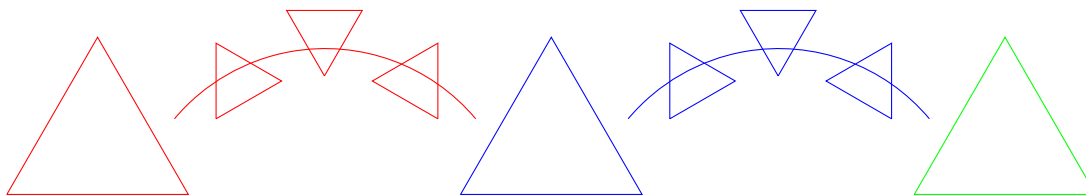
At this point we are equipped with a powerful algorithm by which we are able to derive a unitary transformation that brings a unitary reducible representation into a block diagonal form. In order to show an application of this algorithm we present an example in the coming section.

2.3. Decoupling of ordinary differential equations.

Consider the following linear system of ordinary differential equations written in matrix form

$$\begin{bmatrix} \dot{x}_1 \\ \dot{x}_2 \\ \dot{x}_3 \end{bmatrix} = \begin{bmatrix} 0 & 1 & 1 \\ 1 & 0 & 1 \\ 1 & 1 & 0 \end{bmatrix} \begin{bmatrix} x_1 \\ x_2 \\ x_3 \end{bmatrix} \tag{2.39}$$

We abbreviate this system by $\dot{\mathbf{x}} = A\mathbf{x}$ where A denotes the matrix in the right-hand side of 2.39 and \mathbf{x} a 3×1 vector containing the components x_1, x_2 and x_3 . Note that this linear system of differential equations show signs of symmetry. For instance if we replace x_1 by x_3 , x_2 by x_1 and x_3 by x_2 we obtain the same dynamics as we had before these replacements. If we repeat this process in which we rotate the indices i in x_i among the elements in the set $\{1, 2, 3\}$, then the dynamics will still remain the same. These symmetries of the system of differential equations form a group which can be captured by $\mathbb{Z}_3 := \{E, \rho, \rho^2\}$ where E, ρ, ρ^2 denote the identity element, rotation of the indices by one entry and two entries respectively. The nontrivial symmetries of this symmetry group are depicted in the figure below.



In a linear analysis of such a system as in 2.39 one often diagonalizes the matrix A in order to decouple this system of differential equations. But here we only block diagonalize the matrix A by employing the previous discussed algorithm. This allows us to study the symmetries of system 2.39. In order to clarify our strategy, we assume for the moment that we are in a position where we are allowed to apply the previous discussed algorithm, i.e. that we have a unitary reducible representation $D : \mathbb{Z}_3 \rightarrow GL(V)$. Here, we let $D : \mathbb{Z}_3 \rightarrow GL_3(\mathbb{C})$ be the permutation representation which is always unitary and reducible,

$$D(E) = \begin{bmatrix} 1 & 0 & 0 \\ 0 & 1 & 0 \\ 0 & 0 & 1 \end{bmatrix}, \quad D(\rho) = \begin{bmatrix} 0 & 0 & 1 \\ 1 & 0 & 0 \\ 0 & 1 & 0 \end{bmatrix}, \quad D(\rho^2) = \begin{bmatrix} 0 & 1 & 0 \\ 0 & 0 & 1 \\ 1 & 0 & 0 \end{bmatrix}. \tag{2.40}$$

Before we show how we go about the block diagonalization of matrix A , we first observe that we may block diagonalize the permutation representation matrices $D(g)$ of 2.40 by means of a unitary transformation α as

in the algorithm, i.e. by computing $D'(g) = \alpha^{-1}D(g)\alpha$ for each $g \in G$. Now, we define $\hat{\mathbf{x}} := \alpha^{-1}\mathbf{x}$. In this way we rewrite $\dot{\mathbf{x}} = A\mathbf{x}$ as $\alpha\dot{\hat{\mathbf{x}}} = A\alpha\hat{\mathbf{x}}$ and even as

$$\dot{\hat{\mathbf{x}}} = \alpha^{-1}A\alpha\hat{\mathbf{x}}. \quad (2.41)$$

If we can show that $\alpha^{-1}A\alpha$ takes on a block diagonal form we end up with a block diagonalization of 2.39. To this end, we notice that up to ordering the dynamics of 2.39 remain the same as for each $g \in \mathbb{Z}_3$ in the system

$$D(g)\dot{\hat{\mathbf{x}}} = AD(g)\hat{\mathbf{x}}. \quad (2.42)$$

A simple substitution of $\dot{\hat{\mathbf{x}}} = A\hat{\mathbf{x}}$ into 2.42 yields $D(g)A = AD(g)$ for each $g \in \mathbb{Z}_3$. Hence, the matrix A commutes with each of the representation matrices $D(g)$. Moreover, we have

$$D(g)A = AD(g) \iff \alpha^{-1}D(g)\alpha\alpha^{-1}A\alpha = \alpha^{-1}A\alpha\alpha^{-1}D(g)\alpha \iff D'(g)A' = A'D'(g) \quad (2.43)$$

where $D'(g) := \alpha^{-1}D(g)\alpha$ and $A' := \alpha^{-1}A\alpha$. By unitarity of D we have $D'(g)^{-1} = \alpha^{-1}\overline{D(g)^T}\alpha = \overline{D'(g)^T}$, so entry (u, v) of A' satisfies,

$$A'_{u,v} \stackrel{(i)}{=} \sum_{s,t} \left(\overline{D'(g)^T} \right)_{u,s} A'_{s,t} D'_{t,v}(g) = \sum_{s,t} \overline{D'_{s,u}(g)} A'_{s,t} D'_{t,v}(g) \stackrel{(ii)}{=} \sum_x \sum_y \overline{D_{x,\tilde{u}}^{(i)}(g)} A'_{x,y} D_{y,\tilde{v}}^{(l)}(g) \quad (2.44)$$

where (i) follows from 2.43 and in (ii) we observe that $D'(g)$ is block diagonal as in 2.6, so we confined ourselves to the nonzero contribution given by some subrepresentations $D^{(i)}$ and $D^{(l)}$ of which we denote their entries by (x, \tilde{u}) and (y, \tilde{v}) respectively. A summation over all group elements yields,

$$|G|A'_{u,v} = \sum_x \sum_y \left[\sum_{g \in G} \overline{D_{x,\tilde{u}}^{(i)}(g)} D_{y,\tilde{v}}^{(l)}(g) \right] A'_{x,y}. \quad (2.45)$$

Next, we divide both sides by $|G|$ and apply Schur's orthogonality relations,

$$A'_{u,v} = \sum_x \sum_y \left[\frac{1}{|G|} \sum_{g \in G} \overline{D_{x,\tilde{u}}^{(i)}(g)} D_{y,\tilde{v}}^{(l)}(g) \right] A'_{x,y} = \begin{cases} \frac{1}{d_i} \sum_x A'_{x,y} & \text{if } x = y, \tilde{u} = \tilde{v}, i = l \\ 0 & \text{otherwise} \end{cases} \quad (2.46)$$

This shows that we only have a nonzero contribution whenever blocks $D^{(i)}$ and $D^{(l)}$ are equivalent. Thus, A' is a block diagonal matrix.

The only thing we need to be able to block diagonalize A , is the transformation matrix α that provides the equivalence as in 2.6 of Maschke's Theorem 1. But in order to apply the algorithm we need to know the inequivalent irreducible subrepresentations of the representation in 2.40. By Corollary 4 we know that the number of irreducible representations of the group \mathbb{Z}_3 follow from the distinct number of conjugacy classes of this group. Since we have the following three conjugacy classes, $\mathcal{C}_1 := \{E\}$, $\mathcal{C}_2 := \{\rho\}$ and $\mathcal{C}_3 := \{\rho^2\}$. This means we end up with three irreducible representations of \mathbb{Z}_3 which we denote by $D^{(1)}$, $D^{(2)}$ and $D^{(3)}$. By means of the Dimensionality Theorem 5 we are able to determine the degree d_i of each irreducible representation $D^{(i)}$. We have,

$$|\mathbb{Z}_3| = \sum_{i=1}^3 d_i^2 \implies 3 = d_1^2 + d_2^2 + d_3^2 \implies d_1 = d_2 = d_3 = 1. \quad (2.47)$$

Thus, $D^{(1)}$, $D^{(2)}$ and $D^{(3)}$ are all one-dimensional matrix representations. In order to show that each of these irreducible representations occur as blocks in the block diagonalization we verify that each multiplicity m_i of $D^{(i)}$ is equal to one. This is achieved by using Corollary 3 that relates the multiplicity m_i to the character $\chi_{D^{(i)}}$ of a subrepresentation. To this end, we construct the character table step-by-step. Since we only have to deal with one-dimensional subrepresentations $D^{(i)}$ their characters coincide with their images. Observe that the one-dimensional subrepresentations $D^{(i)}$ are in particular group homomorphisms, so they preserve the identity element. The identity element in the multiplicative group $GL_1(\mathbb{C})$ is 1. The result is presented in the first column of the character table below. Moreover, the one-dimensional trivial subrepresentation is always present which can be seen in the first row of the character table below.

	$\mathcal{C}_1 := \{E\}$	$\mathcal{C}_2 := \{\rho\}$	$\mathcal{C}_3 := \{\rho^2\}$
$D^{(1)}$	1	1	1
$D^{(2)}$	1		
$D^{(3)}$	1		

The group \mathbb{Z}_3 is of order three, so $\rho^3 = E$. Hence by the homomorphism property of $D^{(i)}$ the following holds,

$$\left(D^{(i)}(\rho)\right)^3 = D^{(i)}(\rho^3) = D^{(i)}(E) = 1 \quad (2.48)$$

for each $1 \leq i \leq 3$. This shows that the order of the image of ρ under $D^{(i)}$ must divide 3 for all $1 \leq i \leq 3$. Consequently, its order is either 1 or 3. If its order is 1 we obtain the trivial representation $D^{(1)}$. If its order is equal to 3, we identify the image of each subrepresentation $D^{(i)}$ with the third roots of unity, i.e. $D^{(i)} : \mathbb{Z}_3 \rightarrow \{1, \zeta, \zeta^2\}$ where we define $\zeta := \exp\left(\frac{2\pi i}{3}\right)$. There are clearly only two possibilities in defining $D^{(2)}$ and $D^{(3)}$. These two possibilities complete the character table as shown below.

	$\mathcal{C}_1 := \{E\}$	$\mathcal{C}_2 := \{\rho\}$	$\mathcal{C}_3 := \{\rho^2\}$
$D^{(1)}$	1	1	1
$D^{(2)}$	1	ζ	ζ^2
$D^{(3)}$	1	ζ^2	ζ

It is important to notice that these three one-dimensional representations are irreducible and inequivalent. We only show that $D^{(2)}$ is irreducible as it is verified analogously for the other two representations. Since,

$$\left(\chi_{D^{(2)}} \middle| \chi_{D^{(2)}}\right) = \frac{1}{|\mathbb{Z}_3|} \sum_{g \in \mathbb{Z}_3} \chi_{D^{(2)}}(g) \overline{\chi_{D^{(2)}}(g)} = \frac{1}{3} \left[1 \cdot 1 + \zeta \cdot \bar{\zeta} + \zeta^2 \cdot \bar{\zeta}^2\right] = 1 \quad (2.49)$$

it follows from Corollary 3 that $D^{(2)}$ is irreducible. The inequivalence of the three representations follow from Theorem 2 along with the fact that the three rows of the character table are orthogonal as the sum of the roots of unity is equal to zero. The characters $\chi_{D^{(i)}}$ enable us to apply Corollary 3 to derive the multiplicities m_i as follows.

$$m_1 := \langle \chi_D, \chi_{D^{(1)}} \rangle := \frac{1}{|\mathbb{Z}_3|} \sum_{g \in \mathbb{Z}_3} \chi_D(g) \overline{\chi_{D^{(1)}}(g)} = \frac{1}{3} (3 \cdot 1 + 0 \cdot 1 + 0 \cdot 1) = 1 \quad (2.50)$$

$$m_2 := \langle \chi_D, \chi_{D^{(2)}} \rangle := \frac{1}{|\mathbb{Z}_3|} \sum_{g \in \mathbb{Z}_3} \chi_D(g) \overline{\chi_{D^{(2)}}(g)} = \frac{1}{3} (3 \cdot 1 + 0 \cdot \bar{\zeta} + 0 \cdot \bar{\zeta}^2) = 1 \quad (2.51)$$

$$m_3 := \langle \chi_D, \chi_{D^{(3)}} \rangle := \frac{1}{|\mathbb{Z}_3|} \sum_{g \in \mathbb{Z}_3} \chi_D(g) \overline{\chi_{D^{(3)}}(g)} = \frac{1}{3} (3 \cdot 1 + 0 \cdot \bar{\zeta}^2 + 0 \cdot \bar{\zeta}) = 1 \quad (2.52)$$

By Maschke's Theorem 1 we find the following decomposition,

$$D(g) \cong m_1 D^{(1)}(g) \oplus m_2 D^{(2)}(g) \oplus m_3 D^{(3)}(g) \cong \begin{bmatrix} D^{(1)}(g) & 0 & 0 \\ 0 & D^{(2)}(g) & 0 \\ 0 & 0 & D^{(3)}(g) \end{bmatrix}. \quad (2.53)$$

We denote the representation in the right-hand side of 2.53 by $D'(g)$ for each $g \in \mathbb{Z}_3$. We can write this representation explicitly as,

$$D'(E) := \begin{bmatrix} 1 & 0 & 0 \\ 0 & 1 & 0 \\ 0 & 0 & 1 \end{bmatrix}, \quad D'(\rho) := \begin{bmatrix} 1 & 0 & 0 \\ 0 & \zeta & 0 \\ 0 & 0 & \zeta^2 \end{bmatrix} \quad \text{and} \quad D'(\rho^2) := \begin{bmatrix} 1 & 0 & 0 \\ 0 & \zeta^2 & 0 \\ 0 & 0 & \zeta \end{bmatrix}. \quad (2.54)$$

The block diagonal representation of 2.54 is equivalent to the representation in 2.40 and by means of the algorithm we are able to find the similarity transformation between these representations. In order to apply the first step of Corollary 7 we choose a basis for our vector space V . Here we choose the standard basis $\{e_1, e_2, e_3\}$ where e_i denotes the i -th standard basis vector. Since the vector $P_{1,1}^i e_j$ is just the j -th column of the matrix $P_{1,1}^i$ it suffices to compute the matrices $P_{1,1}^i$. Before we do this, we first simplify the projection operators of 2.30 by using the unitarity of the subrepresentations.

$$P_{d,j}^i := \frac{d_i}{|\mathbb{Z}_3|} \sum_{g \in \mathbb{Z}_3} D_{j,d}^{(i)}(g^{-1}) D(g) = \frac{d_i}{|\mathbb{Z}_3|} \sum_{g \in \mathbb{Z}_3} D_{j,d}^{(i)}(g)^{-1} D(g) = \frac{d_i}{|\mathbb{Z}_3|} \sum_{g \in \mathbb{Z}_3} \overline{D_{d,j}^{(i)}(g)} D(g) \quad (2.55)$$

This last expression is often easier to work with as it avoids taking the inverse of group elements. Finally, we compute the matrices $P_{1,1}^i$ as done below.

$$P_{1,1}^1 = \frac{1}{6} \left[1 \cdot \begin{bmatrix} 1 & 0 & 0 \\ 0 & 1 & 0 \\ 0 & 0 & 1 \end{bmatrix} + 1 \cdot \begin{bmatrix} 0 & 0 & 1 \\ 1 & 0 & 0 \\ 0 & 1 & 0 \end{bmatrix} + 1 \cdot \begin{bmatrix} 0 & 1 & 0 \\ 0 & 0 & 1 \\ 1 & 0 & 0 \end{bmatrix} \right] = \frac{1}{6} \begin{bmatrix} 1 & 1 & 1 \\ 1 & 1 & 1 \\ 1 & 1 & 1 \end{bmatrix} \quad (2.56)$$

$$P_{1,1}^2 = \frac{1}{6} \left[1 \cdot \begin{bmatrix} 1 & 0 & 0 \\ 0 & 1 & 0 \\ 0 & 0 & 1 \end{bmatrix} + \bar{\zeta} \cdot \begin{bmatrix} 0 & 0 & 1 \\ 1 & 0 & 0 \\ 0 & 1 & 0 \end{bmatrix} + \bar{\zeta}^2 \cdot \begin{bmatrix} 0 & 1 & 0 \\ 0 & 0 & 1 \\ 1 & 0 & 0 \end{bmatrix} \right] = \frac{1}{6} \begin{bmatrix} 1 & \bar{\zeta}^2 & \bar{\zeta} \\ \bar{\zeta} & 1 & \bar{\zeta}^2 \\ \bar{\zeta}^2 & \bar{\zeta} & 1 \end{bmatrix} \quad (2.57)$$

$$P_{1,1}^3 = \frac{1}{6} \left[1 \cdot \begin{bmatrix} 1 & 0 & 0 \\ 0 & 1 & 0 \\ 0 & 0 & 1 \end{bmatrix} + \bar{\zeta}^2 \cdot \begin{bmatrix} 0 & 0 & 1 \\ 1 & 0 & 0 \\ 0 & 1 & 0 \end{bmatrix} + \bar{\zeta} \cdot \begin{bmatrix} 0 & 1 & 0 \\ 0 & 0 & 1 \\ 1 & 0 & 0 \end{bmatrix} \right] = \frac{1}{6} \begin{bmatrix} 1 & \bar{\zeta} & \bar{\zeta}^2 \\ \bar{\zeta}^2 & 1 & \bar{\zeta} \\ \bar{\zeta} & \bar{\zeta}^2 & 1 \end{bmatrix} \quad (2.58)$$

In step 2 of Corollary 7 we get rid of the linearly dependent columns in the matrices of 2.56-2.58. This yields the following set of vectors,

$$\left\{ \frac{1}{6} \begin{bmatrix} 1 \\ 1 \\ 1 \end{bmatrix}, \frac{1}{6} \begin{bmatrix} 1 \\ \bar{\zeta} \\ \bar{\zeta}^2 \end{bmatrix}, \frac{1}{6} \begin{bmatrix} 1 \\ \bar{\zeta}^2 \\ \bar{\zeta} \end{bmatrix} \right\}. \quad (2.59)$$

These vectors are linear independent and span a three-dimensional space. Hence, there is no need for step 3 of Corollary 7. The only thing left to do is normalizing these vectors and write them as columns in a matrix to obtain the unitary transformation matrix α ,

$$\alpha = \frac{1}{\sqrt{3}} \begin{bmatrix} 1 & 1 & 1 \\ 1 & \bar{\zeta} & \bar{\zeta}^2 \\ 1 & \bar{\zeta}^2 & \bar{\zeta} \end{bmatrix}. \quad (2.60)$$

It is easily verified that the transformation matrix α makes up the transformation from representation 2.40 to representation 2.54. Moreover, it decouples the system of differential equations as shown in 2.46. Since,

$$\alpha^{-1} A \alpha = \bar{\alpha}^T A \alpha = \frac{1}{3} \begin{bmatrix} 1 & 1 & 1 \\ 1 & \bar{\zeta} & \bar{\zeta}^2 \\ 1 & \bar{\zeta}^2 & \bar{\zeta} \end{bmatrix} \begin{bmatrix} 0 & 1 & 1 \\ 1 & 0 & 1 \\ 1 & 1 & 0 \end{bmatrix} \begin{bmatrix} 1 & 1 & 1 \\ 1 & \bar{\zeta} & \bar{\zeta}^2 \\ 1 & \bar{\zeta}^2 & \bar{\zeta} \end{bmatrix} = \begin{bmatrix} 2 & 0 & 0 \\ 0 & -1 & 0 \\ 0 & 0 & -1 \end{bmatrix} \quad (2.61)$$

it follows that system 2.39 becomes,

$$\begin{bmatrix} \hat{x}_1 \\ \hat{x}_2 \\ \hat{x}_3 \end{bmatrix} = \begin{bmatrix} 2 & 0 & 0 \\ 0 & -1 & 0 \\ 0 & 0 & -1 \end{bmatrix} \begin{bmatrix} \hat{x}_1 \\ \hat{x}_2 \\ \hat{x}_3 \end{bmatrix}. \quad (2.62)$$

In this example the block diagonalization of A by means of the algorithm yields the same result as an eigen-decomposition of the matrix A . This is not always the cases as we will see in the next chapter.

3

Cluster Synchronization

Throughout the years Representation Theory found its way in the study of synchrony in networks. This phenomenon of synchronization shows up in different man-made networks in which it is often an essential requirement for it to operate. In these engineered systems one strives for global synchronization, i.e. a state in which all network nodes are synchronized. This desirable phenomenon may prevent outages and provides a normal operation. Besides its importance in many man-made networks it also occurs naturally in for instance a swarm of animals such as fireflies. Fireflies light up, among other reasons, to identify other members of their species. After a short period of time they tend to light up in synchrony. Due to the occurrence of this phenomenon of global synchronization in many natural systems as well as its importance in engineered networks it became a popular topic of research and has undergone many developments in recent years. Besides a state of global synchrony there are other states of operation in which a loss of synchrony occurs that have gained attention as well. Since a loss of synchrony is often difficult to resolve and may lead to higher operational costs for many man-made networks it is an important subject on its own. In networks with a loss of synchrony there are often clusters of oscillators of which its members are still synchronized and where there is a lack of synchronization between members of different clusters. This phenomenon is referred to as cluster synchronization and fills up the gap between a global synchronous state and a asynchronous state. Knowledge about the transition between a state of global synchronization and synchronization of clusters may provide insights in how a network obtains and retains global synchronization. The stability of a global synchronous state is often addressed via a master stability function [19]. This master stability function is obtained via a decoupling of the variational equations which describe the dynamics of the network nodes. After acquiring a master stability function it allows one to determine the stability by means of a stability measure such as Lyapunov exponents. It turns out that a variety of variables play an important role in whether a network attains a state of global synchrony. In particular, the topology of a network, its nodal dynamics as well as the coupling between the nodes provide an essential contribution to the state of a network. In contrast to this theory of synchronizing networks there is still much to explore in regard to cluster synchronization. Recently published papers have shown that the usage of Representation Theory and Group Theory is well suited for this job. This approach started with the work of Golubitsky and Stewart [8] [21]. It became apparent that the symmetries in the topology of a network or its dynamics provide an important tool in the study of network synchronization. It is even the case that the appearance of network symmetries may lead naturally to synchrony. These network symmetries are often translated into mathematics via groups as we have seen in previous chapters. A more general approach can be taken when one uses groupoids instead of groups. A groupoid is an algebraic structure which generalizes the notion of a group. In a groupoid a product of two elements is not necessarily defined while a group is always closed under its operation. In this report we will restrict ourselves to group structures and advice the reader to look in [9] for a more general approach involving groupoids. Here we will follow the main thread of [22] and [20] which provides us with the theory for this chapter. In these papers one assigns group structures to clusters of network nodes. This is exactly what we will do and so their approach plays a central role in this chapter.

3.1. Symmetry groups for network clusters

A network is described by means of its dynamics along with its topology. This yields a wide variety of possible networks. Hence, we need to limit our scope and choose to deal solely with a particular symmetric network. Nevertheless, the ideas presented below may still be generalized to arbitrary symmetric networks. Below, we will only look at a symmetric ring network with eight nodes, see figure 3.1. The nodes are depicted by red circles and are the oscillators in the network. These oscillators all have their own angle θ_i where i indicates that we deal with the i -th oscillator. Notice that the numbering is provided next to each oscillator in figure 3.1. Each oscillator has its own natural frequency ω_i and is coupled to its neighbours by a link with strength $K > 0$. This eight node network will follow the dynamics provided by the Kuramoto model with second-order oscillators. This means that the angles of each oscillator will change over time according to 1.2 for ring networks,

$$\ddot{\theta}_i = \hat{D}_i \dot{\theta}_i + \omega_i - K \sin(\theta_i - \theta_{i-1}) - K \sin(\theta_i - \theta_{i+1}) \quad (3.1)$$

where $1 \leq i \leq 8$. In order to obtain a ring structure we let the indices of the angles satisfy $0 := 8, 9 := 1$. Although we assume that the dynamics of each angle θ_i follows 3.1, it is often the case that the angles behave differently among the network nodes. This is achieved in this network by differences in parameter values such as the natural frequencies ω_i , coupling strength K and damping parameters \hat{D}_i . The frequencies ω_i provide the intrinsic behaviour of each oscillator. The parameters \hat{D}_i are chosen such that $\hat{D}_i \leq 0$ and these reflect the damping properties in the system. For instance, if $\hat{D}_i = 0$ then there is no damping and we may neglect the first-order derivatives in the system. Differences in these parameters have effects as they can change the dynamics of the network. The coupling strength plays also a very important role since oscillators with the same frequency ω_i may behave differently over time due to the influence of their neighbours. Since we are interested in oscillators within the eight node network which behave similarly we will group these similar oscillators in a cluster. Since all oscillators within such a cluster behave similarly they form a so-called synchronized cluster. This means mathematically that the oscillators within a cluster have angles with equal time derivatives. If a synchronized cluster contains all network nodes, i.e. we have only one cluster with,

$$\dot{\theta}_1 = \dot{\theta}_2 = \dot{\theta}_3 = \dot{\theta}_4 = \dot{\theta}_5 = \dot{\theta}_6 = \dot{\theta}_7 = \dot{\theta}_8 \quad (3.2)$$

then the network is in a global synchronous state. This particular state is often desired in networks, but we will devote more of our time to states where there are multiple synchronized clusters, i.e. the angles of oscillators between two different clusters have a difference in time derivative while the angles of oscillators within each cluster have an equal time derivative. Below we aim to analyze these different synchronized clusters. In particular, we are interested in how clusters retain their synchrony. For this we perform a stability analysis which relies upon an approach which involves symmetries of the underlying network structure and network dynamics. Before we dive into more details we first address the important problem of finding all different clusters. For this, we take a closer look at the symmetry group provided by the network structure of the regular octagon. It has a rotational symmetry of order 8 given by a rotation over an angle $2\pi/8$ and a reflection symmetry in each of the bisectors of its internal angles. This symmetry group is called the Dihedral group of order 16 and is denoted D_{16} . This group is generated by a rotation ρ over an angle of $2\pi/8$ and a reflection σ through a line. These elements satisfy $\rho^8 = E$ and $\sigma^2 = E$ where E denotes the identity element of the group. The symmetry group, D_{16} , may be captured by the set,

$$D_{16} := \{E, \rho, \dots, \rho^7, \sigma, \rho\sigma, \dots, \rho^7\sigma\} \text{ with } \rho = (12345678) \text{ and } \sigma = (28)(37)(46). \quad (3.3)$$

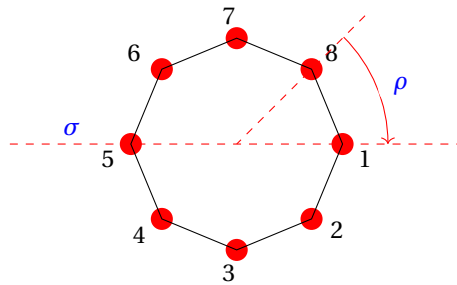


Fig. 3.1: Octagon.

The former table shows a wide variety of allowed symmetry groups for network clusters within an octagon shaped network. However, this characterization by means of direct products of clusters groups is not specific enough as it may lead to network configurations that are dynamically impossible. Moreover, some cluster configurations cannot be uniquely assigned to a specific network configuration. In order to explain these assertions we take a closer look at the cluster configurations \mathbb{Z}_4^2 and $\mathbb{Z}_2^2 \times \langle E \rangle^4$. The non-uniqueness follows from the figures 3.3 and 3.4 below. In these figures we depicted network configurations corresponding to the cluster configuration \mathbb{Z}_4^2 . The clusters are indicated by color such that blue colored nodes belong to one cluster and red colored nodes belong to another cluster. Hence, the dynamics between a red colored node and a blue colored node is different, so the time derivative of their respective angles differ. In figure 3.3 we depicted a network configuration which has an alternating pattern where a blue node is followed by a red node and vice versa. Figure 3.4 shows a similar pattern where two blue nodes are followed by two red nodes and vice versa. These figures show that there are at least two network configurations that are dynamically valid and both of them correspond to the same cluster configuration \mathbb{Z}_4^2 . In essence both of these network configurations may lead to different dynamical behaviour. Due to the fact that there are many allowed network configurations we will later choose only one network configuration for each allowed cluster configuration of table 3.1.

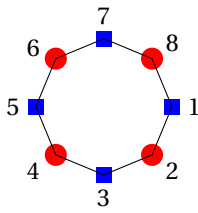


Fig. 3.3: group \mathbb{Z}_4^2 .

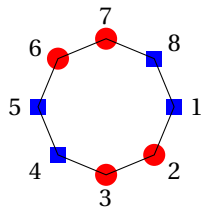


Fig. 3.4: Group \mathbb{Z}_4^2 .

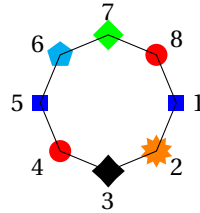


Fig. 3.5: Group $\mathbb{Z}_2^2 \times \langle E \rangle^4$.

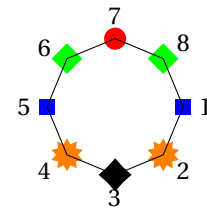


Fig. 3.6: Group $\mathbb{Z}_2^3 \times \langle E \rangle^2$.

The cluster configurations of figures 3.3 and 3.4 are dynamically valid. This is in contrast to all configurations for $\mathbb{Z}_2^2 \times \langle E \rangle^4$. This may be observed from figure 3.5 above. In this figure we depicted the two clusters containing two nodes by either red colored nodes or blue colored nodes. The remaining clusters which only contain one node each are depicted by different colored nodes. It turns out that the dynamically valid network configurations are those in which nodes within a synchronized cluster have neighbouring nodes with a similar behaviour among themselves. This characterization is solely based upon the fact that we are not able to block diagonalize the coupling matrix in a way as discussed in the previous chapter if this property is not satisfied. In order to see what this means graphically, we consider figure 3.5 where one blue node neighbours to an orange node while the other neighbours to a cyan colored node. Since the cyan colored node behaves differently from the orange colored node it leads to an invalid configuration. Since we could not find any allowed network configuration for this group we characterized it as an invalid cluster configuration. However, if we merge two one-node clusters we obtain a valid configuration such as the one in figure 3.6. All of the invalid cluster configurations are highlighted in blue in table 3.1. Hence, from now on we will solely focus upon the remaining allowed cluster configurations. In order to deal with the non-uniqueness of the allowed network configurations we limit our scope and choose the network configurations in which the node dynamics are distributed equally or has the most alternating arrangement. Hence, we choose the network of figure 3.3 over the one presented in figure 3.4. To avoid misunderstandings, we will show networks of table 3.1 graphically whenever we use them.

In table 3.1 we have several allowed cluster configurations. Some of these cluster configurations can be considered as being the same. Notice that the product group $D_8 \times \mathbb{Z}_2^2$ has more symmetries than $\mathbb{Z}_4 \times \mathbb{Z}_2^2$. These groups are not isomorphic, but both direct factors \mathbb{Z}_4 and D_8 will act on four network nodes. Therefore, both cluster configurations lead to the same network configurations. The same holds for the groups $D_8 \times \mathbb{Z}_4$ and $\mathbb{Z}_4 \times \mathbb{Z}_4$ and groups \mathbb{Z}_8 and D_{16} . This observation motivates our decision to choose to consider only the groups in the second and third column of table 3.1. One could argue that the groups in the sixth or last column have more symmetries and lead to a better block diagonalization when we apply the unitary transformation obtained from these groups to a certain coupling matrix of our network. However, the calculations involved to obtain such a unitary transformation involve significantly more calculations. Also, in section 3.3 we show that the groups in the second column allow us to merge clusters which shortens our computations substantially.

3.2. Linearization of Kuramoto dynamics on a ring network.

In the former section we derived all allowed cluster groups for the eight-node network of figure 3.1. These cluster groups correspond to a synchronized state of the entire network. In order to analyse the effects of the different allowed synchronized clusters we intend to linearize the dynamics on the eight-node network as given in 3.1 around a state of cluster synchrony. For this purpose we first rewrite each of the second-order differential equations as a system of first-order differential equations. Let us introduce the notation, $x_{1,i} := \theta_i$ and $x_{2,i} := \dot{\theta}_i$. Then the second-order differential equation is written as system of two first-order differential equations as follows,

$$\begin{aligned}\dot{x}_{1,i} &= x_{2,i} \\ \dot{x}_{2,i} &= \hat{D}x_{2,i} + \omega_i - K \sin(x_{1,i} - x_{1,i-1}) - K \sin(x_{1,i} - x_{1,i+1}).\end{aligned}\quad (3.4)$$

This system contains only first-order derivatives and allows us to linearize the system around a trajectory. Since we have n second-order oscillators we obtain n of these systems and therefore $2n$ first-order differential equations in total. We write the total system of $2n$ equations in vector form as,

$$\begin{aligned}\dot{\mathbf{x}}_1 &= \mathbf{x}_2 \\ \dot{\mathbf{x}}_2 &= \hat{D}\mathbf{x}_2 + \boldsymbol{\omega} - Kf(\mathbf{x}_1).\end{aligned}\quad (3.5)$$

The vector \mathbf{x}_1 has n entries of the form $x_{1,i}$. Similarly, the vector \mathbf{x}_2 has n entries of the form $x_{2,i}$. At last, the vector $\boldsymbol{\omega}$ contains n intrinsic frequencies. At this point, we combine the two equations by writing it as,

$$\dot{\mathbf{x}} = F(\mathbf{x}) \quad (3.6)$$

where $\mathbf{x} = [\mathbf{x}_1, \mathbf{x}_2]^T$ has $2n$ entries and the right-hand side of both equations in 3.5 is contained in $F(\mathbf{x})$. Our next goal is to linearize it around a state of cluster synchrony. For an arbitrary cluster group we denote a state of cluster synchrony by the vector \mathbf{s} . This vector contains for every node within the eight node network a certain angle position and angle velocity which is determined by the synchronous state of each cluster. By linearizing around such a state we are able to analyse the effects of small deviations in the angles positions and angle velocities of the oscillators. To this end, we write $\mathbf{x} = \mathbf{s} + \boldsymbol{\delta}$ where $\boldsymbol{\delta}$ is a vector of arbitrarily small deviations from the cluster synchronous state \mathbf{s} . We substitute this expression into 3.6 and find by means of linearization the following equation

$$\dot{\mathbf{s}} + \dot{\boldsymbol{\delta}} = F(\mathbf{s} + \boldsymbol{\delta}) = F(\mathbf{s}) + DF(\mathbf{s})\boldsymbol{\delta} + \mathcal{O}(\boldsymbol{\delta}^2). \quad (3.7)$$

The D in front of f shows that we deal with the Jacobian of f . We discard the second order terms in the previous equation and simplify accordingly,

$$\dot{\boldsymbol{\delta}} = DF(\mathbf{s})\boldsymbol{\delta}. \quad (3.8)$$

We can work backwards and expand this expression by taking $\boldsymbol{\delta} := [\boldsymbol{\delta}_1, \boldsymbol{\delta}_2]^T$ where $\boldsymbol{\delta}_1$ captures the deviations with respect to the first n equations and $\boldsymbol{\delta}_2$ the deviations with respect to the second n equations. This results in a system of the form,

$$\begin{bmatrix} \dot{\boldsymbol{\delta}}_1 \\ \dot{\boldsymbol{\delta}}_2 \end{bmatrix} = \begin{bmatrix} \mathbf{0} & I \\ -KDf(\mathbf{s}_1) & \hat{D}I \end{bmatrix} \begin{bmatrix} \boldsymbol{\delta}_1 \\ \boldsymbol{\delta}_2 \end{bmatrix}. \quad (3.9)$$

Here I denotes an $n \times n$ identity matrix and $Df(\mathbf{s}_1)$ is the Jacobian of f evaluated in a state of synchrony \mathbf{s}_1 that corresponds to the deviations vector $\boldsymbol{\delta}_1$. In particular, this Jacobian matrix consists of cosines and it has row sums equal to zero. Its structure is given explicitly below where we used the abbreviation $s_{i,j}$ for $\cos(s_i - s_j)$ to get

$$Df(\mathbf{s}_1) = \begin{bmatrix} s_{1,8} + s_{1,2} & -s_{1,2} & 0 & 0 & 0 & 0 & 0 & -s_{1,8} \\ -s_{1,2} & s_{1,2} + s_{2,3} & -s_{2,3} & 0 & 0 & 0 & 0 & 0 \\ 0 & -s_{2,3} & s_{2,3} + s_{3,4} & -s_{3,4} & 0 & 0 & 0 & 0 \\ 0 & 0 & -s_{3,4} & s_{3,4} + s_{4,5} & -s_{4,5} & 0 & 0 & 0 \\ 0 & 0 & 0 & -s_{4,5} & s_{4,5} + s_{5,6} & -s_{5,6} & 0 & 0 \\ 0 & 0 & 0 & 0 & -s_{5,6} & s_{5,6} + s_{6,7} & -s_{6,7} & 0 \\ 0 & 0 & 0 & 0 & 0 & -s_{6,7} & s_{6,7} + s_{7,8} & -s_{7,8} \\ -s_{1,8} & 0 & 0 & 0 & 0 & 0 & -s_{7,8} & s_{1,8} + s_{7,8} \end{bmatrix}.$$

The system in 3.9 is a coupled system of ordinary differential equations which are linear in the deviations vector. It describes how deviations in the angles affect the synchronous state. This last dynamical system will therefore be suitable to study the stability of synchronous states. Since we only consider the first order terms in the linearization of f we have to keep in mind that the analysis we are about to do is only valid for small deviations. Besides this assumption we also assume that synchronized oscillators within a cluster have not only equal derivatives but also equal angles. This means that for instance in the network configuration of figure 3.4 we take $s_{1,2} = s_{3,4} = s_{5,6} = s_{7,8}$ and $s_{2,3} = s_{6,7}$. This allows us to simplify the Jacobian matrix Df . In general, this assumption allows us to decouple the former linearized system by means of a unitary transformation which is obtained by using representations based on cluster groups from table 3.1. We denote the unitary transformation based on the cluster groups for the angles as in the previous chapter by α . By using the substitution $\alpha\delta$ it follows that system 3.9 can be written as

$$\begin{bmatrix} \dot{\delta}_1 \\ \dot{\delta}_2 \end{bmatrix} = \begin{bmatrix} \mathbf{0} & I \\ -K\alpha^T Df(\mathbf{s})\alpha & \hat{D}I \end{bmatrix} \begin{bmatrix} \delta_1 \\ \delta_2 \end{bmatrix} \quad (3.10)$$

where we used that $\alpha^T \hat{D}I\alpha = \alpha^T \alpha \hat{D}I = \hat{D}I$ by unitarity of the transformation matrix α . The lower left block in the matrix of the previous system yields a block diagonalization of Df . We emphasize that $\alpha^T Df(\mathbf{s}_1)\alpha$ only block diagonalizes under the assumption that all angles within a cluster are equal or in this case differ by a multiple of 2π due to the invariance of the cosine function. The resulting block diagonal matrix has in the upper left corner a block of dimension equal to the number of clusters in the network. This block corresponds to deviations on a synchronized manifold. The other blocks correspond to deviations in the so-called transverse manifold and we will call these blocks, transverse blocks [22]. These represent deviations in a direction perpendicular to that of the synchronization manifold. Hence, these are the blocks that are of importance in our stability analysis of synchronous states. To illustrate this we consider for the moment the network configuration of figure 3.3. The transformation $\alpha^T Df(\mathbf{s})\alpha$ results in a block diagonal matrix of the form as depicted in figure 3.7.

$$\begin{bmatrix} B_1 & 0 & 0 & 0 \\ 0 & B_2 & 0 & 0 \\ 0 & 0 & B_3 & 0 \\ 0 & 0 & 0 & B_4 \end{bmatrix}$$

Fig. 3.7: Block diagonal matrix.

The block diagonal matrix depicted above has a two-dimensional block B_1 , two one-dimensional blocks B_2 and B_3 and a four-dimensional block B_4 . Notice that the system in 3.10 is only partially decoupled by this transformation due to two higher dimensional blocks B_1 and B_4 . The block B_1 corresponds to deviations on a synchronization manifold while blocks B_2 down to B_4 correspond to deviations perpendicular to that of the synchronization manifold [22]. The blocks B_2 , B_3 and B_4 are of interest to us as they can distort the cluster synchronous state of figure 3.3. Since the block B_4 has dimension 4×4 we diagonalize this matrix by using an eigendecomposition. In this way, we further decouple the system of 3.10 by using a suitable transformation. To make this explicit we write 3.10 according to the block diagonalization as depicted in figure 3.7.

$$\begin{bmatrix} \dot{\delta}_1 \\ \dot{\delta}_{2,1} \\ \dot{\delta}_{2,2} \\ \dot{\delta}_{2,3} \\ \dot{\delta}_{2,4} \end{bmatrix} = \begin{bmatrix} \mathbf{0} & I \\ \hline -KB_1 & 0 & 0 & 0 \\ 0 & -KB_2 & 0 & 0 \\ 0 & 0 & -KB_3 & 0 \\ 0 & 0 & 0 & -KP^{-1}B_4P \end{bmatrix} \begin{bmatrix} \delta_1 \\ \delta_{2,1} \\ \delta_{2,2} \\ \delta_{2,3} \\ \delta_{2,4} \end{bmatrix}$$

Here P denotes the matrix with eigenvectors resulting from the eigendecomposition of B_4 . It decouples the differential equations such that we only need to consider the decoupled differential equations corresponding to the deviations $\delta_{2,1}$ up to $\delta_{2,4}$. Hence we do not consider the first component δ_1 , but only the components $\delta_{2,i}$ where the index i refers to the deviations that correspond to the i -th block of figure 3.7. A stability analysis for these deviations by means of Lyapunov exponents will determine the linear stability of the synchronous state

3.3. Merging clusters in a ring network.

Since there are many cluster configurations valid in our eight-node network, see table 3.1, we would have to determine many similarity transformations. Luckily, there is a way to avoid such a cumbersome process. This is done by merging clusters and we will treat this procedure below.

The table 3.1 contains several columns with different cluster groups. We did this on purpose since a cluster group appearing below another cluster group within the same column can be formed by merging clusters. Hence, if we start with a network that has a cluster group as presented at the top of one of the columns, then we can work our way down the table to obtain a network having a cluster group at a bottom row of this column. Moreover, if we have a unitary transformation corresponding to a permutation representation of a cluster group at the top row of table 3.1, then we are just a small step away from a unitary transformation for each of its underlying cluster groups. One way to go about this process of merging clusters is presented below for the second column of table 3.1.

Consider the group $\mathbb{Z}_2^4 := \mathbb{Z}_2 \times \mathbb{Z}_2 \times \mathbb{Z}_2 \times \mathbb{Z}_2$ of order sixteen. This group can be viewed as an analogue of the cartesian product for sets in which each entry has a group structure of addition modulo two on the integers. This cluster group is given in the first row and second column of table 3.1. This group can act on the set of network nodes as depicted in figure 3.8 below where each direct factor \mathbb{Z}_2 represents the possibility to interchange two network nodes having the same color.

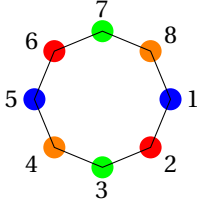


Fig. 3.8: Four clusters.

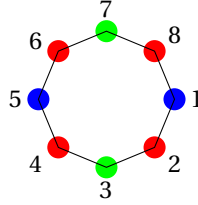


Fig. 3.9: Three clusters.

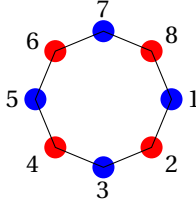


Fig. 3.10: Two clusters.

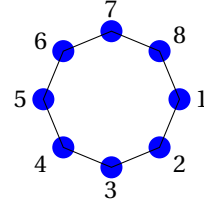


Fig. 3.11: One cluster.

Similarly, the network configurations of figure 3.9 up to figure 3.11 correspond to cluster groups $\mathbb{Z}_4 \times \mathbb{Z}_2^2$, \mathbb{Z}_4^2 and \mathbb{Z}_8 . Our goal is to derive a unitary transformation based on a cluster group of the network configuration in figure 3.8 to a unitary transformation that is based on a cluster group of the network configuration in figure 3.9. From there, we repeat this process and go from the network configuration in figure 3.9 to the one in figure 3.10. Notice, that the transition from the network in figure 3.8 to that of figure 3.9 is given by merging the clusters (2, 6) and (4, 8).

Before we merge clusters we first derive the unitary transformation with respect to the cluster group \mathbb{Z}_2^4 . This group is generated by four elements $a := (1, 0, 0, 0)$, $b := (0, 1, 0, 0)$, $c := (0, 0, 1, 0)$ and $d := (0, 0, 0, 1)$.

A permutation representation of this group is given by,

$$D(a) = \begin{bmatrix} 0 & 0 & 0 & 0 & 1 & 0 & 0 & 0 \\ 0 & 1 & 0 & 0 & 0 & 0 & 0 & 0 \\ 0 & 0 & 1 & 0 & 0 & 0 & 0 & 0 \\ 0 & 0 & 0 & 1 & 0 & 0 & 0 & 0 \\ 1 & 0 & 0 & 0 & 0 & 0 & 0 & 0 \\ 0 & 0 & 0 & 0 & 0 & 1 & 0 & 0 \\ 0 & 0 & 0 & 0 & 0 & 0 & 1 & 0 \\ 0 & 0 & 0 & 0 & 0 & 0 & 0 & 1 \end{bmatrix}, D(b) = \begin{bmatrix} 1 & 0 & 0 & 0 & 0 & 0 & 0 & 0 \\ 0 & 0 & 0 & 0 & 0 & 1 & 0 & 0 \\ 0 & 0 & 1 & 0 & 0 & 0 & 0 & 0 \\ 0 & 0 & 0 & 1 & 0 & 0 & 0 & 0 \\ 0 & 0 & 0 & 0 & 1 & 0 & 0 & 0 \\ 0 & 0 & 0 & 0 & 1 & 0 & 0 & 0 \\ 0 & 1 & 0 & 0 & 0 & 0 & 0 & 0 \\ 0 & 0 & 0 & 0 & 0 & 0 & 1 & 0 \\ 0 & 0 & 0 & 0 & 0 & 0 & 0 & 1 \end{bmatrix}, D(c) = \begin{bmatrix} 1 & 0 & 0 & 0 & 0 & 0 & 0 & 0 \\ 0 & 1 & 0 & 0 & 0 & 0 & 0 & 0 \\ 0 & 0 & 0 & 0 & 0 & 0 & 1 & 0 \\ 0 & 0 & 0 & 1 & 0 & 0 & 0 & 0 \\ 0 & 0 & 0 & 0 & 1 & 0 & 0 & 0 \\ 0 & 0 & 0 & 0 & 1 & 0 & 0 & 0 \\ 0 & 0 & 0 & 0 & 0 & 1 & 0 & 0 \\ 0 & 1 & 0 & 0 & 0 & 0 & 0 & 0 \\ 0 & 0 & 0 & 0 & 0 & 0 & 0 & 1 \end{bmatrix}, D(d) = \begin{bmatrix} 1 & 0 & 0 & 0 & 0 & 0 & 0 & 0 \\ 0 & 1 & 0 & 0 & 0 & 0 & 0 & 0 \\ 0 & 0 & 1 & 0 & 0 & 0 & 0 & 0 \\ 0 & 0 & 0 & 1 & 0 & 0 & 0 & 0 \\ 0 & 0 & 0 & 0 & 1 & 0 & 0 & 0 \\ 0 & 0 & 0 & 0 & 1 & 0 & 0 & 0 \\ 0 & 0 & 0 & 0 & 0 & 1 & 0 & 0 \\ 0 & 0 & 0 & 0 & 0 & 0 & 1 & 0 \\ 0 & 0 & 0 & 1 & 0 & 0 & 0 & 0 \end{bmatrix} \quad (3.11)$$

This group has sixteen conjugacy classes, each containing one group element. This follows from the fact that the direct factors are abelian groups, so in particular the direct product itself is abelian. Hence, there are sixteen irreducible representations and the Dimensionality Theorem tells us that they are all one-dimensional. We let the conjugacy classes be defined as follows,

$$\begin{aligned} \mathcal{C}_1 &= \{E\}, \mathcal{C}_2 = \{a\}, \mathcal{C}_3 = \{b\}, \mathcal{C}_4 = \{c\}, \mathcal{C}_5 = \{d\}, \mathcal{C}_6 = \{ab\}, \mathcal{C}_7 = \{ac\}, \mathcal{C}_8 = \{ad\} \\ \mathcal{C}_9 &= \{bc\}, \mathcal{C}_{10} = \{bd\}, \mathcal{C}_{11} = \{cd\}, \mathcal{C}_{12} = \{abc\}, \mathcal{C}_{13} = \{bcd\}, \mathcal{C}_{14} = \{acd\}, \mathcal{C}_{15} = \{abd\}, \mathcal{C}_{16} = \{abcd\} \end{aligned} \quad (3.12)$$

Each character of an irreducible representation of our group coincides with the representation itself as they are all one-dimensional. The character table is easily found since each element is either of order one or two so it must be sent to either 1 or -1 by the homomorphism property. The character table is presented below.

	\mathcal{C}_1	\mathcal{C}_2	\mathcal{C}_3	\mathcal{C}_4	\mathcal{C}_5	\mathcal{C}_6	\mathcal{C}_7	\mathcal{C}_8	\mathcal{C}_9	\mathcal{C}_{10}	\mathcal{C}_{11}	\mathcal{C}_{12}	\mathcal{C}_{13}	\mathcal{C}_{14}	\mathcal{C}_{15}	\mathcal{C}_{16}
$D^{(1)}$	1	1	1	1	1	1	1	1	1	1	1	1	1	1	1	1
$D^{(2)}$	1	-1	1	1	1	-1	-1	-1	1	1	1	-1	1	-1	-1	-1
$D^{(3)}$	1	1	-1	1	1	-1	1	1	-1	-1	1	-1	-1	1	-1	-1
$D^{(4)}$	1	1	1	-1	1	1	-1	1	-1	1	-1	-1	-1	-1	1	-1
$D^{(5)}$	1	1	1	1	-1	1	1	-1	1	-1	-1	1	-1	-1	-1	-1
$D^{(6)}$	1	-1	-1	1	1	1	-1	-1	-1	-1	1	1	-1	-1	1	1
$D^{(7)}$	1	-1	1	-1	1	-1	1	-1	1	-1	1	-1	1	-1	1	1
$D^{(8)}$	1	-1	1	1	-1	-1	-1	1	1	-1	-1	-1	-1	1	1	1
$D^{(9)}$	1	1	-1	-1	1	-1	-1	1	1	-1	-1	1	1	-1	-1	1
$D^{(10)}$	1	1	-1	1	-1	-1	1	-1	-1	1	-1	-1	1	-1	1	1
$D^{(11)}$	1	1	1	-1	-1	1	-1	-1	-1	-1	1	-1	1	1	-1	1
$D^{(12)}$	1	-1	-1	-1	1	1	1	-1	1	-1	-1	-1	1	1	1	-1
$D^{(13)}$	1	1	-1	-1	-1	-1	-1	-1	1	1	1	1	-1	1	1	-1
$D^{(14)}$	1	-1	1	-1	-1	-1	1	1	-1	-1	1	1	1	-1	1	-1
$D^{(15)}$	1	-1	-1	1	-1	1	-1	1	-1	1	-1	1	1	1	-1	-1
$D^{(16)}$	1	-1	-1	-1	-1	1	1	1	1	1	1	-1	-1	-1	-1	1

Notice that all rows are orthogonal, so these are indeed inequivalent representations by Corollary 3. They are necessarily irreducible being one-dimensional representations. At this point, we may calculate the unitary transformation by means of the projection operator as given in 2.55. This is done in Matlab due to the lengthy computation. It turns out that the unitary transformation, denoted by α , is as given in 3.13 below.

$$\alpha = \frac{1}{2}\sqrt{2} \begin{bmatrix} 1 & 0 & 0 & 0 & 1 & 0 & 0 & 0 \\ 0 & 1 & 0 & 0 & 0 & 1 & 0 & 0 \\ 0 & 0 & 1 & 0 & 0 & 0 & 1 & 0 \\ 0 & 0 & 0 & 1 & 0 & 0 & 0 & 1 \\ 1 & 0 & 0 & 0 & -1 & 0 & 0 & 0 \\ 0 & 1 & 0 & 0 & 0 & -1 & 0 & 0 \\ 0 & 0 & 1 & 0 & 0 & 0 & -1 & 0 \\ 0 & 0 & 0 & 1 & 0 & 0 & 0 & -1 \end{bmatrix}, \quad \beta = \frac{1}{2}\sqrt{2} \begin{bmatrix} 1 & 0 & 0 & 0 & 1 & 0 & 0 & 0 \\ 0 & \frac{1}{\sqrt{2}} & 0 & \frac{1}{\sqrt{2}} & 0 & \frac{1}{\sqrt{2}} & 0 & \frac{1}{\sqrt{2}} \\ 0 & 0 & 1 & 0 & 0 & 0 & 1 & 0 \\ 1 & 0 & 0 & 0 & -1 & 0 & 0 & 0 \\ 0 & 1 & 0 & 0 & 0 & -1 & 0 & 0 \\ 0 & 0 & 1 & 0 & 0 & 0 & -1 & 0 \\ 0 & 0 & 0 & 1 & 0 & 0 & 0 & -1 \end{bmatrix}. \quad (3.13)$$

At this point we only consider the matrix α , the matrix β is used later on. The clusters (2,6) and (4,8) can be merged such that we only have three clusters instead of four. In this way we obtain the configuration as presented in figure 3.9. The unitary transformation can then be obtained by repeating a similar computation as done above, but this time with a different symmetry group. The group we should use here is the one corresponding to the merged clusters as in figure 3.9. This provides yet another permutation representation. Since the resulting permutation representation will differ from the original one of 3.11 it will lead to a different unitary transformation. The computations we need in order to obtain a unitary transformation are often long due to the fact that we have to determine all irreducible representations. Luckily, we can avoid this long computation by using the structure of the unitary transformation we already found. We will explain this process that we found in [22]. A closer look at the unitary transformation in 3.13 shows that the clusters (2,6) and (4,8) have corresponding columns of the form $(0, 1, 0, 0, 0, 1, 0, 0)^T$ and $(0, 0, 0, 1, 0, 0, 0, 1)^T$, i.e. a column with a nonzero contribution on the entries 2 and 6 for cluster (2,6) and a nonzero contribution on the entries 4 and 8 for cluster (4,8). These are the second and fourth column in α . By taking the sum of these columns we end up with a vector $(0, 1, 0, 1, 0, 1, 0, 1)^T$ which has a one at each node within the merged cluster, i.e. a one at position i for node i within the merged cluster (2,6,4,8). Next, we normalize this vector to get $\frac{1}{2}(0, 1, 0, 1, 0, 1, 0, 1)^T$. Now we remove the second and fourth columns of α which correspond to the clusters (2,6) and (4,8). We replace one of these columns with the new column $\frac{1}{2}(0, 1, 0, 1, 0, 1, 0, 1)^T$. We choose to delete the fourth column and replace the second column. This results in a matrix with only seven columns. At this point, we are missing one column in order to form a basis. This missing column will be the orthogonal complement of the column space, i.e. the nullspace of these seven columns. The kernel of the linear map β in 3.13, that represents the transpose of this matrix with seven columns, is the linear span of the vector

$\frac{1}{2}(0, 1, 0, -1, 0, 1, 0, -1)^T$. This will be the missing column in our new similarity transformation. In summary we obtain the similarity transformation α' as given in 3.14 below.

$$\alpha' = \frac{1}{2}\sqrt{2} \begin{bmatrix} 1 & 0 & 0 & 0 & 1 & 0 & 0 & 0 \\ 0 & \frac{1}{\sqrt{2}} & 0 & \frac{1}{\sqrt{2}} & 0 & 1 & 0 & 0 \\ 0 & 0 & 1 & 0 & 0 & 0 & 1 & 0 \\ 0 & \frac{1}{\sqrt{2}} & 0 & -\frac{1}{\sqrt{2}} & 0 & 0 & 0 & 1 \\ 1 & 0 & 0 & 0 & -1 & 0 & 0 & 0 \\ 0 & \frac{1}{\sqrt{2}} & 0 & \frac{1}{\sqrt{2}} & 0 & -1 & 0 & 0 \\ 0 & 0 & 1 & 0 & 0 & 0 & -1 & 0 \\ 0 & \frac{1}{\sqrt{2}} & 0 & -\frac{1}{\sqrt{2}} & 0 & 0 & 0 & -1 \end{bmatrix}, \quad \alpha'' = \frac{1}{2}\sqrt{2} \begin{bmatrix} \frac{1}{2} & 0 & \frac{\sqrt{3}}{2} & 0 & 1 & 0 & 0 & 0 \\ \frac{1}{2} & \frac{1}{\sqrt{6}} & -\frac{1}{2\sqrt{3}} & \frac{1}{\sqrt{2}} & 0 & 1 & 0 & 0 \\ \frac{1}{2} & -\frac{\sqrt{2}}{3} & -\frac{1}{2\sqrt{3}} & 0 & 0 & 0 & 1 & 0 \\ \frac{1}{2} & \frac{1}{\sqrt{6}} & \frac{1}{2\sqrt{3}} & -\frac{1}{\sqrt{2}} & 0 & 0 & 0 & 1 \\ \frac{1}{2} & 0 & \frac{\sqrt{3}}{2} & 0 & -1 & 0 & 0 & 0 \\ \frac{1}{2} & \frac{1}{\sqrt{6}} & -\frac{1}{2\sqrt{3}} & \frac{1}{\sqrt{2}} & 0 & -1 & 0 & 0 \\ \frac{1}{2} & -\frac{\sqrt{2}}{3} & -\frac{1}{2\sqrt{3}} & 0 & 0 & 0 & -1 & 0 \\ \frac{1}{2} & \frac{1}{\sqrt{6}} & \frac{1}{2\sqrt{3}} & -\frac{1}{\sqrt{2}} & 0 & 0 & 0 & -1 \end{bmatrix}. \quad (3.14)$$

The matrix α'' will be used later on. A similar computation can be carried out to obtain a similarity transformation that corresponds to the network configuration of figure 3.10. From there on it is possible to find a similarity transformation for the global synchronous state of figure 3.11 too. This can also be achieved in one step by essentially the same process. To this end, we observe that in order to go from the network of figure 3.9 to the one in figure 3.11 we need to merge the clusters (2, 4, 6, 8), (1, 5) and (3, 7). Again, we have are looking for columns in α' with solely a nonzero contribution at entries indicated by the clusters. We see that the first column corresponds to cluster (1, 5), while the second and third column correspond to the clusters (2, 4, 6, 8) and (3, 7) respectively. Hence, we take the sum of the vectors $(1, 0, 0, 0, 1, 0, 0, 0)^T$, $(0, 1, 0, 1, 0, 1, 0, 1)^T$ and $(0, 0, 1, 0, 0, 1, 0)^T$. This results in a vector that becomes after normalizing, $8^{-1/2}(1, 1, 1, 1, 1, 1, 1, 1)^T$. We replace the first column of α' and replace the second and third columns by vectors containing only zeros. The orthogonal complement is this time spanned by two vectors. These two vectors replace the two empty columns. The result is the unitary transformation α'' of 3.14.

This seems very convenient as it provides the possibility to go quickly from one cluster configuration to another. However, the unitary transformation α'' will be different than the one obtained by taking an intermediate step where one first merges clusters (1, 5) and (3, 7) of figure 3.9. To be more precise, the α'' of 3.14 decouples the matrix in 3.10 in a different way than the unitary transformation obtained by an intermediate step. In the first case, there appears a 2×2 block while in the last case this 2×2 block are two 1×1 blocks. We rather have fewer large blocks after applying the similarity transformation. Hence, we only use the similarity transformations that are obtained by taking all intermediate steps into account. To give the complete picture we provide the two unitary transformations corresponding to figures 3.10 and 3.11 below by α''' and $\alpha^{(iv)}$ respectively.

$$\alpha''' = \frac{1}{2}\sqrt{2} \begin{bmatrix} \frac{1}{\sqrt{2}} & 0 & \frac{1}{\sqrt{2}} & 0 & 1 & 0 & 0 & 0 \\ 0 & \frac{1}{\sqrt{2}} & 0 & \frac{1}{\sqrt{2}} & 0 & 1 & 0 & 0 \\ \frac{1}{\sqrt{2}} & 0 & -\frac{1}{\sqrt{2}} & 0 & 0 & 0 & 1 & 0 \\ 0 & \frac{1}{\sqrt{2}} & 0 & -\frac{1}{\sqrt{2}} & 0 & 0 & 0 & 1 \\ \frac{1}{\sqrt{2}} & 0 & \frac{1}{\sqrt{2}} & 0 & -1 & 0 & 0 & 0 \\ 0 & \frac{1}{\sqrt{2}} & 0 & \frac{1}{\sqrt{2}} & 0 & -1 & 0 & 0 \\ \frac{1}{\sqrt{2}} & 0 & -\frac{1}{\sqrt{2}} & 0 & 0 & 0 & -1 & 0 \\ 0 & \frac{1}{\sqrt{2}} & 0 & -\frac{1}{\sqrt{2}} & 0 & 0 & 0 & -1 \end{bmatrix}, \quad \alpha^{(iv)} = \begin{bmatrix} \frac{1}{2} & -\frac{1}{2} & \frac{1}{\sqrt{2}} & 0 & 1 & 0 & 0 & 0 \\ \frac{1}{2} & \frac{1}{2} & 0 & \frac{1}{\sqrt{2}} & 0 & 1 & 0 & 0 \\ \frac{1}{2} & -\frac{1}{2} & -\frac{1}{\sqrt{2}} & 0 & 0 & 0 & 1 & 0 \\ \frac{1}{2} & \frac{1}{2} & 0 & -\frac{1}{\sqrt{2}} & 0 & 0 & 0 & 1 \\ \frac{1}{2} & -\frac{1}{2} & \frac{1}{\sqrt{2}} & 0 & -1 & 0 & 0 & 0 \\ \frac{1}{2} & \frac{1}{2} & 0 & \frac{1}{\sqrt{2}} & 0 & -1 & 0 & 0 \\ \frac{1}{2} & -\frac{1}{2} & -\frac{1}{\sqrt{2}} & 0 & 0 & 0 & -1 & 0 \\ \frac{1}{2} & \frac{1}{2} & 0 & -\frac{1}{\sqrt{2}} & 0 & 0 & 0 & -1 \end{bmatrix}. \quad (3.15)$$

The unitary matrices $\alpha, \alpha', \alpha'''$ and $\alpha^{(iv)}$ are the matrices we use for the cluster configurations as given in the second column of table 3.1. A similar computation can be carried out for the cluster group $\mathbb{Z}_2^3 \times \langle E \rangle^2$ as presented in the third column of table 3.1. For this cluster group we have a network configuration as depicted in figure 3.6. It turns out that a merge of two two-node clusters for this cluster configuration yields an invalid network configuration. In particular, we are not able to carry out the process of merging clusters to obtain a unitary matrix with a better diagonalization property.

4

Basin of Attraction

The dynamics of a network is often vulnerable to perturbations. For instance the dynamics of a power-grid could be disturbed by the seasonal volatility in demand. Moreover, power-grids may also suffer under large scale perturbations such as a power outage. The consequences of these different types of perturbations as well as methods to analyze them has drawn much attention throughout the years. In the case of small perturbations in network dynamics there are practical analytical tools available such as a linear analysis by means of the Lyapunov exponents. On the other hand, the influence of large perturbations is often difficult to derive analytically. This problem plays a central role in this chapter. We will analyse these large perturbations by taking all points in phase space into account which tend to evolve towards a specific attractor of the dynamical system. These points fall within the so called basin of attraction. This basin of attraction can be quantified by a (higher dimensional) volume in phase space. Below, we intend to determine the basin of attraction of a general n -node ring network capturing the dynamics provided by the Kuramoto model. We measure the size of the basin of attraction by fitting a ball of appropriate dimensions. Moreover, we will provide a proof for the largest ball we can fit inside the basin of attraction for a three node network, i.e. we determine the smallest distance between the chosen attractor and its neighbouring equilibrium points.

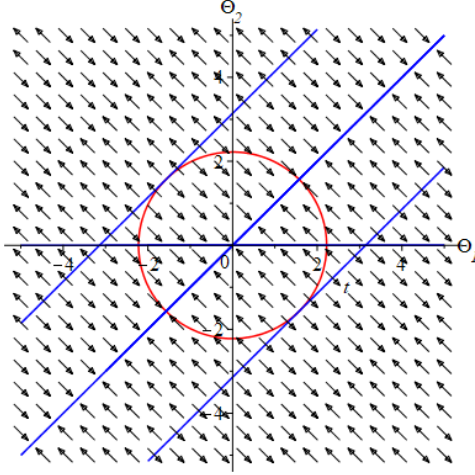
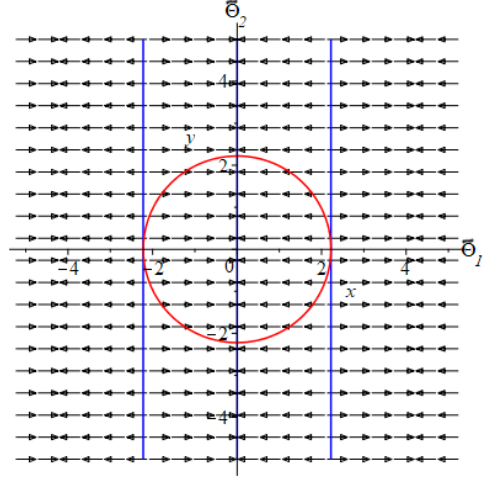
The outline of this chapter is as follows. We start with a motivation of our approach to determine the size of the basin of attraction. Next, we consider a simple ring network consisting of three oscillators. This toy model serves to illustrate the ideas used in the general n -node ring network. Moreover, it shows that our approach is computationally efficient for relatively low dimensions. At last we consider the general n -node ring network where we point out the nontrivial generalization of the argument used in the three oscillator network.

4.1. Motivation

The dynamics in the networks we are about to discuss follow the Kuramoto model as presented in (1.1). Since we are in particular interested in ring networks which only have a coupling between neighbouring nodes. This observation along with the assumption that $\omega_i = 0$ reduces the dynamics to,

$$\frac{d\theta_i}{dt} = -K \sin(\theta_i - \theta_{i-1}) - K \sin(\theta_i - \theta_{i+1}) \quad (4.1)$$

for $i = 1, \dots, n$ and where we define $\theta_0 := \theta_n$ and $\theta_{n+1} := \theta_1$. In order to determine the size of the basin of attraction analytically it would be satisfactory to have information about the location of the equilibria of (4.1). However, the nonlinearity due to the sine functions in (4.1) makes it very difficult to locate all equilibria. In [26] the synchronization of a similar model is studied and a novel algorithm is provided to find equilibria. Below we won't find all equilibria explicitly, but we will find analytical expressions for the angles along with an approximation for the minimal Euclidean distance between an attractor and any other equilibrium point. To this end, we first reduce the dimension of system (4.1). This is done, by using a property of the equilibria which can be readily verified. Note that if we find an equilibrium point of (4.1) then an equal adjustment of each of its coordinates yields another equilibrium point, i.e. the equilibria of (4.1) form lines in phase space.

Fig. 4.1: Phase plane with $n = 2$ and $K = 1$.Fig. 4.2: Rotated phase plane with $n = 2$ and $K = 1$.

In figure 4.1 we have depicted the phase plane corresponding to (4.1) with $n = 2$ and $K = 1$. We also added three blue lines consisting of equilibrium points. Notice that there is a change in angle in the horizontal direction as well as in the vertical direction. Since the dynamics is only present in the orthogonal direction relative to each blue line it makes sense to rotate the vector field such that a blue line going through the origin coincides with the θ_2 axis. The result of such a 'rotation' is given in figure 4.2. Here there is no change in angle in the vertical direction, so $\dot{\theta}_2$ will be constant. This is mathematically visible in the system corresponding to the dynamics of figure 4.2 by the fact that the time derivative of θ_2 will be equal to zero. Besides this reduction of dimension of the system of differential equations, we will also benefit from this rotation when we try to determine the size of the basin of attraction by means of fitting a circle around an attractor. In order to determine the radius of the circle we only need to measure in the θ_1 direction in the rotated phase plane while we need both directions in the original phase plane. As an example of an approximation of the basin of attraction we depicted in both figures the same red circle of maximal radius $\frac{1}{2}\sqrt{2}\pi$ around the attractor $(0, 0)$.

For $n = 2$ it is relatively easy to determine the radius of the circle we try to fit in the basin of attraction. However, for large n this is still a crucial question that remains unanswered. To cope with this problem one often searches for a way to apply a well known theorem of LaSalle [13]. For convenience, we first rewrite system (4.1) as,

$$\frac{d\boldsymbol{\theta}}{dt} = V(\boldsymbol{\theta}) \quad (4.2)$$

where $\boldsymbol{\theta}$ denotes a $n \times 1$ vector containing the phase angles of each oscillator and $V: \mathbb{R}^n \rightarrow \mathbb{R}^n$ a vector field with its i -th component given by the right-hand side of (4.1). At this moment we are able to formulate the theorem of LaSalle as follows.

Theorem 8 [13]: *Let $V(\boldsymbol{\theta})$ be a locally Lipschitz function defined over $D \subseteq \mathbb{R}^n$ and $\Omega \subseteq D$ a compact set that is positively invariant with respect to (4.2), i.e. $\boldsymbol{\theta}(0) \in \Omega$ implies $\boldsymbol{\theta}(t) \in \Omega$ for all $t \geq 0$. Let $L(\boldsymbol{\theta})$ a continuously differentiable function defined over D such that the total derivative $\dot{L}(\boldsymbol{\theta})$ satisfies $\dot{L}(\boldsymbol{\theta}) \leq 0$ in Ω . Define E to be the set of all points in Ω where $\dot{L}(\boldsymbol{\theta}) = 0$. Let M be the largest invariant set in E with respect to (4.2), i.e. $\boldsymbol{\theta}(0) \in M$ implies $\boldsymbol{\theta}(t) \in M$ for all $t \in \mathbb{R}$. Then every solution starting in Ω approaches M as $t \rightarrow \infty$.*

At this point we make a couple of remarks. All functions we will deal with are continuously differentiable over \mathbb{R}^n so in particular locally Lipschitz over a domain $D \subseteq \mathbb{R}^n$. Besides this technicality we are only interested in the domain of attraction of the origin so the set E and in particular the set M will contain only the origin. Since we want to determine the size of the basin of attraction radially we take Ω to be a closed ball around the origin excluding any other root of $\dot{L}(\boldsymbol{\theta})$.

The main issue in the application of this theorem is that it doesn't tell you how to choose $L(\boldsymbol{\theta})$. We make an attempt to apply this theorem by means of a natural choice for this function. We introduce our approach in the following section for a complete network.

4.2. A Complete Network

Suppose we have a ring network consisting of three oscillators, each following the dynamics provided by the Kuramoto model. Since all oscillators are coupled to each other we call this a complete network. We assume a constant coupling $K > 0$ and denote the phase angle of oscillator i by θ_i . Moreover, we set the natural frequency ω_i of each oscillator i equal to zero. This results in the following system of differential equations,

$$\frac{d\boldsymbol{\theta}}{dt} = V(\boldsymbol{\theta}) \quad (4.3)$$

where $\boldsymbol{\theta}$ denotes a 3×1 vector containing the phase angles of each oscillator and $V : \mathbb{R}^3 \rightarrow \mathbb{R}^3$ denotes a vector field. More specifically we have

$$\boldsymbol{\theta} = \begin{bmatrix} \theta_1 \\ \theta_2 \\ \theta_3 \end{bmatrix} \quad \text{and} \quad V(\boldsymbol{\theta}) = \begin{bmatrix} -K \sin(\theta_1 - \theta_3) - K \sin(\theta_1 - \theta_2) \\ -K \sin(\theta_2 - \theta_1) - K \sin(\theta_2 - \theta_3) \\ -K \sin(\theta_3 - \theta_2) - K \sin(\theta_3 - \theta_1) \end{bmatrix}$$

It can be readily verified that (4.3) is invariant under a cyclic permutation of the phase angles and a translation of each phase angle by the same amount. These transformations are captured by the following expressions,

$$\rho : (\theta_1, \theta_2, \theta_3) \mapsto (\theta_3, \theta_1, \theta_2) \quad \text{and} \quad \tau_\epsilon : (\theta_1, \theta_2, \theta_3) \mapsto (\theta_1 + \epsilon, \theta_2 + \epsilon, \theta_3 + \epsilon) \quad (4.4)$$

where $\epsilon > 0$ arbitrarily. We will take advantage of the translation invariance τ_ϵ as it enables us to rewrite system (4.3) in a more convenient form. To this end, we observe that the translation invariance takes place in the $\mathbf{n} := (\mathbf{1}, \mathbf{1}, \mathbf{1})$ direction. It turns out that a rotation of the vector field such that the θ_3 -axis collapses with \mathbf{n} reduces the dimension of (4.3) to only 2 dimensions. Moreover, it preserves the Euclidean distance between points in phase space. Hence, it will not affect the size of the basin of attraction around any point in phase space. To illustrate this rotation mathematically we provide the rotation matrices about the θ_3 and θ_1 -axis over angles φ_3 and φ_1 in counter-clockwise direction by

$$R_{\theta_3}(\varphi_3) = \begin{bmatrix} \cos(\varphi_3) & -\sin(\varphi_3) & 0 \\ \sin(\varphi_3) & \cos(\varphi_3) & 0 \\ 0 & 0 & 1 \end{bmatrix} \quad \text{and} \quad R_{\theta_1}(\varphi_1) = \begin{bmatrix} 1 & 0 & 0 \\ 0 & \cos(\varphi_1) & -\sin(\varphi_1) \\ 0 & \sin(\varphi_1) & \cos(\varphi_1) \end{bmatrix} \quad (4.5)$$

respectively. The rotation which makes \mathbf{n} coincide with the θ_3 -axis is done in two steps. First we rotate \mathbf{n} about the θ_3 -axis over an angle φ_3 . Secondly, we rotate the result of the previous step about the θ_1 -axis over an angle φ_1 . From figure (4.3) it is clear that the red colored arrow, which depicts the first and second component of \mathbf{n} , yields an angle of size $\varphi_3 = \frac{\pi}{4}$ with respect to the θ_2 -axis.

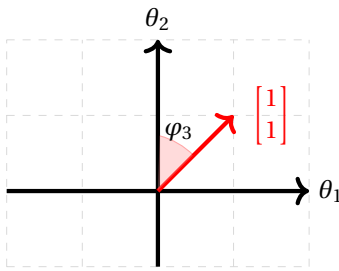


Fig. 4.3: Rotation about the θ_3 -axis

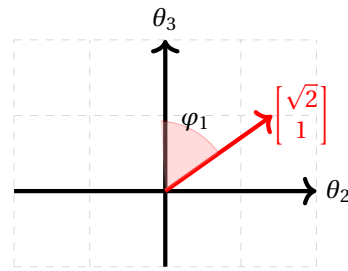


Fig. 4.4: Rotation about the θ_1 -axis

A simple substitution of $\varphi_3 = \frac{\pi}{4}$ into the expression of $R_{\theta_3}(\varphi_3)$ in (5.4) yields a rotated vector of \mathbf{n} given by,

$$R_{\theta_3}\left(\frac{\pi}{4}\right) \cdot \mathbf{n} = \begin{bmatrix} \frac{1}{\sqrt{2}} & -\frac{1}{\sqrt{2}} & 0 \\ \frac{1}{\sqrt{2}} & \frac{1}{\sqrt{2}} & 0 \\ 0 & 0 & 1 \end{bmatrix} \begin{bmatrix} 1 \\ 1 \\ 1 \end{bmatrix} = \begin{bmatrix} 0 \\ \sqrt{2} \\ 1 \end{bmatrix}. \quad (4.6)$$

The result lies clearly in the θ_2 - θ_3 plane. The red arrow in figure 4.4 is given by the result of (4.6) where we neglect the first entry. Since we want an explicit representation of $R_{\theta_1}(\varphi_1)$ we determine both $\cos(\varphi_1)$ and $\sin(\varphi_1)$. Recall that $\cos(\varphi_1)$ is equal to the dot product between the red vector and an arbitrary vector along the θ_3 axis divided by the product of their magnitudes, i.e.

$$\cos(\varphi_1) = \frac{1}{\sqrt{3} \cdot 1} [\sqrt{2} \ 1] \cdot \begin{bmatrix} 0 \\ 1 \end{bmatrix} = \frac{1}{\sqrt{3}}. \quad (4.7)$$

The angle φ_1 is clearly in the interval $[0, \pi]$. Hence we write $\varphi_1 = \arccos(x)$ where $x = (\sqrt{3})^{-1}$ by (4.7). A simple derivation yields,

$$\sin(\varphi_1) = \sin(\arccos(x)) = \sin(\varphi_1) = \sqrt{1 - \cos^2(\varphi_1)} = \sqrt{1 - (\cos(\arccos(x)))^2} = \sqrt{1 - x^2} = \sqrt{\frac{2}{3}} \quad (4.8)$$

By using (4.7) and (4.8) we are able to write $R_{\theta_1}(\varphi_1)$ explicitly and provide the final rotation,

$$R_{\theta_1}(\varphi_1) R_{\theta_3}\left(\frac{\pi}{4}\right) \cdot \mathbf{n} = R_{\theta_1}(\varphi_1) \cdot \begin{bmatrix} 0 \\ \sqrt{2} \\ 1 \end{bmatrix} = \begin{bmatrix} 1 & 0 & 0 \\ 0 & \frac{1}{\sqrt{3}} & -\sqrt{\frac{2}{3}} \\ 0 & \sqrt{\frac{2}{3}} & \frac{1}{\sqrt{3}} \end{bmatrix} \begin{bmatrix} 0 \\ \sqrt{2} \\ 1 \end{bmatrix} = \begin{bmatrix} 0 \\ 0 \\ \sqrt{3} \end{bmatrix}. \quad (4.9)$$

These two rotations can be captured by a single rotation matrix R which is defined by $R := R_{\theta_1}(\varphi_1) R_{\theta_3}(\varphi_3)$. In this way, the rotation of \mathbf{n} can be done in only one step,

$$R \cdot \mathbf{n} = \begin{bmatrix} \frac{1}{\sqrt{2}} & -\frac{1}{\sqrt{2}} & 0 \\ \frac{1}{\sqrt{6}} & \frac{1}{\sqrt{6}} & -\sqrt{\frac{2}{3}} \\ \frac{1}{\sqrt{3}} & \frac{1}{\sqrt{3}} & \frac{1}{\sqrt{3}} \end{bmatrix} \begin{bmatrix} 1 \\ 1 \\ 1 \end{bmatrix} = \begin{bmatrix} 0 \\ 0 \\ \sqrt{3} \end{bmatrix}. \quad (4.10)$$

The result clearly lies on the θ_3 axis. This rotation matrix allows us to rotate the vector field of (4.3). Since a vector field is a vector-valued function, it attaches to each point in the plane a vector. Hence, we need to rotate each point by the same angle as the vectors that are attached to these points. This yields the rotated version of (4.3),

$$\frac{d\boldsymbol{\theta}}{dt} = RV(R^{-1}\boldsymbol{\theta}) \quad (4.11)$$

where R is a rotation matrix such as the one in (4.10). It can be readily verified that the rotation amounts to a transformation $\boldsymbol{\theta} \mapsto R^{-1}\boldsymbol{\theta}$. Since R is a rotation matrix its inverse is equal to its transpose, i.e. $R^{-1} = R^T$. This property will simplify our next calculation in which we determine the rotated vector field explicitly. We have,

$$\begin{aligned} RV(R^{-1}\boldsymbol{\theta}) &= RV\left(\begin{bmatrix} \frac{1}{\sqrt{2}} & \frac{1}{\sqrt{6}} & \frac{1}{\sqrt{3}} \\ -\frac{1}{\sqrt{2}} & \frac{1}{\sqrt{6}} & \frac{1}{\sqrt{3}} \\ 0 & -\sqrt{\frac{2}{3}} & \frac{1}{\sqrt{3}} \end{bmatrix} \begin{bmatrix} \theta_1 \\ \theta_2 \\ \theta_3 \end{bmatrix}\right) = RV\left(\begin{bmatrix} \frac{\theta_1}{\sqrt{2}} + \frac{\theta_2}{\sqrt{6}} + \frac{\theta_3}{\sqrt{3}} \\ -\frac{\theta_1}{\sqrt{2}} + \frac{\theta_2}{\sqrt{6}} + \frac{\theta_3}{\sqrt{3}} \\ -\sqrt{\frac{2}{3}}\theta_2 + \frac{\theta_3}{\sqrt{3}} \end{bmatrix}\right) \\ &= R \begin{bmatrix} -K \sin\left(\frac{\theta_1}{\sqrt{2}} + \sqrt{\frac{3}{2}}\theta_2\right) - K \sin(\sqrt{2}\theta_1) \\ K \sin(\sqrt{2}\theta_1) - K \sin\left(-\frac{\theta_1}{\sqrt{2}} + \sqrt{\frac{3}{2}}\theta_2\right) \\ K \sin\left(-\frac{\theta_1}{\sqrt{2}} + \sqrt{\frac{3}{2}}\theta_2\right) + K \sin\left(\frac{\theta_1}{\sqrt{2}} + \sqrt{\frac{3}{2}}\theta_2\right) \end{bmatrix} = \begin{bmatrix} -\sqrt{2}K \sin(\sqrt{2}\theta_1) - \frac{K}{\sqrt{2}} \sin\left(\frac{\theta_1}{\sqrt{2}} + \sqrt{\frac{3}{2}}\theta_2\right) + \frac{K}{\sqrt{2}} \sin\left(-\frac{\theta_1}{\sqrt{2}} + \sqrt{\frac{3}{2}}\theta_2\right) \\ -K\sqrt{\frac{3}{2}} \sin\left(\frac{\theta_1}{\sqrt{2}} + \sqrt{\frac{3}{2}}\theta_2\right) - K\sqrt{\frac{3}{2}} \sin\left(-\frac{\theta_1}{\sqrt{2}} + \sqrt{\frac{3}{2}}\theta_2\right) \\ 0 \end{bmatrix}. \end{aligned}$$

Notice that the last entry is zero due to the fact that the θ_3 -axis of the original system coincides with the \mathbf{n} direction. This means that there is no change in dynamics along the θ_3 axis of the rotated system, so we may as well neglect this last equation and consider the dynamics given by

$$\begin{bmatrix} \dot{\theta}_1 \\ \dot{\theta}_2 \end{bmatrix} = \begin{bmatrix} -\sqrt{2}K \sin(\sqrt{2}\theta_1) - \frac{K}{\sqrt{2}} \sin\left(\frac{\theta_1}{\sqrt{2}} + \sqrt{\frac{3}{2}}\theta_2\right) + \frac{K}{\sqrt{2}} \sin\left(-\frac{\theta_1}{\sqrt{2}} + \sqrt{\frac{3}{2}}\theta_2\right) \\ -K\sqrt{\frac{3}{2}} \sin\left(\frac{\theta_1}{\sqrt{2}} + \sqrt{\frac{3}{2}}\theta_2\right) - K\sqrt{\frac{3}{2}} \sin\left(-\frac{\theta_1}{\sqrt{2}} + \sqrt{\frac{3}{2}}\theta_2\right) \end{bmatrix} \quad (4.12)$$

The figures below show the original three dimensional phase space from two different viewpoints. Figure 4.5 can be seen as the dynamics provided by the original dynamics given by three differential equations, while figure 4.6 depicts the dynamics given by the two dimensional rotated system of differential equations. The red ball indicates an approximation of the basin of attraction which we intend to find below. In figure 4.5 we see diagonal lines which are lines consisting of equilibria. These diagonal lines are points in figure 4.6 due to the different point of view of the dynamics depicted in figure 4.5.

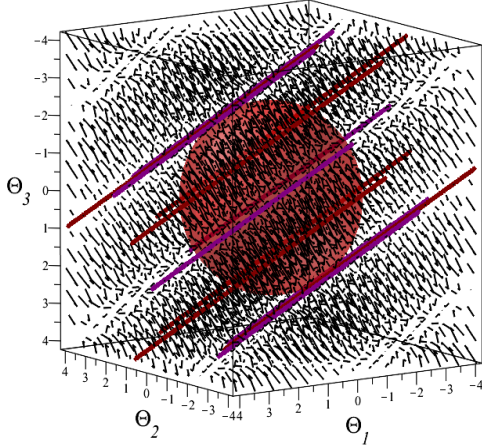


Fig. 4.5: Phase space of 5.1 with $K = 1$.

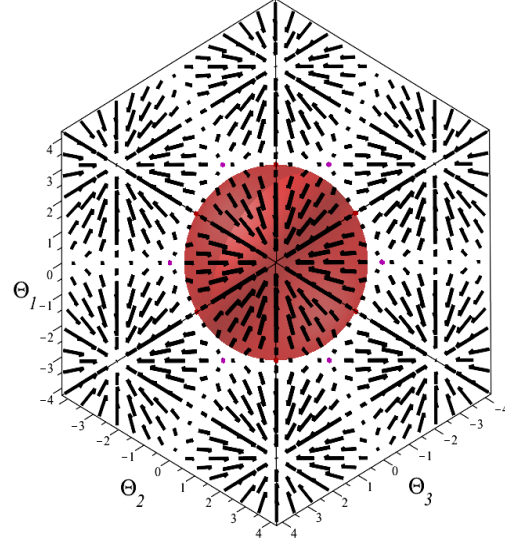


Fig. 4.6: Rotation phase space of 5.1 with $K = 1$.

In order to determine the basin of attraction of this rotated system of differential equations, we apply Theorem 8 as presented in the motivation of this chapter. In this exposition we restrict our 3×1 vector $\boldsymbol{\theta}$ to a 2×1 vector containing only θ_1 and θ_2 . Moreover, the sets $D \subseteq \mathbb{R}^n$ and $\Omega \subseteq D$ in Theorem 8 will be determined along the way. First, we will find a suitable continuously differentiable function $L : \mathbb{R}^2 \rightarrow \mathbb{R}$. To this end, we observe that (4.12) is a gradient system, i.e. there is a scalar function $\hat{V} : \mathbb{R}^2 \rightarrow \mathbb{R}$ such that $\dot{\boldsymbol{\theta}} = \nabla \hat{V}(\boldsymbol{\theta})$. The scalar function $\hat{V}(\boldsymbol{\theta})$ may be written explicitly as,

$$\hat{V}(\boldsymbol{\theta}) = K \cos(\sqrt{2}\theta_1) + K \cos\left(\frac{\theta_1}{\sqrt{2}} + \sqrt{\frac{3}{2}}\theta_2\right) + K \cos\left(-\frac{\theta_1}{\sqrt{2}} + \sqrt{\frac{3}{2}}\theta_2\right). \quad (4.13)$$

This provides us with the following candidate, $L(\boldsymbol{\theta}) := -\hat{V}(\boldsymbol{\theta})$. To verify whether it satisfies the required conditions of Theorem 8 we calculate its total derivative. Although it is not difficult to find it explicitly as shown in Appendix A, we may also derive it as follows.

$$\dot{L}(\boldsymbol{\theta}) = \frac{d}{dt} [-\nabla \hat{V}(\boldsymbol{\theta})] = -\nabla \hat{V}(\boldsymbol{\theta}) \cdot \dot{\boldsymbol{\theta}} = -\nabla \hat{V}(\boldsymbol{\theta}) \cdot [\nabla \hat{V}(\boldsymbol{\theta})] = -\|\nabla \hat{V}(\boldsymbol{\theta})\|^2 \quad (4.14)$$

Hence, $\dot{L}(\boldsymbol{\theta}) \leq 0$. Moreover, it shows that its roots coincide with the equilibria of our system of differential equations in 4.12. Since we want to determine the size of the basin of attraction of the origin we want E as in Theorem 8 to contain only the origin. By 4.14 it is clear that the origin is indeed a root of $\dot{L}(\boldsymbol{\theta})$. However, there are more roots of $\dot{L}(\boldsymbol{\theta})$ over \mathbb{R}^2 . These other roots need to be excluded from the ball $\Omega \subseteq \mathbb{R}^2$ of Theorem 8. Moreover, we want this ball Ω to be as large as possible to obtain the best bound of the basin of attraction in arbitrary radial direction. Therefore we determine the smallest Euclidean distance between the origin and an arbitrary equilibrium of 4.12 by finding all roots of $\dot{L}(\boldsymbol{\theta})$. To find all roots of $\dot{L}(\boldsymbol{\theta})$ we turn our attention to system 4.12 and see that the equilibria must satisfy,

$$\sin(\sqrt{2}\theta_1) = -\sin\left(\frac{\theta_1}{\sqrt{2}} + \sqrt{\frac{3}{2}}\theta_2\right) = \sin\left(-\frac{\theta_1}{\sqrt{2}} + \sqrt{\frac{3}{2}}\theta_2\right). \quad (4.15)$$

The last equality in 4.15 leads with the help of a little trigonometry to,

$$0 = \sin\left(-\frac{\theta_1}{\sqrt{2}} + \sqrt{\frac{3}{2}}\theta_2\right) + \sin\left(\frac{\theta_1}{\sqrt{2}} + \sqrt{\frac{3}{2}}\theta_2\right) = 2\cos\left(\frac{\theta_1}{\sqrt{2}}\right)\sin\left(\sqrt{\frac{3}{2}}\theta_2\right) \quad (4.16)$$

If $\cos\left(\frac{1}{2}\sqrt{2}\theta_1\right) = 0$, then $\theta_1 = \frac{1}{2}\sqrt{2}(2k_1 - 1)\pi$ with $k_1 \in \mathbb{Z}$ and so $\sin\left(\sqrt{2}\theta_1\right) = 0$. This means that every term in 4.15 vanishes. A substitution of $\theta_1 = \frac{1}{2}\sqrt{2}(2k_1 - 1)\pi$ in the first equation of 4.15 yields $\cos\left(\sqrt{\frac{3}{2}}\theta_2\right) = 0$, i.e. $\theta_2 = \frac{1}{2}\sqrt{\frac{2}{3}}(2k_2 - 1)\pi$. On the other hand, if $\sin\left(\sqrt{\frac{3}{2}}\theta_2\right)$ in 4.16 vanishes, we have $\theta_2 = \sqrt{\frac{2}{3}}\ell_2\pi$. Consequently, the first equality in 4.15 yields

$$0 = \sin\left(\sqrt{2}\theta_1\right) \pm \sin\left(\frac{1}{2}\sqrt{2}\theta_1\right) = 2\sin\left(\frac{1}{2}\left[\sqrt{2}\theta_1 \pm \frac{1}{2}\sqrt{2}\theta_1\right]\right)\cos\left(\frac{1}{2}\left[\sqrt{2}\theta_1 \mp \frac{1}{2}\sqrt{2}\theta_1\right]\right) \quad (4.17)$$

Thus,

$$\theta_1 = \frac{2}{3}\sqrt{2}\ell_1\pi, \quad \theta_1 = 2\sqrt{2}\ell_1\pi, \quad \theta_1 = \frac{1}{3}\sqrt{2}(2\ell_1 - 1)\pi \quad \text{or} \quad \theta_1 = \sqrt{2}\ell_1\pi. \quad (4.18)$$

The roots that lie as close as possible to the origin lie $\sqrt{\frac{2}{3}}\pi$ away from the origin and are given by

$$\left(0, \pm\sqrt{\frac{2}{3}}\pi\right) \quad \text{and} \quad \left(\pm\frac{1}{2}\sqrt{2}\pi, \pm\frac{\pi}{\sqrt{6}}\right). \quad (4.19)$$

These six points are depicted in figure 4.7 by blue points lying on the red circle which provides an approximation of the basin of attraction. We also depicted six magenta colored points lying further away from the origin. As can be seen in figure 4.8 we have a repeating hexagon shape and all equilibria of 4.12 are translations of the blue and magenta colored points.

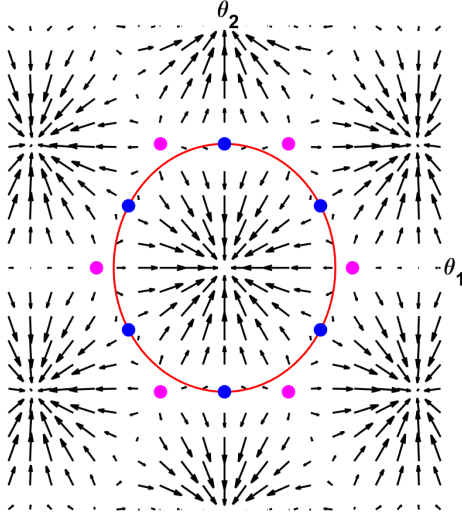


Fig. 4.7: Phase plane corresponding to 5.12 with $K = 1$.

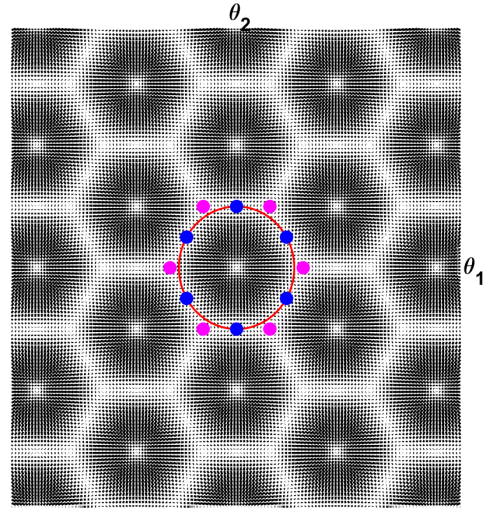


Fig. 4.8: Phase plane corresponding to 5.12 with $K = 1$.

For completeness we provide the magenta colored points of figure 4.7 explicitly,

$$\left(\pm 2\sqrt{2}\frac{\pi}{3}, 0\right) \quad \text{and} \quad \left(\pm\frac{\sqrt{2}\pi}{3}, \pm\sqrt{\frac{2}{3}}\pi\right). \quad (4.20)$$

In order to complete the proof we need to show that a circle with a radius $\epsilon > 0$ smaller than the one in figure 4.7 doesn't let any trajectory leave this circle. More specifically, we need to show that the closed ball $B\left[0, \sqrt{\frac{2}{3}}\pi - \epsilon\right]$ with $\epsilon > 0$ sufficiently small is positively invariant with respect to 4.12. This we do not show mathematically as it may be observed from the direction fields.

4.3. Ring networks of odd-dimension

In the previous section we successfully determined the size of the basin of attraction of the origin of a complete network with three oscillators. This three-oscillator network is not only a complete network but also a ring network. Here, we will try to extend the ideas used in the previous section to ring networks of arbitrary size but with an odd number of oscillators. Ring networks are often encountered in practice, examples include electrical circuits and communication networks such as computer networks. A malfunction within such a network may cause severe problems. Thereby, it is of practical importance to gain insights into their global dynamics to be able to prevent such problems from happening. We do this by studying the size of the basin of attraction. This is often difficult due to nonlinearities in the dynamics as seen in the previous section. The main tool to perform such a study about the basin of attraction is Theorem 8. It turns out that the biggest obstacle is the unknown location of all equilibria in phase space. This wasn't a problem for the complete network of the previous section. However, for arbitrary networks it is even harder to find the best radial bound of the basin by a number solely depending on the number of oscillators in the ring network. The results presented in this section require many lengthy calculations for validating certain conditions of Theorem 8, but for the most part they follow the same ideas as presented above. Therefore we choose to move these computations to the appendix and solely address the main line of the argument as well as points in the argument where we deviate from the case of the complete network as presented in the previous section.

We are dealing with dynamics provided by the n -dimensional system 4.1. This system is invariant under an analogous translation τ_ϵ as the one in 4.4. The only difference is that instead of translating three angles we translate all n angles by the same amount $\epsilon > 0$. This property is related to an invariance into the $\mathbf{n} = \mathbf{1}_n$ direction in phase space, where $\mathbf{1}_n$ denotes a $n \times 1$ vector with on each entry a 1. In this way, we are capable to rotate system 4.1 by means of a rotation matrix. This rotation matrix is given in Appendix B. The resulting system only shows change in dynamics along the first $n - 1$ -dimensions, so we may neglect the n -th differential equation describing the change in the n -th dimension. The following equation provides the general form of the first $n - 2$ equations of the rotated system.

$$\begin{aligned} \frac{d\theta_i}{dt} = & -\frac{K}{\sqrt{i(i+1)}} \sin\left(\sum_{i=1}^{n-2} \frac{\theta_i}{\sqrt{i(i+1)}} + \sqrt{\frac{n}{n-1}}\theta_{n-1}\right) - \sqrt{\frac{i+1}{i}} K \sin\left(-\sqrt{\frac{i-1}{i}}\theta_{i-1} + \sqrt{\frac{i+1}{i}}\theta_i\right) \\ & + \sqrt{\frac{i}{i+1}} K \sin\left(-\sqrt{\frac{i}{i+1}}\theta_i + \sqrt{\frac{i+2}{i+1}}\theta_{i+1}\right) \end{aligned} \quad (4.21)$$

where $i \in \{1, \dots, n-2\}$ and $\theta_0 := 0$. The last $n - 1$ -th equation takes on the form

$$\frac{d\theta_{n-1}}{dt} = -\sqrt{\frac{n}{n-1}} K \sin\left(\sum_{i=1}^{n-2} \frac{\theta_i}{\sqrt{i(i+1)}} + \sqrt{\frac{n}{n-1}}\theta_{n-1}\right) - \sqrt{\frac{n}{n-1}} K \sin\left(-\sqrt{\frac{n-2}{n-1}}\theta_{n-2} + \sqrt{\frac{n}{n-1}}\theta_{n-1}\right). \quad (4.22)$$

If we take $n = 3$ we obtain system 4.12 for the complete network of three oscillators. In this special case each sine function in 4.21 and 4.22 contains at most two angles as argument. However, for larger n we see that the number of angles in the argument of the first sine term in both 4.21 and 4.22 grows with the number of oscillators. This makes it very difficult to determine the equilibria of this system in a straightforward manner. In particular, it becomes difficult to determine the size of the basin of attraction. Luckily, we are still able to provide expressions for the angles as well as an approximation for the size of the basin for ring network with an odd number of nodes.

Notice that the system given by the combination 4.21 and 4.22 has no translation invariance over an infinitesimal amount along the angles. This tells us that the equilibria do not lie on lines as is the case in the original system. In this way we prevent the usage of a free parameter to describe these lines. Moreover, the equilibria will be points instead of lines. As in the case of the complete network we note that the combination 4.21 and 4.22 gives a gradient system, i.e. $\dot{\boldsymbol{\theta}} = \nabla \hat{V}(\boldsymbol{\theta})$ where

$$\hat{V}(\boldsymbol{\theta}) = K \cos\left(\sum_{i=1}^{n-2} \frac{\theta_i}{\sqrt{i(i+1)}} + \sqrt{\frac{n}{n-1}}\theta_{n-1}\right) + K \cos(\sqrt{2}\theta_1) + K \sum_{i=1}^{n-2} \cos\left(-\sqrt{\frac{i}{i+1}}\theta_i + \sqrt{\frac{i+2}{i+1}}\theta_{i+1}\right). \quad (4.23)$$

For clarification we emphasize that $\boldsymbol{\theta}$ is a $(n-1) \times 1$ vector containing angles θ_i with $1 \leq i \leq n-1$. In similar fashion as before we have a natural candidate for the $L(\boldsymbol{\theta})$ function of Theorem 8, $L(\boldsymbol{\theta}) := -\hat{V}(\boldsymbol{\theta})$. In order to

verify whether the condition $\dot{L}(\boldsymbol{\theta}) \leq 0$ of Theorem 8 is satisfied we observe that 4.14 still holds. We may also calculate the total derivative or orbital derivative $\dot{L}(\boldsymbol{\theta})$, but this computation is rather long and can be found in Appendix B. From the calculation provided in appendix B it follows that the total derivative can be written as,

$$\begin{aligned} \dot{L}(\boldsymbol{\theta}) = & -K^2 \left[\sin(\sqrt{2}\theta_1) + \sin\left(\sum_{i=1}^{n-2} \frac{\theta_i}{\sqrt{i(i+1)}} + \sqrt{\frac{n}{n-1}}\theta_{n-1}\right) \right]^2 \\ & - K^2 \sum_{i=1}^{n-2} \left[\sin\left(-\sqrt{\frac{i}{i+1}}\theta_i + \sqrt{\frac{i+2}{i+1}}\theta_{i+1}\right) - \sin\left(-\sqrt{\frac{i-1}{i}}\theta_{i-1} + \sqrt{\frac{i+1}{i}}\theta_i\right) \right]^2 \\ & - K^2 \left[\sin\left(-\sqrt{\frac{n-2}{n-1}}\theta_{n-2} + \sqrt{\frac{n}{n-1}}\theta_{n-1}\right) + \sin\left(\sum_{i=1}^{n-2} \frac{\theta_i}{\sqrt{i(i+1)}} + \sqrt{\frac{n}{n-1}}\theta_{n-1}\right) \right]^2 \end{aligned} \quad (4.24)$$

Due to the sum of squares we have indeed $\dot{L}(\boldsymbol{\theta}) \leq 0$. However, the question remains when we have equality $\dot{L}(\boldsymbol{\theta}) = 0$. This boils down to the calculation of all equilibria of the system given by 4.21-4.22. We won't calculate all equilibria, but we try to determine the equilibria lying closest to the origin. To this end, we observe that for the complete network we have two types of equilibria excluding their translations. We have the equilibria provided by 4.19 which are the blue colored points in figure 4.7 and the equilibria provided by 4.20 which are the magenta colored points in figure 4.7. The blue points make each sine term in 4.15 vanish while this does not happen for the magenta colored points. Although we are not able to prove it, we do expect that this observation generalized to ring networks of arbitrary size. From here on, we assume that $n > 3$ and n odd. It is easily seen from the recurrence in the second line of 4.24 that a root of 4.24 or equivalently an equilibrium point of 4.21-4.22 satisfies the following equalities.

$$\begin{aligned} -\sin\left(\sum_{i=1}^{n-2} \frac{\theta_i}{\sqrt{i(i+1)}} + \sqrt{\frac{n}{n-1}}\theta_{n-1}\right) &= \sin(\sqrt{2}\theta_1) = \sin\left(-\frac{\theta_1}{\sqrt{2}} + \sqrt{\frac{3}{2}}\theta_2\right) = \sin\left(-\sqrt{\frac{2}{3}}\theta_2 + \sqrt{\frac{4}{3}}\theta_3\right) = \dots \\ &= \sin\left(-\sqrt{\frac{i-1}{i}}\theta_{i-1} + \sqrt{\frac{i+1}{i}}\theta_i\right) = \dots \\ &= \sin\left(-\sqrt{\frac{n-2}{n-1}}\theta_{n-2} + \sqrt{\frac{n}{n-1}}\theta_{n-1}\right) \end{aligned} \quad (4.25)$$

Notice, that for every $n \in \mathbb{N}_{\geq 3}$ there are roots that make the sine term with argument $\sqrt{2}\theta_1$ vanish. These type of roots were also present for $n = 3$. The other roots occur when not all sine terms vanish and these will depend on the dimension of the problem at hand. Unfortunately we are not able to compute all the zeros explicitly. This would be a daunting task. This can simply be observed by looking at all the equalities. Notice that each expression in 4.25 that comes after the sine term with only θ_1 as argument contains a new angle which introduces a new degree of freedom. Therefore we need at least these $n - 2$ equalities in the determination of the equilibria. Moreover, we need a restriction on all of the angles which can only be provided by the first sine term. This first sine term contains $n - 1$ angles as argument, so in order to simplify one could use trigonometric identities that will necessarily introduce cosine terms. But it turns out that for these cosine terms we do not have enough information that could enable us to reduce this problem. Luckily, we are still able to provide expressions for the equilibria which gives us information on their location. To this end, we first make the following observation,

$$\begin{aligned} \sum_{i=1}^{n-1} -\sqrt{\frac{i-1}{i}}\theta_{i-1} + \sqrt{\frac{i+1}{i}}\theta_i &= \sum_{i=2}^{n-1} -\sqrt{\frac{i-1}{i}}\theta_{i-1} + \sum_{i=1}^{n-1} \sqrt{\frac{i+1}{i}}\theta_i \\ &= \sum_{i=1}^{n-2} -\sqrt{\frac{i}{i+1}}\theta_i + \sum_{i=1}^{n-2} \sqrt{\frac{i+1}{i}}\theta_i + \sqrt{\frac{n}{n-1}}\theta_{n-1} \\ &= \sum_{i=1}^{n-2} \frac{\theta_i}{\sqrt{i(i+1)}} + \sqrt{\frac{n}{n-1}}\theta_{n-1} \end{aligned} \quad (4.26)$$

This shows that the argument of the first sine function in 4.25 is equal to the sum of the arguments of all other sine functions of 4.25. For small n it is possible to use this fact to find all equilibria. However, this remains problematic for large networks.

At this point, we introduce coupling terms $k_i \in \mathbb{Z}$. These coupling terms act as a coupling between the argument of the sine function with only θ_1 as argument and all other sine functions that have a two angle argument, i.e.

$$(-1)^{k_i} \sqrt{2}\theta_1 + k_i\pi = -\sqrt{\frac{i-1}{i}}\theta_{i-1} + \sqrt{\frac{i+1}{i}}\theta_i. \quad (4.27)$$

We define $k_1 := 0$ such that this expression holds for all $1 \leq i \leq n-1$. Note, that we only translated the arguments of each sine function to the interval stretching from $-\pi/2$ up to $\pi/2$ where the sine function has a well-defined inverse. This translation is captured by the coupling terms $k_i \in \mathbb{Z}$. Hence, the equality in 4.27 defines planes in phase space for each $k_i \in \mathbb{Z}$. By using these planes we are able to define each angle in terms of the first angle,

$$\begin{aligned} \theta_i &= \sqrt{\frac{1}{i(i+1)}} \sum_{j=1}^i -\sqrt{j(j-1)}\theta_{j-1} + \sqrt{j(j+1)}\theta_j \\ &= \sqrt{\frac{1}{i(i+1)}} \sum_{j=1}^i j \left[-\sqrt{\frac{j-1}{j}}\theta_{j-1} + \sqrt{\frac{j+1}{j}}\theta_j \right] \\ &= \sqrt{\frac{1}{i(i+1)}} \sum_{j=1}^i j \left[(-1)^{k_j} \sqrt{2}\theta_1 + k_j\pi \right]. \end{aligned} \quad (4.28)$$

In this derivation we used that the first equality holds due to the fact that the finite sum has the telescoping property and that the third equality holds by means of 4.27. It is likely that the triangular sum appearing in the former expression cannot be simplified due to its dependence on the coupling terms k_j . On the other hand, we are still able to find an expression for the first angle. For this, we use the first equality in 4.25 and introduce an additional coupling term $k_n \in \mathbb{Z}$ to couple the arguments in the same way as we did in 4.27.

$$-(-1)^{k_n} \sqrt{2}\theta_1 - k_n\pi = \sum_{i=1}^{n-2} \frac{\theta_i}{\sqrt{i(i+1)}} + \sqrt{\frac{n}{n-1}}\theta_{n-1}. \quad (4.29)$$

In combination with 4.27 and 4.26 this will result in,

$$\begin{aligned} \sum_{i=1}^{n-1} \left[(-1)^{k_i} \sqrt{2}\theta_1 + k_i\pi \right] &= \sum_{i=1}^{n-1} -\sqrt{\frac{i-1}{i}}\theta_{i-1} + \sqrt{\frac{i+1}{i}}\theta_i \\ &= \sum_{i=1}^{n-2} \frac{\theta_i}{\sqrt{i(i+1)}} + \sqrt{\frac{n}{n-1}}\theta_{n-1} \\ &= -(-1)^{k_n} \sqrt{2}\theta_1 - k_n\pi. \end{aligned} \quad (4.30)$$

Consequently,

$$\theta_1 = \frac{-\sum_{i=1}^n k_i\pi}{\sqrt{2}\sum_{i=1}^n (-1)^{k_i}}. \quad (4.31)$$

when the denominator is unequal to zero. Notice that the denominator can only be equal to zero whenever the number of odd coupling terms is equal to the number of even coupling terms. Thus, for odd n it follows that 4.31 gives always the right formula for the first angle. On the other hand, if n is even then the number of even coupling terms may be equal to the number of odd coupling terms. Hence the denominator could end up being equal to zero. For this reason we assumed n to be an odd number.

Now that we have an expression for all angles, see 4.28 and 4.31. We will study the equilibria by calculating Euclidean distances between the origin and points defined by the formulas given above. In order to perform such a calculation efficiently we observe that some equilibria can be found easily from the equalities in 4.25. For instance, if we take the first $n-2$ angles equal to zero and the last angle equal to $\sqrt{(n-1)/n}\pi$ then this defines an equilibrium point. There are more equilibria lying $\sqrt{(n-1)/n}\pi$ away from the origin. Another example is given by taking $\theta_i = \pi/\sqrt{i(i+1)}$ for all $1 \leq i \leq n-1$. Since we were not able to find any point, except for the origin, lying within a radius of $\sqrt{(n-1)/n}\pi$ we claim that a ball with this radius provides an approximation of the basin of attraction for the origin. To test this claim, we use the expressions derived for

the angles along with a restriction on the coupling terms. This restriction follows from the planes defined by 4.27. For each coupling term we are able to calculate the shortest distance between the plane and the origin. To this end, we recall that the point-to-plane distance d for a point p and a plane $c'x - e = 0$ is given by the formula [17] [6],

$$d := \frac{|c'p - e|}{\|c\|_2} \quad (4.32)$$

This means that the distance between the origin and a plane defined by 4.27 is given by,

$$d = \frac{|k_i|\pi}{2} \quad (4.33)$$

Therefore we may take $k_i \in \{-1, 0, 1\}$ for $1 \leq i \leq n-1$ as any other choice would mean that the shortest origin-plane distance would exceed the radius of the ball in our claim. Similarly, it follows that for the higher dimensional plane of 4.29 holds $k_n \in \{-2, -1, 0, 1, 2\}$. These results will be used in the next section to validate our claim about the size of the basin for many ring networks.

At this point we have a reasonable restriction on the coupling terms. However, it seems that these bounds on the coupling terms are not strict enough to find the equilibrium closest to the origin. The expressions for the angles and restriction on the coupling terms even suggest that there are many possible different equilibria. To test if this is indeed the case we exploit the fact that the equilibria must satisfy formula 4.25. For convenience we abbreviate the arguments of the sine functions that appear in this formula. We let,

$$x_i := -\sqrt{\frac{i-1}{i}}\theta_{i-1} + \sqrt{\frac{i+1}{i}}\theta_i, \quad \text{where } 1 \leq i \leq n-1. \quad (4.34)$$

By the result presented in formula 4.26 we may write 4.25 as follows,

$$-\sin\left(\sum_{i=1}^{n-1} x_i\right) = \sin(x_1) = \dots = \sin(x_i) = \dots = \sin(x_n). \quad (4.35)$$

As done earlier, we are able to couple the arguments of each of these sine functions by introducing coupling terms and express x_i for $1 \leq i \leq n-1$ in terms of x_1 , see e.g. 4.27. By this process we can replace each x_i in the argument of the first sine term in 4.35 by an expression in terms of x_1 . The number of possibilities in which this can be achieved depends on the size of the network and the parity of the coupling terms. These possibilities are easily determined by making a tree as the one depicted below.

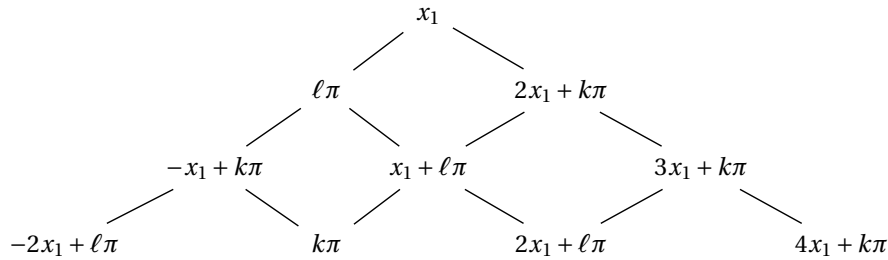


Fig. 4.9: Tree for the sine argument replacement.

where $k \in 2\mathbb{Z}$ and $\ell \in 1 + 2\mathbb{Z}$. The j -th row corresponds to the case $n = j + 1$, e.g. the second row corresponds to $n = 3$. The tree is constructed by taking the argument of the first sine in 4.35, i.e. $\sum_{i=1}^{n-1} x_i$, and replacing each x_i with $2 \leq i \leq n-1$ by an expression of the form $(-1)^y x_1 + \gamma\pi$ where $\gamma \in \{k, \ell\}$. Each even row in this tree corresponds to an odd number for n . Hence, we may replace the first equality in 4.35 by,

$$-\sin([n - (4m + 1)]x_1) = \sin(x_1) \quad \text{or} \quad \sin([n - (4m + 3)]x_1) = \sin(x_1) \quad (4.36)$$

where $m \in \{0, 1, 2, \dots, ((n-1)/2) - 1\}$ and n odd. Since $x_1 := \sqrt{2}\theta_1$ we are able to find all possibilities for the first angle by using the former formulas. Since there are many possibilities to choose m it is already clear that there are many possibilities for the first angle as well. This observation will be made explicit in the next chapter.

5

Results

In this chapter we discuss our findings with respect to the phenomena of cluster synchronization in an eight node network as well as global stability in ring networks with an odd number of oscillators. These results follow directly by employing the techniques as discussed in previous chapters. Since these topics address different properties of a dynamical system, we make a distinction between the results obtained for cluster synchronization and those obtained for global stability.

We will start our discussion with the topic of cluster synchronization. Since the method we used to analyse this phenomenon doesn't allow us to study arbitrary networks we were forced to pick a certain topological structure. We chose to consider a network with the shape of a regular octagon with dynamics of the second-order Kuramoto model. This choice was made due to fact that it is a network with a decent number of oscillators for which we could still perform a large part of our analysis by hand. Moreover, the method we use requires the knowledge of configurations of angles and parameters that cause a state of cluster synchrony. Since we could not find these configurations in the literature we decided to write a program that enables us to find those configurations for an eight-node network. Unfortunately, this process depends on inspection and remains difficult to measure for large networks. Hence, we emphasize that the results presented in the coming section are only valid for this particular eight-node ring network with certain configurations.

After the cluster synchronization section we discuss results of global stability in a ring network with an odd number of oscillators that follow the Kuramoto dynamics. In particular, we present results that revolve around the size of the basin of attraction of an attractor in phase space. The attractor we chose for our analysis is the origin. This choice is made purely for convenience purposes. Due to the translation invariance of the sine function within the dynamical system, we may translate other attractors to the origin as well. Therefore, our analysis is not restricted to only one attractor.

5.1. Cluster synchronization in a ring network.

We studied methods based on network symmetries that allow us to determine the stability of synchronous network clusters. In Chapter 3 we devoted much of our attention to a network with dynamics provided by the Kuramoto model on the topological structure of a regular octagon. These dynamics were linearized around a state of cluster synchrony for each of the top row cluster configurations provided by table 3.1 with the exception of the blue-highlighted configurations. After this linearization we applied a unitary transformation in order to decouple the dynamical system at least partially. A similar computation was done for the cluster configurations presented in second down to the fourth row of table 3.1. However for these three rows of cluster configurations we were able to merge clusters in the unitary transformation corresponding to the top row cluster configurations. In this way we could shorten the computation for obtaining unitary transformations corresponding to particular cluster configurations that are able to decouple the linearized system. The resulting decoupled blocks, except for the upper left block, determine whether the system remains in a state of cluster synchrony or not. We will devote more of our attention to these transverse blocks in this section and analyze the stability of each cluster configuration presented in table 3.1 except for those highlighted in blue.

The linearization of the second order system as provided by 3.11 contains unknown parameters D , K and α . The parameters D and K are adjustable, so it makes sense to derive a stability condition that depends on these parameters. In order to achieve such a stability condition one needs the α matrix that depends on the cluster configuration. Besides we also need a yet unknown synchronous state \mathbf{s}_1 around which the original system was linearized. This state is characterized by means of a set of initial angles and angle velocities. Notice that not all synchronous states are valid, since some states are not compatible with the cluster configuration at hand. Hence, each synchronous state depends on the cluster configuration we intend to use in our analysis. Since a certain cluster configuration does not correspond to a unique synchronous state we are forced to choose a particular allowed state. This state must be a point on a trajectory that is part of the synchronization manifold corresponding to a certain cluster configuration. However there is, at least to our knowledge, no method available that is capable of detecting cluster synchrony. Therefore we choose to find at least some of the cluster synchronous states by inspection. To this end, we have written a Java code. In this program we solved the second order system by means of the RK4 method for a particular set of parameters. The solution is a vector of angles where each angle θ_i is graphically represented by a line that makes an angle θ_i with respect to the positive horizontal axis. Since the RK4 method solves the system of differential equations over time, we were able to let the program automatically update these angles and therefore also the lines. If there are lines moving in the same pace for at least a relative short period of time we treat the corresponding oscillators as being synchronized. In this way, we are able to detect trajectories corresponding to certain cluster configurations of table 3.1. For the cluster synchronous state \mathbf{s}_1 we just choose a certain point on such a trajectory. The easiest way to choose such a point is by taking the initial conditions at which the program starts to solve the system and this is exactly what we have done. The table below contains the chosen points and parameters that lead to a trajectory corresponding to the cluster configuration as indicated in the first column. The format is such that the i -th entry in the cartesian product corresponds to the i -th angle or frequency in the state of synchrony. The synchronous state vector \mathbf{s}_1 has sixteen entries and we use powers to denote repeated terms, so for instance 0^8 denotes eight zeros in the cartesian product.

Group	State \mathbf{s}_1	Frequency ω	Coupling K	Damping D
\mathbb{Z}_2^4	$(0^8, 0.1^8)$	$(1, 1.5, 0.5, 0, 1, 1.5, 0.5, 0)$	(0.1^8)	-1
$\mathbb{Z}_4 \times \mathbb{Z}_2^2$	$(0^8, 0.1^8)$	$(1, 0, 0.5, 0, 1, 0, 0.5, 0)$	(0.1^8)	-1
\mathbb{Z}_4^2	$(0^8, 0.1^8)$	$(1, 0, 1, 0, 1, 0, 1, 0)$	(0.1^8)	-1
\mathbb{Z}_8	$(0^8, 0.1^8)$	(1^8)	(0.1^8)	-1
$\mathbb{Z}_2^3 \times \langle E \rangle^2$	$(0^8, 0.1^8)$	$(0, 1, 1.45, 1, 0, 0.9, 1.55, 0.9)$	(0.1^8)	-1

Table 5.1: Characterization of trajectories on a synchronization manifold.

This table shows that we are able to take the initial state such that the eight angles are equal to zero and their velocities equal to 0.1 for each cluster configuration. In order to obtain a particular cluster configuration we only have to change the intrinsic frequencies of the oscillators. These frequencies must be compatible with the group structure on the underlying network. This is mostly achieved by equally distributing oscillators that have the same intrinsic frequency. Moreover, each trajectory starts from a cluster configuration that has a weak coupling of 0.1 and a significant damping given by minus one.

The synchronous states in the second column and the chosen parameter as in the third up to the last column of table 5.1 lead to network configurations as those depicted in figures 3.8 up to 3.11 and 3.6. In order to perform a stability analysis with respect to the different cluster configurations, we block diagonalize the system by means of an appropriate unitary transformation to get system 3.10. The figures below show an approximate solution of system 3.10 for all eight angle deviations and its derivatives. We stress that not all of these angle deviations cause the system to leave a state of cluster synchrony. The angle deviations that do cause the system to leave a synchronous state will be discussed later on. For the moment, we take a closer look at the matrix $-\alpha' Df(\mathbf{s})\alpha$ in the lower-left block of the system. It has the following eight eigenvalues,

$$\lambda_1 = 0, \quad \lambda_2 = -4, \quad \lambda_3 = -2(\times 2), \quad \lambda_4 = -0.5858(\times 2), \quad \lambda_5 = -3.4142(\times 2).$$

The numbers in the curly brackets denote the corresponding algebraic multiplicities of the eigenvalues. We observe that there is a zero eigenvalue present. This is always the case due to the zero row-sum property of the lower-left block in the system. Due to the diagonal structure of the system it follows that repeated eigenvalues lead to the same solution. Hence we will distinguish between the approximate solutions of the angle

deviations by means of the corresponding eigenvalues. The angle deviations and their velocities are indicated by corresponding eigenvalues with different colors as shown in the legends of figures 5.1 and 5.2.

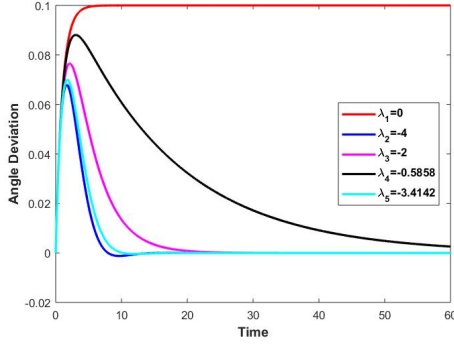


Fig. 5.1: Angle deviations approximated by RK4.

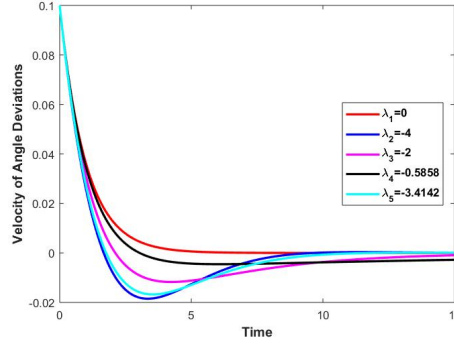


Fig. 5.2: Velocity of deviations approximated by RK4.

These figures show that the angle deviations and velocities converge to zero except for the solution that corresponds to eigenvalue λ_1 which converges to one. Since these two figures correspond to solutions of the linearized system 3.10, we emphasize that the intrinsic frequencies do not contribute to these solutions. Hence, these figures show that the clusters are completely determined by the chosen intrinsic frequencies.

Let us consider system 3.10. Recall that the upper-left block of $-\alpha' Df(s)\alpha$ corresponds to deviations in the synchronization manifold, so we are only interested in the lower-right blocks that correspond to deviations in the transverse directions. These transverse blocks have eigenvalues that form a subset of those mentioned before and they correspond to angle deviations that may cause the system to leave a state of synchrony. Hence, these are the eigenvalues that are of importance here. We summarize the eigenvalues of the transverse blocks for each cluster configuration in the table below.

Groups	Eigenvalues
\mathbb{Z}_2^4	$\lambda_4 (\times 2), \lambda_5 (\times 2)$
$\mathbb{Z}_4 \times \mathbb{Z}_2^2$	$\lambda_3, \lambda_4 (\times 2), \lambda_5 (\times 2)$
\mathbb{Z}_4^2	$\lambda_3 (\times 2), \lambda_4 (\times 2), \lambda_5 (\times 2)$
\mathbb{Z}_8	$\lambda_1, \lambda_2, \lambda_3 (\times 2), \lambda_4 (\times 2), \lambda_5 (\times 2)$
$\mathbb{Z}_2^3 \times \langle E \rangle^2$	$\lambda_3, \lambda_4, \lambda_5$

Table 5.2: Eigenvalues of transverse blocks

Observe that the number of eigenvalues increases when the direct product contains less direct factors. The network configurations with respect to the groups $\mathbb{Z}_4 \times \mathbb{Z}_2^4$ down to \mathbb{Z}_8 were obtained by merging clusters. Hence, this table shows that the number of transverse blocks in the block diagonalization of $-\alpha' Df(s)\alpha$ increases by the process of merging clusters. This means, that the synchronization manifold decreases in dimension while the transverse manifold increases in dimension. For \mathbb{Z}_8 the block diagonalization is the same as an eigendecomposition and we obtain all eigenvalues in this case. Moreover, the eigenvalue λ_1 that corresponds to the red-colored graph in figures 5.1 and 5.2 is only observed for the group \mathbb{Z}_8 .

After diagonalization of the transverse blocks in $-\alpha' Df(s)\alpha$ of system 3.10 we end up with a partially decoupled system. We are only interested in the differential equations that correspond to the diagonalized transverse blocks. These differential equations take on the following form,

$$\begin{bmatrix} \dot{\delta}_{1,i} \\ \dot{\delta}_{2,i} \end{bmatrix} = \begin{bmatrix} 0 & 1 \\ \lambda_i K & D \end{bmatrix} \begin{bmatrix} \delta_{1,i} \\ \delta_{2,i} \end{bmatrix} \quad (5.1)$$

where λ_i denotes an eigenvalue of a transverse block, $\delta_{1,i}$ denotes the i -th component of δ_1 and similarly $\delta_{2,i}$ denotes the i -th component of δ_2 . Notice that the range of the index i depends on the transverse blocks of system 3.10, i.e. it depends on the cluster configuration. It is easily seen that the eigenvalues of the matrix in the former system are given by,

$$\gamma_i = \frac{1}{2} \left(D \pm \sqrt{D^2 + 4K\lambda_i} \right). \quad (5.2)$$

The eigenvalues of the transverse blocks λ_i depend on the cluster configuration. Hence, the previous table shows exactly all possibilities λ_i for each cluster configuration. In order to perform a linear stability analysis we need to determine when the real part of γ_i is negative. This depends on the parameters D and K , but also on the eigenvalues of the transverse blocks λ_i . The case of λ_1 is easy as it simplifies the expression such that γ_1 has a negative real part if and only if $D < 0$. For γ_i where $1 < i < 5$ it is harder to determine the outcome. Due to the many dependencies in the expression for γ_i we divide this problem in subproblems where we restrict the range of the parameters D and K . From here on we may assume $\lambda_i < 0$ since eigenvalues of the transverse blocks in $-aDf(s)\alpha$ are either negative or equal to zero.

1. Assume $D > 0$ and $K \leq 0$. In this case we have $D^2 + 4K\lambda_i > 0$ and therefore $D + \sqrt{D^2 + 4K\lambda_i} > 0$. Hence γ_i does not have a negative real part in this region.
2. Assume $D > 0$ and $K > 0$. If $D^2 + 4\lambda_i K > 0$ then $D + \sqrt{D^2 + 4K\lambda_i} > 0$, so this does not lead to γ_i having a negative real part. On the other hand, if $D^2 + 4\lambda_i K < 0$ then γ_i has a real part given by $\frac{1}{2}D$. Since $D > 0$, it follows that its real part is positive. We conclude that γ_i has no negative real part in the region where $D > 0$ and $K > 0$.
3. Assume $D < 0$ and $K \leq 0$. In this case we have $D^2 + 4\lambda_i K > 0$. Suppose $K < 0$ holds, then it is clearly true that $D - \sqrt{D^2 + 4\lambda_i K} < 0$, so at least one of the eigenvalues for γ_i is negative. For the other possibility we observe that $D + \sqrt{D^2 + 4K\lambda_i} < 0$ if and only if $D < -\sqrt{D^2 + 4\lambda_i K}$. This last inequality holds by monotonicity of the square root and the fact that $\lambda_i K > 0$. Finally, if $K = 0$ then γ_i simplifies to $\frac{1}{2}(D \pm D)$, so one of these two eigenvalues is positive. We conclude that the region specified by $D < 0$ and $K < 0$ yields stability.
4. Assume $D < 0$ and $K > 0$. If $D^2 + 4K\lambda_i > 0$, then $D - \sqrt{D^2 + 4K\lambda_i} < 0$, so we have at least one negative eigenvalue. Now, $D + \sqrt{D^2 + 4K\lambda_i} < 0$ if and only if $D < -\sqrt{D^2 + 4K\lambda_i}$. This last inequality cannot hold since $4K\lambda_i < 0$. On the other hand if we have $D^2 + 4K\lambda_i < 0$ it follows that the real part of γ_i is given by $\frac{1}{2}D$ which is negative. We conclude that we have stability for the region specified by $D < 0$, $K > 0$ and $D^2 + 4K\lambda_i < 0$.
5. Assume $D = 0$. If $K = 0$, then $\gamma_i = 0$. If $K > 0$ then γ_i is purely imaginary, so it has a zero real part. If $K < 0$ then we have at least one positive eigenvalue. We conclude that the linearized system is stable for $D = 0$ and $K \geq 0$.

The eigenvalues γ_i depend on the eigenvalues of the transverse blocks λ_i . In item four we derived that a part of the stability region depends on λ_i . Since the presence of a λ_i differ for each cluster configuration, it could be the case that the stability region either shrinks or grows. It turns out that the largest stability region is achieved for λ_4 . This value appears in each cluster configuration as an eigenvalue of a transverse block. Therefore the size of the stability region remains unchanged over the different cluster configurations. The size of this stability region is depicted in the figure below.

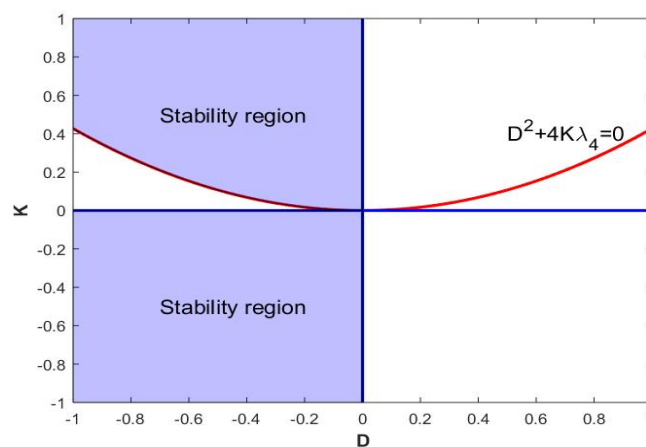


Fig. 5.3: The largest stability region for each cluster configuration.

5.2. Size of the Basin of Attraction.

In Chapter 4 we discussed the size of the basin of attraction for ring networks with an arbitrary odd number of oscillators. We claimed that the largest ball we could fit in the basin of attraction with respect to the origin would be a ball of radius $r := ((n-1)/n)\pi$. Although we were not able to provide a decisive conclusion on whether this is true or not, we were in fact able to provide expressions for the angles that may lie within this ball of radius r centered around the origin. For the sake of completeness we recall these expressions,

$$\theta_i = \frac{1}{\sqrt{i(i+1)}} \sum_{j=1}^i j \left[(-1)^{k_j} \sqrt{2}\theta_1 + k_j \pi \right] \quad \text{with } \theta_1 = -\frac{\sum_{i=1}^n k_i \pi}{\sqrt{2} \sum_{i=1}^n (-1)^{k_i}} \quad \text{and } k_i \in \{-1, 0, 1\}, \quad (5.3)$$

except for $k_1 := 0$ and $k_n \in \{-2, -1, 0, 1, 2\}$. We could neglect the restriction on the coupling terms, but then we have to deal with all equilibria. Since we want to know if there are equilibria within the ball of radius r we only have to take coupling terms either equal to ± 1 or equal to zero with the exception of $k_1 := 0$ and $k_n \in \{-2, -1, 0, 1, 2\}$. To test if our claim is true, we consider several ring networks of different sizes. We have written a code that determines the Euclidean distances for the points defined by 5.3 with the size of the ring network as parameter. Due to the many possibilities for the coupling terms, we were only able to consider a few networks.

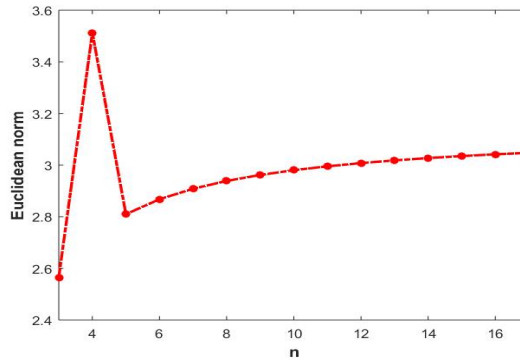


Fig. 5.4: Distance between origin and closest equilibrium.

In order to obtain the figure presented above we have written a program in Java that determines for each possible arrangement of the k_i 's an Euclidean distance between the point determined by such an arrangement and the origin. Moreover, this program determines from all these distances the minimum Euclidean distance. This minimum distance is depicted in the figure above by means of red circles. At the same time, the program also determines the arrangement of k_i 's corresponding to such a minimum distance. Although this arrangement is not unique, it does enable us to provide an explicit expression for the minimum Euclidean distance between the nearest equilibrium with respect to the origin. It turns out that for networks that have an odd number of oscillators, the minimum Euclidean distance is what we expected, namely $\sqrt{(n-1)/n}\pi$. For a network with four oscillators, i.e. $n = 4$, it is $\frac{1}{2}\sqrt{5}\pi$. Since the case $n = 4$ defines a network with an even number of oscillators it could be the case that there are angles that do not satisfy the relation for the first angle as given by 5.3. This is due to the division by zero possibility in the expression for the first angle. However, from the relations in 4.26 we observe that we could assign zeros to the first two angles and to the third angle a contribution of $\sqrt{3/4}\pi$. This assignment leads to an equilibrium that satisfies our claim. Hence, we still expect the claim to be true for networks with an even number of oscillators.

The implementation of the angles by means of the formulas above plays an important role in the range of n on the horizontal axis of the figure. We have written a Java program that explores two different approaches. In one approach we determined all possible arrangements for the k_i 's recursively and in another approach we did this iteratively. Although recursive methods are often less efficient, it did pay out in this case. Our iterative approach takes much more computation time in comparison to the recursive approach. Hence, the results depicted in the figure are obtained by means of a recursive approach.

Since the problem of determining the minimal distance between an attractor and a neighbouring node involves many possibilities for the coupling numbers k_i , we decided to look at how the number of different equilibria increases when the number of oscillators in the network increases. This is difficult to verify, but we can find the number of different possibilities for the first angle within an equilibrium point. To this end, we recall the formulas in 4.36,

$$-\sin\left([n - (4m + 1)]\sqrt{2}\theta_1\right) = \sin\left(\sqrt{2}\theta_1\right) \quad \text{and} \quad \sin\left([n - (4m + 3)]\sqrt{2}\theta_1\right) = \sin\left(\sqrt{2}\theta_1\right). \quad (5.4)$$

By means of simple trigonometry one finds,

$$\sin\left(\frac{1}{2}[n - (4m + 1) + 1]\sqrt{2}\theta_1\right) \cos\left(\frac{1}{2}[n - (4m + 1) - 1]\sqrt{2}\theta_1\right) = 0 \quad (5.5)$$

and

$$\sin\left(\frac{1}{2}[n - (4m + 3) - 1]\sqrt{2}\theta_1\right) \cos\left(\frac{1}{2}[n - (4m + 3) + 1]\sqrt{2}\theta_1\right) = 0. \quad (5.6)$$

Thus,

$$\theta_1 = \frac{2\gamma\pi}{\sqrt{2}(n - 4m)} \quad \text{and} \quad \theta_1 = \frac{(2\gamma + 1)\pi}{\sqrt{2}(n - (4m + 2))} \quad (5.7)$$

where $m \in \{0, 1, 2, \dots, \frac{n-1}{2} + 1\}$. In order to get a bound on $\gamma \in \mathbb{Z}$, we observe that the period of the functions in 5.4 is $\sqrt{2}\pi$. Thus each fraction in 5.7 should be between $-\sqrt{2}\pi$ and $\sqrt{2}\pi$. Also, one has to be cautious since it could be the case that for certain γ and m one could simplify these fractions. Therefore, we filtered these possibilities out. The resulting number of different possibilities for the first angle is displayed below.

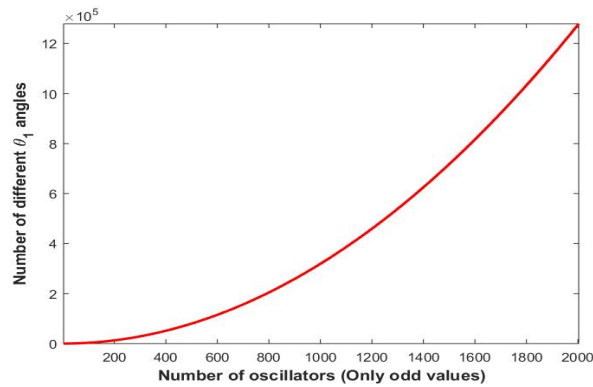


Fig. 5.5: Number of different first angles.

The result as depicted in figure 5.5 is only valid for networks with an odd number of oscillators. It provides an indication for the number of equilibria. Note that for each first angle there is at least one corresponding equilibrium point. Hence, the result in the figure above provides a lower bound for the number of different equilibrium points. Moreover, it gives us an indication of how difficult it is to find all different equilibria due to the rapid growth of the number of equilibria. It can be seen from this figure that for a network of say 2001 oscillators one has already more than a million different equilibria. Hence, it would be a daunting maybe even impossible task to find formulas for all equilibria that could help us in the determination of the shortest distance between the origin and the other equilibria. However, we think that the shortest distance is attained when each of the sine functions in 4.25 vanish for those equilibria that lie on the boundary of the basin of attraction. If it were possible to show that this statement is true then it would be easier to find the size of the basin of attraction.

6

Conclusion

In this thesis we discussed the phenomena of cluster synchronization and global stability in Kuramoto networks. A relatively large part of this report is inspired by recent studies in which the phenomenon of cluster synchronization is addressed by means of techniques from representation theory. In the second chapter we discussed the algorithm that lies at the heart of these studies. This algorithm allowed us to study cluster synchronization on the basis of both the topology of the network and its dynamics. In the third chapter we discussed the concept of cluster synchronization and introduced a ring network. Although the ideas presented in this chapter are applicable to a wide range of networks we decided to consider only a network with eight oscillators which follow the Kuramoto dynamics. For this eight-node ring network we addressed the problem of finding all network configurations. The main approach is taken from [22] and [20]. In order to tackle this problem we focussed upon the subgroups that follow from the largest group that presents itself in the network topology. By combining these subgroups as direct factors in direct products we were able to find all possible cluster configurations. Some of these cluster configurations were not compatible with the dynamics and therefore not allowed as network configuration. The remaining allowed cluster configurations could lead to many different network configurations, so we were forced to make a choice. We decided to consider only those networks in which oscillators with similar dynamics were distributed evenly among the network. The drawback in this approach is that we were not able to analyse all possible network configurations.

In order to analyse the different network configurations, we linearized the system around a state of cluster synchrony. This state depends on the chosen network configuration. Moreover, we could distinguish between these different states by means of each oscillators' intrinsic frequency. Due to this linearization we were able to apply the algorithm of the second chapter and block diagonalize the entire system accordingly. Afterwards, we made a distinction between deviations that occur within a synchronization manifold and deviations in transverse directions. Since only the deviations in transverse directions could take the system out of synchrony we focussed ourselves on the corresponding transverse blocks in the system. By the process of merging clusters we could easily find all transverse blocks for each network configuration. A linear stability analysis based on these transverse blocks allowed us to determine the stability of each synchronous state on the basis of their eigenvalues. It turns out that the largest negative eigenvalue determines the range in which one could deviate the coupling strength and damping parameter. Since this largest negative eigenvalue is present for each of the five network configurations, we conclude that the stability for each state of cluster synchrony depends in the same way on the coupling strength and damping parameter. However, we only considered one point on a specific trajectory in our linearization process. If we chose another point it could be the case that the stability region as depicted in figure 5.3 changes in size. The main point here is that the usage of representation theory simplifies the dimension of the problem. The block diagonalization of the linearized system by means of the algorithm tells us exactly which blocks are responsible for taking the system out of synchrony. Hence, we end up with less equations that we need to analyze in a linear stability analysis. For the eight-node network it turns out that this strategy is more relevant if there are many direct factors present in the network configuration. To justify this statement we recall table 5.2. This table shows that there are less eigenvalues of transverse blocks when there are many direct factors in the direct product group. Hence, we only need to consider a few equations for these groups and this simplifies the stability problem significantly.

In order to obtain an approximation for the size of the basin of attraction of an attractor we tried to fit a ball in this basin. Since this basin is bounded by the Euclidean distance between the attractor and its nearest equilibrium, we tried to estimate this distance. The ball with a radius defined by this minimum distance would therefore provide an approximation of the size of the basin. In our approach we rotated the entire system of differential equations. This rotation preserves distances, so the size of the basin remains unaffected by this operation. This process leads to a system that has equilibria that are easier to obtain for a relatively small number of oscillators. This is mostly due to the fact that the rotated system has no line invariance so each equilibrium is a point instead of a line. Moreover, the rotated system provides a condition on the equilibria, see 4.26. However, for large systems it remains a difficult task to obtain the distance between the attractor and its nearest equilibrium point. Luckily, we were able to determine the size of the basin of attraction for many ring networks. Since all minimum distances we found satisfy $\sqrt{(n-1)/n\pi}$, we think that this is the minimum distance for ring networks of arbitrary size. Hence, we conjecture that the largest ball that could be fitted inside the basin of attraction of the origin has radius $\sqrt{(n-1)/n\pi}$.

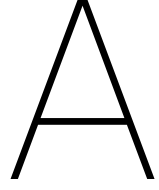
6.1. Recommendation

The algorithm for block diagonalizing the coupling matrix in a system of differential equations uses information about the topology of the network and its dynamics. This is exactly why this approach is attractive in solving stability issues that revolve around synchronous clusters. The main drawback of this approach is that the unitary transformation that should bring the coupling matrix in block diagonal form could be difficult to obtain for large networks. In particular the explicit form of the irreducible representations are generally difficult to find. With this in mind I recommend to use the easiest group that still captures the topology of the entire network. This is exactly what we did with all of the groups in table 3.1. Moreover, the usage of the algorithm pays off for large networks as it may reduce the number of differential equations. Moreover, the analysis we did for the eight-node network shows that whenever we have to deal with a network configuration that has an underlying direct group with many direct factors, it might be beneficial to use the block diagonalization process by means of the algorithm since it reduces the number of equations significantly. To this end, I recommend to use this algorithm for large dynamical networks with network configurations where the underlying group has many direct factors. On the other hand, if one studies a network configuration in which there is full synchronization than one might as well use an eigenvalue decomposition. This last recommendation follows from our experience that using the entire group of the topological network structure tends to diagonalize the system entirely. Since an eigendecomposition generally requires less computations than the block diagonalizing algorithm it is recommended to use the first method in this case.

For the determination of the size of the basin of attraction for cyclic networks we used a rotation to reduce the dimension of the system. Moreover, it deals also with the translation invariance along a line. Therefore the equilibria become points instead of lines. For networks with an odd number of nodes we were able to find expressions for the equilibria that enabled us to find the minimal distance between an attractor and its nearest equilibrium. We conjectured that the minimal distance is given by $\sqrt{(n-1)/n\pi}$. Since we were not able to find a computer with high processing speed, we recommend to run our Java program for higher odd numbered networks. This would be the easiest way to verify if our conjecture is true or not for specific networks.

6.2. Future Research

We think that the long computations that are required in the application of the block diagonalizing algorithm could be shortened by theoretical improvements. Moreover, the approach of finding all possible network configurations is still complicated since it needs a verification for the compatibility of the network dynamics with its network structure. This verification is done by inspection, but may be improved by a more mathematical approach. We feel that these type of improvements could benefit future research on the topic of cluster synchronization. In order to verify our conjecture for the size of the basin of attraction we think that a logical step would be to verify that the nearest equilibria with respect to an attractor makes each sine term in 4.26 vanish. This improvement would be a big step towards solving the problem.



Appendix

Below we provide an expression for the total derivative of $L(\boldsymbol{\theta}) := -\hat{v}(\boldsymbol{\theta})$ where $\hat{V}(\boldsymbol{\theta})$ is given by formula 5.13. Notice,

$$\begin{aligned}
\dot{L}(\boldsymbol{\theta}) &= \sqrt{2}K \sin(\sqrt{2}\theta_1) \dot{\theta}_1 + K \sin\left(\frac{\theta_1}{\sqrt{2}} + \sqrt{\frac{3}{2}}\theta_2\right) \left[\frac{\dot{\theta}_1}{\sqrt{2}} + \sqrt{\frac{3}{2}}\dot{\theta}_2 \right] + K \sin\left(-\frac{\theta_1}{\sqrt{2}} + \sqrt{\frac{3}{2}}\theta_2\right) \left[-\frac{\dot{\theta}_1}{\sqrt{2}} + \sqrt{\frac{3}{2}}\dot{\theta}_2 \right] \\
&= \sqrt{2}K \sin(\sqrt{2}\theta_1) \left[-\sqrt{2}K \sin(\sqrt{2}\theta_1) - \frac{K}{\sqrt{2}} \sin\left(\frac{\theta_1}{\sqrt{2}} + \sqrt{\frac{3}{2}}\theta_2\right) + \frac{K}{\sqrt{2}} \sin\left(-\frac{\theta_1}{\sqrt{2}} + \sqrt{\frac{3}{2}}\theta_2\right) \right] \\
&+ \frac{K}{\sqrt{2}} \sin\left(\frac{\theta_1}{\sqrt{2}} + \sqrt{\frac{3}{2}}\theta_2\right) \left[-\sqrt{2}K \sin(\sqrt{2}\theta_1) - \frac{K}{\sqrt{2}} \sin\left(\frac{\theta_1}{\sqrt{2}} + \sqrt{\frac{3}{2}}\theta_2\right) + \frac{K}{\sqrt{2}} \sin\left(-\frac{\theta_1}{\sqrt{2}} + \sqrt{\frac{3}{2}}\theta_2\right) \right] \\
&+ \sqrt{\frac{3}{2}}K \sin\left(\frac{\theta_1}{\sqrt{2}} + \sqrt{\frac{3}{2}}\theta_2\right) \left[-K\sqrt{\frac{3}{2}} \sin\left(\frac{\theta_1}{\sqrt{2}} + \sqrt{\frac{3}{2}}\theta_2\right) - K\sqrt{\frac{3}{2}} \sin\left(-\frac{\theta_1}{\sqrt{2}} + \sqrt{\frac{3}{2}}\theta_2\right) \right] \\
&- \frac{K}{\sqrt{2}} \sin\left(-\frac{\theta_1}{\sqrt{2}} + \sqrt{\frac{3}{2}}\theta_2\right) \left[-\sqrt{2}K \sin(\sqrt{2}\theta_1) - \frac{K}{\sqrt{2}} \sin\left(\frac{\theta_1}{\sqrt{2}} + \sqrt{\frac{3}{2}}\theta_2\right) + \frac{K}{\sqrt{2}} \sin\left(-\frac{\theta_1}{\sqrt{2}} + \sqrt{\frac{3}{2}}\theta_2\right) \right] \\
&+ \sqrt{\frac{3}{2}}K \sin\left(-\frac{\theta_1}{\sqrt{2}} + \sqrt{\frac{3}{2}}\theta_2\right) \left[-K\sqrt{\frac{3}{2}} \sin\left(\frac{\theta_1}{\sqrt{2}} + \sqrt{\frac{3}{2}}\theta_2\right) - K\sqrt{\frac{3}{2}} \sin\left(-\frac{\theta_1}{\sqrt{2}} + \sqrt{\frac{3}{2}}\theta_2\right) \right]
\end{aligned} \tag{A.1}$$

This expression can easily be simplified by collecting equal terms.

$$\begin{aligned}
\dot{L}(\boldsymbol{\theta}) &= -2K^2 \left[\sin^2(\sqrt{2}\theta_1) + \sin^2\left(\frac{\theta_1}{\sqrt{2}} + \sqrt{\frac{3}{2}}\theta_2\right) + \sin^2\left(-\frac{\theta_1}{\sqrt{2}} + \sqrt{\frac{3}{2}}\theta_2\right) + \sin(\sqrt{2}\theta_1) \sin\left(\frac{\theta_1}{\sqrt{2}} + \sqrt{\frac{3}{2}}\theta_2\right) \right. \\
&\quad \left. + \sin\left(\frac{\theta_1}{\sqrt{2}} + \sqrt{\frac{3}{2}}\theta_2\right) \sin\left(-\frac{\theta_1}{\sqrt{2}} + \sqrt{\frac{3}{2}}\theta_2\right) - \sin(\sqrt{2}\theta_1) \sin\left(-\frac{\theta_1}{\sqrt{2}} + \sqrt{\frac{3}{2}}\theta_2\right) \right]
\end{aligned}$$

It is easily verified that we are able to complete the square three times to obtain the following expression.

$$\begin{aligned}
\dot{L}(\boldsymbol{\theta}) &= -K^2 \left[\sin(\sqrt{2}\theta_1) + \sin\left(\frac{\theta_1}{\sqrt{2}} + \sqrt{\frac{3}{2}}\theta_2\right) \right]^2 - K^2 \left[\sin\left(-\frac{\theta_1}{\sqrt{2}} + \sqrt{\frac{3}{2}}\theta_2\right) - \sin(\sqrt{2}\theta_1) \right]^2 \\
&\quad - K^2 \left[\sin\left(-\frac{\theta_1}{\sqrt{2}} + \sqrt{\frac{3}{2}}\theta_2\right) + \sin\left(\frac{\theta_1}{\sqrt{2}} + \sqrt{\frac{3}{2}}\theta_2\right) \right]^2
\end{aligned} \tag{A.2}$$

Due to the squares it follows that $\dot{L}(\boldsymbol{\theta}) \leq 0$ over \mathbb{R}^2 . One may also verify that its roots coincide with those of system 5.12.

At this point, we are ready to compute $V(\theta')$ by substituting the θ'_i in the right-hand side of (B1).

$$V(\theta') := \begin{pmatrix} -K \sin \left[\frac{\theta'_1}{\sqrt{2}} + \frac{\theta'_2}{\sqrt{2 \cdot 3}} + \dots + \frac{\theta'_{n-2}}{\sqrt{(n-2)(n-1)}} + \frac{n}{\sqrt{(n-1)n}} \theta'_{n-1} \right] - K \sin \left[\sqrt{2} \theta'_1 \right] \\ -K \sin \left[-\sqrt{2} \theta'_1 \right] - K \sin \left[-\frac{\theta'_1}{\sqrt{2}} + \frac{3}{\sqrt{2 \cdot 3}} \theta'_2 \right] \\ -K \sin \left[\frac{\theta'_1}{\sqrt{2}} - \frac{3\theta'_2}{\sqrt{2 \cdot 3}} \right] - K \sin \left[-\sqrt{\frac{2}{3}} \theta'_2 + \frac{4\theta'_3}{\sqrt{3 \cdot 4}} \right] \\ -K \sin \left[\sqrt{\frac{2}{3}} \theta'_2 - \frac{4\theta'_3}{\sqrt{3 \cdot 4}} \right] - K \sin \left[-\sqrt{\frac{3}{4}} \theta'_3 + \frac{5\theta'_4}{\sqrt{4 \cdot 5}} \right] \\ -K \sin \left[\sqrt{\frac{3}{4}} \theta'_3 - \frac{5\theta'_4}{\sqrt{4 \cdot 5}} \right] - K \sin \left[-\sqrt{\frac{4}{5}} \theta'_4 + \frac{6\theta'_5}{\sqrt{5 \cdot 6}} \right] \\ \vdots \\ -K \sin \left[\sqrt{\frac{i-2}{i-1}} \theta'_{i-2} - \frac{i\theta'_{i-1}}{\sqrt{(i-1)i}} \right] - K \sin \left[-\sqrt{\frac{i-1}{i}} \theta'_{i-1} + \frac{(i+1)\theta'_i}{\sqrt{i(i+1)}} \right] \\ \vdots \\ -K \sin \left[\sqrt{\frac{n-3}{n-2}} \theta'_{n-3} - \frac{(n-1)\theta'_{n-2}}{\sqrt{(n-2)(n-1)}} \right] - K \sin \left[-\sqrt{\frac{n-2}{n-1}} \theta'_{n-2} + \frac{n\theta'_{n-1}}{\sqrt{(n-1)n}} \right] \\ -K \sin \left[\sqrt{\frac{n-2}{n-1}} \theta'_{n-2} - \frac{n\theta'_{n-1}}{\sqrt{(n-1)n}} \right] - K \sin \left[-\frac{\theta'_1}{\sqrt{2}} - \frac{\theta'_2}{\sqrt{2 \cdot 3}} - \frac{\theta'_3}{\sqrt{3 \cdot 4}} - \dots - \frac{\theta'_{n-2}}{\sqrt{(n-2)(n-1)}} - \frac{n\theta'_{n-1}}{\sqrt{(n-1)n}} \right] \end{pmatrix} \quad (\text{B.4})$$

In order to finish the rotation of this vector field we determine $RV(\theta')$ and write the obtained system using the appropriate angle vector θ' . For readability, we define

$$S_n := \sin \left(\sum_{i=1}^{n-2} \frac{\theta'_i}{\sqrt{i(i+1)}} + \sqrt{\frac{n}{n-1}} \theta'_{n-1} \right)$$

and find that $RV(\theta')$ equals,

$$\begin{pmatrix} \dot{\theta}'_1 \\ \dot{\theta}'_2 \\ \dot{\theta}'_2 \\ \dot{\theta}'_3 \\ \dot{\theta}'_4 \\ \dot{\theta}'_5 \\ \vdots \\ \dot{\theta}'_i \\ \vdots \\ \dot{\theta}'_{n-2} \\ \dot{\theta}'_{n-1} \\ \dot{\theta}'_n \end{pmatrix} := \begin{pmatrix} -\sqrt{2} K \sin(\sqrt{2} \theta'_1) - \frac{K}{\sqrt{2}} S_n + \frac{K}{\sqrt{2}} \sin \left(-\frac{\theta'_1}{\sqrt{2}} + \frac{3}{\sqrt{2 \cdot 3}} \theta'_2 \right) \\ -\frac{K}{\sqrt{2 \cdot 3}} S_n - \frac{3K}{\sqrt{2 \cdot 3}} \sin \left(-\frac{\theta'_1}{\sqrt{2}} + \frac{3\theta'_2}{\sqrt{2 \cdot 3}} \right) + K \sqrt{\frac{2}{3}} \sin \left(-\sqrt{\frac{2}{3}} \theta'_2 + \frac{4\theta'_3}{\sqrt{3 \cdot 4}} \right) \\ -\frac{K}{\sqrt{3 \cdot 4}} S_n - \frac{4K}{\sqrt{3 \cdot 4}} \sin \left(-\sqrt{\frac{2}{3}} \theta'_2 + \frac{4}{\sqrt{3 \cdot 4}} \theta'_3 \right) + K \sqrt{\frac{3}{4}} \sin \left(-\sqrt{\frac{3}{4}} \theta'_3 + \frac{5\theta'_4}{\sqrt{4 \cdot 5}} \right) \\ -\frac{K}{\sqrt{4 \cdot 5}} S_n - \frac{5K}{\sqrt{4 \cdot 5}} \sin \left(-\sqrt{\frac{3}{4}} \theta'_3 + \frac{5\theta'_4}{\sqrt{4 \cdot 5}} \right) + K \sqrt{\frac{4}{5}} \sin \left(-\sqrt{\frac{4}{5}} \theta'_4 + \frac{6\theta'_5}{\sqrt{5 \cdot 6}} \right) \\ -\frac{K}{\sqrt{5 \cdot 6}} S_n - \frac{6K}{\sqrt{5 \cdot 6}} \sin \left(-\sqrt{\frac{4}{5}} \theta'_4 + \frac{6\theta'_5}{\sqrt{5 \cdot 6}} \right) + K \sqrt{\frac{5}{6}} \sin \left(-\sqrt{\frac{5}{6}} \theta'_5 + \frac{7\theta'_6}{\sqrt{6 \cdot 7}} \right) \\ \vdots \\ -\frac{K S_n}{\sqrt{i(i+1)}} - \sqrt{\frac{i+1}{i}} K \sin \left(-\sqrt{\frac{i-1}{i}} \theta'_{i-1} + \sqrt{\frac{i+1}{i}} \theta'_i \right) + K \sqrt{\frac{i}{i+1}} \sin \left(-\sqrt{\frac{i}{i+1}} \theta'_i + \sqrt{\frac{i+2}{i+1}} \theta'_{i+1} \right) \\ \vdots \\ -\frac{K S_n}{\sqrt{(n-2)(n-1)}} - \sqrt{\frac{n-1}{n-2}} K \sin \left(-\sqrt{\frac{n-3}{n-2}} \theta'_{n-3} + \sqrt{\frac{n-1}{n-2}} \theta'_{n-2} \right) + K \sqrt{\frac{n-2}{n-1}} \sin \left(-\sqrt{\frac{n-2}{n-1}} \theta'_{n-2} + \sqrt{\frac{n}{n-1}} \theta'_{n-1} \right) \\ -\sqrt{\frac{n}{n-1}} K S_n - \sqrt{\frac{n}{n-1}} K \sin \left(-\sqrt{\frac{n-2}{n-1}} \theta'_{n-2} + \sqrt{\frac{n}{n-1}} \theta'_{n-1} \right) \\ 0 \end{pmatrix} \quad (\text{B.5})$$

Note that this system is a gradient system since it can be readily verified that it can be written as $\dot{\theta}' = \nabla \hat{V}$, where

$$\hat{V} = K \cos(\sqrt{2} \theta'_1) + K \cos \left(\sum_{i=1}^{n-2} \frac{\theta'_i}{\sqrt{i(i+1)}} + \sqrt{\frac{n}{n-1}} \theta'_{n-1} \right) + K \sum_{i=1}^{n-2} \cos \left(-\sqrt{\frac{i}{i+1}} \theta'_i + \sqrt{\frac{i+2}{i+1}} \theta'_{i+1} \right)$$

Note that $\nabla \hat{V}$ is continuously differentiable, so it is in particular locally Lipschitz over a domain $D \subset \mathbb{R}^{n-1}$ containing the origin. Moreover, $\nabla \hat{V}|_{\theta'=0} = 0$. We let $L(\theta') = n - \hat{V}(\theta')$. It is clearly a positive semidefinite function, that is $L(\theta') \geq 0$ for $\theta' \neq 0$. Also, $L(\theta') = 0$ for $\theta' = 0$. We take a closer look at the total derivative of L . We want $\dot{L}(\theta') \leq 0$ in a domain D . Hence it suffices to show that $\hat{V} \geq 0$. We have,

$$\begin{aligned} \dot{V} &= -\sqrt{2}K \sin(\sqrt{2}\theta'_1)\dot{\theta}'_1 - K \left(\sqrt{\frac{n}{n-1}}\dot{\theta}'_{n-1} + \sum_{i=1}^{n-2} \frac{\dot{\theta}'_i}{\sqrt{i(i+1)}} \right) S_n \\ &- K \sum_{i=1}^{n-2} \left(-\sqrt{\frac{i}{i+1}}\dot{\theta}'_i + \sqrt{\frac{i+2}{i+1}}\dot{\theta}'_{i+1} \right) \sin \left(-\sqrt{\frac{i}{i+1}}\theta'_i + \sqrt{\frac{i+2}{i+1}}\theta'_{i+1} \right) \end{aligned}$$

We substitute the differential equations,

$$\begin{aligned} &= -\sqrt{2}K \sin(\sqrt{2}\theta_1) \left[-\sqrt{2}K \sin(\sqrt{2}\theta_1) - \frac{K}{\sqrt{2}}S_n + \frac{K}{\sqrt{2}} \sin \left(-\frac{\theta_1}{\sqrt{2}} + \sqrt{\frac{3}{2}}\theta_2 \right) \right] \\ &- K \sqrt{\frac{n}{n-1}} S_n \left[-\sqrt{\frac{n}{n-1}} K S_n - \sqrt{\frac{n}{n-1}} K \sin \left(-\sqrt{\frac{n-2}{n-1}}\theta_{n-2} + \sqrt{\frac{n}{n-1}}\theta_{n-1} \right) \right] \\ &- S_n K \sum_{i=1}^{n-2} \frac{1}{\sqrt{i(i+1)}} \left[-\frac{K S_n}{\sqrt{i(i+1)}} - \sqrt{\frac{i+1}{i}} K \sin \left(-\sqrt{\frac{i-1}{i}}\theta_{i-1} + \sqrt{\frac{i+1}{i}}\theta_i \right) \right. \\ &\quad \left. + K \sqrt{\frac{i}{i+1}} \sin \left(-\sqrt{\frac{i}{i+1}}\theta_i + \sqrt{\frac{i+2}{i+1}}\theta_{i+1} \right) \right] \\ &+ K \sum_{i=1}^{n-2} \sqrt{\frac{i}{i+1}} \sin \left(-\sqrt{\frac{i}{i+1}}\theta_i + \sqrt{\frac{i+2}{i+1}}\theta_{i+1} \right) \left[-\frac{K S_n}{\sqrt{i(i+1)}} - \sqrt{\frac{i+1}{i}} K \sin \left(-\sqrt{\frac{i-1}{i}}\theta_{i-1} + \sqrt{\frac{i+1}{i}}\theta_i \right) \right. \\ &\quad \left. + K \sqrt{\frac{i}{i+1}} \sin \left(-\sqrt{\frac{i}{i+1}}\theta_i + \sqrt{\frac{i+2}{i+1}}\theta_{i+1} \right) \right] \\ &- K \sum_{i=1}^{n-3} \sqrt{\frac{i+2}{i+1}} \sin \left(-\sqrt{\frac{i}{i+1}}\theta_i + \sqrt{\frac{i+2}{i+1}}\theta_{i+1} \right) \left[-\frac{K S_n}{\sqrt{(i+1)(i+2)}} - \sqrt{\frac{i+2}{i+1}} K \sin \left(-\sqrt{\frac{i}{i+1}}\theta_i + \sqrt{\frac{i+2}{i+1}}\theta_{i+1} \right) \right. \\ &\quad \left. + K \sqrt{\frac{i+1}{i+2}} \sin \left(-\sqrt{\frac{i+1}{i+2}}\theta_{i+1} + \sqrt{\frac{i+3}{i+2}}\theta_{i+2} \right) \right] \\ &- K \sqrt{\frac{n}{n-1}} \sin \left(-\sqrt{\frac{n-2}{n-1}}\theta_{n-2} + \sqrt{\frac{n}{n-1}}\theta_{n-1} \right) \left[-\sqrt{\frac{n}{n-1}} K S_n - \sqrt{\frac{n}{n-1}} K \sin \left(-\sqrt{\frac{n-2}{n-1}}\theta_{n-2} + \sqrt{\frac{n}{n-1}}\theta_{n-1} \right) \right] \end{aligned}$$

Notice that in a summation we used θ_0 as auxiliary variable for $i = 1$. This term won't be of any concern here and in the derivation presented below since it has zero contribution due to the square root which appears before θ_0 . If we write out every term we obtain,

$$= 2K^2 \sin^2(\sqrt{2}\theta_1) + \boxed{K^2 S_n \sin(\sqrt{2}\theta_1)} - K^2 \sin \left(-\frac{\theta_1}{\sqrt{2}} + \sqrt{\frac{3}{2}}\theta_2 \right) \sin(\sqrt{2}\theta_1) + \frac{K^2 S_n^2 n}{n-1}$$

$$+ \boxed{\frac{K^2 S_n n}{n-1} \sin \left(-\sqrt{\frac{n-2}{n-1}}\theta_{n-2} + \sqrt{\frac{n}{n-1}}\theta_{n-1} \right)} + \sum_{i=1}^{n-2} \frac{K^2 S_n^2}{i(i+1)}$$

$$+ \sum_{i=1}^{n-2} \frac{K^2 S_n}{i} \sin \left(-\sqrt{\frac{i-1}{i}}\theta_{i-1} + \sqrt{\frac{i+1}{i}}\theta_i \right)$$

$$- \sum_{i=1}^{n-2} \frac{K^2 S_n}{i+1} \sin \left(-\sqrt{\frac{i}{i+1}}\theta_i + \sqrt{\frac{i+2}{i+1}}\theta_{i+1} \right) - \sum_{i=1}^{n-2} \frac{K^2 S_n}{i+1} \sin \left(-\sqrt{\frac{i}{i+1}}\theta_i + \sqrt{\frac{i+2}{i+1}}\theta_{i+1} \right)$$

$$-K^2 \sum_{i=1}^{n-2} \sin\left(-\sqrt{\frac{i}{i+1}}\theta_i + \sqrt{\frac{i+2}{i+1}}\theta_{i+1}\right) \sin\left(-\sqrt{\frac{i-1}{i}}\theta_{i-1} + \sqrt{\frac{i+1}{i}}\theta_i\right)$$

$$+ \sum_{i=1}^{n-2} \frac{iK^2}{i+1} \sin^2\left(-\sqrt{\frac{i}{i+1}}\theta_i + \sqrt{\frac{i+2}{i+1}}\theta_{i+1}\right)$$

$$+ \sum_{i=1}^{n-3} \frac{K^2 S_n}{i+1} \sin\left(-\sqrt{\frac{i}{i+1}}\theta_i + \sqrt{\frac{i+2}{i+1}}\theta_{i+1}\right)$$

$$+ \sum_{i=1}^{n-3} \frac{(i+2)K^2}{i+1} \sin^2\left(-\sqrt{\frac{i}{i+1}}\theta_i + \sqrt{\frac{i+2}{i+1}}\theta_{i+1}\right)$$

$$-K^2 \sum_{i=1}^{n-3} \sin\left(-\sqrt{\frac{i}{i+1}}\theta_i + \sqrt{\frac{i+2}{i+1}}\theta_{i+1}\right) \sin\left(-\sqrt{\frac{i+1}{i+2}}\theta_{i+1} + \sqrt{\frac{i+3}{i+2}}\theta_{i+2}\right)$$

$$+ \frac{K^2 S_n n}{n-1} \sin\left(-\sqrt{\frac{n-2}{n-1}}\theta_{n-2} + \sqrt{\frac{n}{n-1}}\theta_{n-1}\right)$$

$$+ \frac{K^2 n}{n-1} \sin^2\left(-\sqrt{\frac{n-2}{n-1}}\theta_{n-2} + \sqrt{\frac{n}{n-1}}\theta_{n-1}\right)$$

The parts of the above equation in boxes with a black border may be captured by the single expression,

$$+2K^2 \sum_{i=1}^{n-2} \sin^2\left(-\sqrt{\frac{i}{i+1}}\theta_i + \sqrt{\frac{i+2}{i+1}}\theta_{i+1}\right)$$

Further, the terms in the blue box may be simplified to the expression,

$$-2K^2 \sum_{i=1}^{n-2} \frac{S_n}{i+1} \sin\left(-\sqrt{\frac{i}{i+1}}\theta_i + \sqrt{\frac{i+2}{i+1}}\theta_{i+1}\right)$$

Similarly, the terms in the red boxes may be replaced by the expression

$$-2K^2 \sum_{i=2}^{n-2} \sin\left(-\sqrt{\frac{i-1}{i}}\theta_{i-1} + \sqrt{\frac{i+1}{i}}\theta_i\right) \sin\left(-\sqrt{\frac{i}{i+1}}\theta_i + \sqrt{\frac{i+2}{i+1}}\theta_{i+1}\right) - K^2 \sin(\sqrt{2}\theta_1) \sin\left(-\frac{\theta_1}{\sqrt{2}} + \sqrt{\frac{3}{2}}\theta_2\right)$$

The terms in the green boxes may be replaced by,

$$+2K^2 \frac{nS_n}{n-1} \sin\left(-\sqrt{\frac{n-2}{n-1}}\theta_{n-2} + \sqrt{\frac{n}{n-1}}\theta_{n-1}\right)$$

The terms in the magenta boxes may be replaced by,

$$+2K^2 \sum_{i=1}^{n-2} \frac{S_n}{i} \sin\left(-\sqrt{\frac{i-1}{i}}\theta_{i-1} + \sqrt{\frac{i+1}{i}}\theta_i\right)$$

These replacements simplify the expression to

$$= 2K^2 \sin^2(\sqrt{2}\theta_1) + 2K^2 \sum_{i=1}^{n-2} \frac{S_n}{i} \sin\left(-\sqrt{\frac{i-1}{i}}\theta_{i-1} + \sqrt{\frac{i+1}{i}}\theta_i\right)$$

$$-2K^2 \sin\left(-\frac{\theta_1}{\sqrt{2}} + \sqrt{\frac{3}{2}}\theta_2\right) \sin(\sqrt{2}\theta_1)$$

$$+ \frac{nK^2 S_n^2}{n-1}$$

$$+2K^2 \frac{nS_n}{n-1} \sin\left(-\sqrt{\frac{n-2}{n-1}}\theta_{n-2} + \sqrt{\frac{n}{n-1}}\theta_{n-1}\right) \left[+ \sum_{i=1}^{n-2} \frac{K^2 S_n^2}{i(i+1)} \right]$$

$$\left[-2K^2 \sum_{i=1}^{n-2} \frac{S_n}{i+1} \sin\left(-\sqrt{\frac{i}{i+1}}\theta_i + \sqrt{\frac{i+2}{i+1}}\theta_{i+1}\right) \right] + 2K^2 \sum_{i=1}^{n-2} \sin^2\left(-\sqrt{\frac{i}{i+1}}\theta_i + \sqrt{\frac{i+2}{i+1}}\theta_{i+1}\right)$$

$$\left[-2K^2 \sum_{i=2}^{n-2} \sin\left(-\sqrt{\frac{i-1}{i}}\theta_{i-1} + \sqrt{\frac{i+1}{i}}\theta_i\right) \sin\left(-\sqrt{\frac{i}{i+1}}\theta_i + \sqrt{\frac{i+2}{i+1}}\theta_{i+1}\right) \right]$$

The terms in the black boxes may be replaced by,

$$-2K^2 \sum_{i=1}^{n-2} \sin\left(-\sqrt{\frac{i-1}{i}}\theta_{i-1} + \sqrt{\frac{i+1}{i}}\theta_i\right) \sin\left(-\sqrt{\frac{i}{i+1}}\theta_i + \sqrt{\frac{i+2}{i+1}}\theta_{i+1}\right)$$

If we use the telescoping series, we may replace the terms in the blue boxes by $2K^2 S_n^2$. Finally, the terms in the red boxes may be replaced by

$$2K^2 S_n \sin(\sqrt{2}\theta_1) - 2 \frac{K^2 S_n}{n-1} \sin\left(-\sqrt{\frac{n-2}{n-1}}\theta_{n-2} + \sqrt{\frac{n}{n-1}}\theta_{n-1}\right)$$

These replacements lead to,

$$= 2K^2 \sin^2(\sqrt{2}\theta_1) + 2K^2 S_n \sin(\sqrt{2}\theta_1) \left[-2 \frac{K^2 S_n}{n-1} \sin\left(-\sqrt{\frac{n-2}{n-1}}\theta_{n-2} + \sqrt{\frac{n}{n-1}}\theta_{n-1}\right) \right]$$

$$-2K^2 \sum_{i=1}^{n-2} \sin\left(-\sqrt{\frac{i-1}{i}}\theta_{i-1} + \sqrt{\frac{i+1}{i}}\theta_i\right) \sin\left(-\sqrt{\frac{i}{i+1}}\theta_i + \sqrt{\frac{i+2}{i+1}}\theta_{i+1}\right) + 2K^2 S_n^2$$

$$\left[+2K^2 \frac{nS_n}{n-1} \sin\left(-\sqrt{\frac{n-2}{n-1}}\theta_{n-2} + \sqrt{\frac{n}{n-1}}\theta_{n-1}\right) \right] + 2K^2 \sum_{i=1}^{n-2} \sin^2\left(-\sqrt{\frac{i}{i+1}}\theta_i + \sqrt{\frac{i+2}{i+1}}\theta_{i+1}\right)$$

We replace the terms in the black boxes by

$$+2K^2 S_n \sin\left(-\sqrt{\frac{n-2}{n-1}}\theta_{n-2} + \sqrt{\frac{n}{n-1}}\theta_{n-1}\right).$$

Thus,

$$\begin{aligned} \dot{V} = & 2K^2 \sin^2(\sqrt{2}\theta_1) + 2K^2 S_n^2 + 2K^2 \sum_{i=1}^{n-2} \sin^2\left(-\sqrt{\frac{i}{i+1}}\theta_i + \sqrt{\frac{i+2}{i+1}}\theta_{i+1}\right) + 2K^2 S_n \sin(\sqrt{2}\theta_1) \\ & + 2K^2 S_n \sin\left(-\sqrt{\frac{n-2}{n-1}}\theta_{n-2} + \sqrt{\frac{n}{n-1}}\theta_{n-1}\right) \end{aligned} \quad (\text{B.6})$$

$$-2K^2 \sum_{i=1}^{n-2} \sin\left(-\sqrt{\frac{i-1}{i}}\theta_{i-1} + \sqrt{\frac{i+1}{i}}\theta_i\right) \sin\left(-\sqrt{\frac{i}{i+1}}\theta_i + \sqrt{\frac{i+2}{i+1}}\theta_{i+1}\right)$$

Now, we observe that

$$\sum_{i=1}^{n-2} \left[\sin\left(-\sqrt{\frac{i}{i+1}}\theta_i + \sqrt{\frac{i+2}{i+1}}\theta_{i+1}\right) - \sin\left(-\sqrt{\frac{i-1}{i}}\theta_{i-1} + \sqrt{\frac{i+1}{i}}\theta_i\right) \right]^2 \quad (\text{B.7})$$

$$\begin{aligned}
&= \sin^2 \left(-\sqrt{\frac{n-2}{n-1}} \theta_{n-2} + \sqrt{\frac{n}{n-1}} \theta_{n-1} \right) + 2 \sum_{i=1}^{n-3} \sin^2 \left(-\sqrt{\frac{i}{i+1}} \theta_i + \sqrt{\frac{i+2}{i+1}} \theta_{i+1} \right) \\
&+ \sin^2(\sqrt{2}\theta_1) - 2 \sum_{i=1}^{n-2} \sin \left(-\sqrt{\frac{i-1}{i}} \theta_{i-1} + \sqrt{\frac{i+1}{i}} \theta_i \right) \sin \left(-\sqrt{\frac{i}{i+1}} \theta_i + \sqrt{\frac{i+2}{i+1}} \theta_{i+1} \right) \\
&= -\sin^2 \left(-\sqrt{\frac{n-2}{n-1}} \theta_{n-2} + \sqrt{\frac{n}{n-1}} \theta_{n-1} \right) + 2 \sum_{i=1}^{n-2} \sin^2 \left(-\sqrt{\frac{i}{i+1}} \theta_i + \sqrt{\frac{i+2}{i+1}} \theta_{i+1} \right) \\
&+ \sin^2(\sqrt{2}\theta_1) - 2 \sum_{i=1}^{n-2} \sin \left(-\sqrt{\frac{i-1}{i}} \theta_{i-1} + \sqrt{\frac{i+1}{i}} \theta_i \right) \sin \left(-\sqrt{\frac{i}{i+1}} \theta_i + \sqrt{\frac{i+2}{i+1}} \theta_{i+1} \right)
\end{aligned}$$

We compare terms in the expanded form of (3) with terms in equation (2) and simplify (2),

$$\begin{aligned}
\dot{V} &= K^2 \sin^2(\sqrt{2}\theta_1) + 2K^2 S_n^2 + K^2 \sum_{i=1}^{n-2} \left[\sin \left(-\sqrt{\frac{i}{i+1}} \theta_i + \sqrt{\frac{i+2}{i+1}} \theta_{i+1} \right) - \sin \left(-\sqrt{\frac{i-1}{i}} \theta_{i-1} + \sqrt{\frac{i+1}{i}} \theta_i \right) \right]^2 \\
&+ K^2 \sin^2 \left(-\sqrt{\frac{n-2}{n-1}} \theta_{n-2} + \sqrt{\frac{n}{n-1}} \theta_{n-1} \right) + 2K^2 S_n \sin(\sqrt{2}\theta_1) + 2K^2 S_n \sin \left(-\sqrt{\frac{n-2}{n-1}} \theta_{n-2} + \sqrt{\frac{n}{n-1}} \theta_{n-1} \right)
\end{aligned}$$

Finally we observe that we can rewrite this last expression as a sum of squares.

$$\begin{aligned}
\dot{V} &= K^2 \left[\sin(\sqrt{2}\theta_1) + S_n \right]^2 + K^2 \sum_{i=1}^{n-2} \left[\sin \left(-\sqrt{\frac{i}{i+1}} \theta_i + \sqrt{\frac{i+2}{i+1}} \theta_{i+1} \right) - \sin \left(-\sqrt{\frac{i-1}{i}} \theta_{i-1} + \sqrt{\frac{i+1}{i}} \theta_i \right) \right]^2 \\
&+ K^2 \left[\sin \left(-\sqrt{\frac{n-2}{n-1}} \theta_{n-2} + \sqrt{\frac{n}{n-1}} \theta_{n-1} \right) + S_n \right]^2
\end{aligned}$$

This is a sum of squares. For this expression to be equal to zero we need that each squared term is equal to zero. This results in the expression of 4.25.

C

Appendix

```
1
2 import java.util.*;
3 import java.lang.*;
4 import java.io.*;
5
6 public class Equilibria
7 {
8
9     static double Nom=100.0;
10    static int counter=0;
11    static int intermediateLevel=2;
12
13    public static void main(String[] args)
14    {
15        int n=7;
16        int[] rij = new int[1];
17        System.out.println();
18        combinations(rij,0,n-1);
19
20    }
21    /*
22    public static int[] replace(int[] posValues, int[] rijIn)
23    {
24        int[] res = new int[rijIn.length];
25        for(int i=0; i<rijIn.length; i++)
26        {
27            if(rijIn[i]==0)
28            {
29                res[i]=posValues[0];
30            }
31            else if(rijIn[i]==1)
32            {
33                res[i]=posValues[1];
34            }
35            else if(rijIn[i]==2)
36            {
37                res[i]=posValues[2];
38            }
39            else if(rijIn[i]==3)
40            {
41                res[i]=posValues[3];
42            }
43            else if(rijIn[i]==4)
44            {
45                res[i]=posValues[4];
46            }
47        }
48        return res;
49    }
50
```

```

51 public static void combinationsTwo(int sz, int[] posValues)
52 {
53     int track; int iterator=0; double norm=100;
54     int[] res = new int[sz];
55     do
56     {
57         int[] result = replace(posValues, res);
58         if(norm>=EuclideanNorm(result, sz-1) && EuclideanNorm(result, sz-1)>0)
59         {
60             norm = EuclideanNorm(result, sz-1);
61             System.out.println(norm);
62         }
63         if(iterator==Math.pow(3, sz-2)*5-1)
64         {
65             System.out.println(norm);
66             break;
67         }
68         iterator+=1;
69         //System.out.println("");
70         track=1;
71         for(int j=sz-1; j>=0; j--)
72         {
73             if(track==0)
74             {
75                 break;
76             }
77             res[j]+=track;
78             track=0;
79             if(j==sz-1)
80             {
81                 if(res[j]==5)
82                 {
83                     track=1;
84                     res[j]=0;
85                 }
86             }
87             if(j<sz-1)
88             {
89                 if(res[j]==3)
90                 {
91                     track=1;
92                     res[j]=0;
93                 }
94             }
95         }
96     } while(track !=1);
97 }
98
99
100 */
101 public static int[] addToRij(int[] rij, int a)
102 {
103     int[] res = Arrays.copyOf(rij, rij.length+1);
104     res[rij.length]=a;
105     return res;
106 }
107
108 public static void combinations(int[] rij, int i, int n)
109 {
110     int[] res;
111     if(i==n)
112     {
113         //System.out.println(Arrays.toString(rij));
114         if(Nom>=EuclideanNorm(rij, n) && EuclideanNorm(rij, n) != 0.0)
115         {
116             Nom=EuclideanNorm(rij, n);
117         }
118         counter=counter+1;
119         if(counter==Math.pow(3, n-1)*5)
120         {
121             System.out.println("Minimal distance : "+Nom);

```

```

122     }
123
124 }
125 else if (i==n-1)
126 {
127     for (int j=-2;j<=2;j++)
128     {
129         res = addToRij(rij , j);
130         combinations(res , i+1,n);
131     }
132 }
133 else
134 {
135     for (int j=-1;j<=1;j++)
136     {
137         res = addToRij(rij , j);
138         combinations(res , i+1,n);
139     }
140 }
141 }
142
143
144
145 public static double getThetaOne(int[] rijIn)
146 {
147     double tempOne =0;
148     double tempTwo =0;
149     for (int i=0; i<rijIn.length; i++)
150     {
151         tempOne = tempOne+Math.pow(-1,rijIn [ i ] );
152         tempTwo = tempTwo+rijIn [ i ];
153     }
154     double ThetaOne = (-1*tempTwo*Math.PI)/(Math.sqrt(2)*tempOne);
155     return ThetaOne;
156 }
157
158 public static double getThetaI(int[] rijIn , int index)
159 {
160     double ThetaI=0;
161     for (int j=0; j<index; j++)
162     {
163         double temp =(Math.pow(-1,rijIn [ j ])*Math.sqrt(2)*getThetaOne(rijIn)+rijIn [ j ]*Math.PI);
164         ThetaI=ThetaI+(1./(Math.sqrt(index*(index+1))))*(j+1)*temp;
165     }
166     return ThetaI;
167 }
168
169 public static double EuclideanNorm(int[] rijIn , int n)
170 {
171     double res =0;
172     for (int i=0; i<n; i++)
173     {
174         res = res+Math.pow(getThetaI(rijIn , i+1) , 2);
175     }
176     res = Math.sqrt(res);
177     return res;
178 }
179
180
181 }

```


Bibliography

- [1] M. Artin. *Algebra*. Prentice Hall, 1991. ISBN 9780130047632. URL https://books.google.nl/books?id=C_juAAAAAMAAJ.
- [2] Jared C Bronski and Lee DeVille. Spectral theory for dynamics on graphs containing attractive and repulsive interactions. *SIAM Journal on Applied Mathematics*, 74(1):83–105, 2014.
- [3] David Cumin and CP Unsworth. Generalising the kuramoto model for the study of neuronal synchronisation in the brain. *Physica D: Nonlinear Phenomena*, 226(2):181–196, 2007.
- [4] Robin Delabays, Melvyn Tyloo, and Philippe Jacquod. The size of the sync basin revisited. *Chaos: An Interdisciplinary Journal of Nonlinear Science*, 27(10):103109, 2017.
- [5] Bard Ermentrout. An adaptive model for synchrony in the firefly pteroptyx malaccae. *Journal of Mathematical Biology*, 29(6):571–585, 1991.
- [6] Francis J Flanigan and Jerry L Kazdan. *Calculus two: linear and nonlinear functions*. Springer Science & Business Media, 1998.
- [7] John B Fraleigh. *A first course in abstract algebra*. Pearson Education India, 2003.
- [8] Martin Golubitsky and Ian Stewart. *The symmetry perspective: from equilibrium to chaos in phase space and physical space*, volume 200. Springer Science & Business Media, 2003.
- [9] Martin Golubitsky and Ian Stewart. Nonlinear dynamics of networks: the groupoid formalism. *Bulletin of the american mathematical society*, 43(3):305–364, 2006.
- [10] Hermann Haken and Hans Christoph Wolf. *Molecular physics and elements of quantum chemistry: introduction to experiments and theory*. Springer Science & Business Media, 2013.
- [11] Adalbert Kerber. *Applied finite group actions*, volume 19. Springer Science & Business Media, 2013.
- [12] David Marlow Kerns. *Analysis of symmetrical waveguide junctions*. PhD thesis, Catholic University of America Press, 1951.
- [13] Hassan K Khalil. *Nonlinear control*. Pearson New York, 2015.
- [14] Mike Krebs and Anthony Shaheen. *Expander families and Cayley graphs: a beginner's guide*. Oxford University Press, 2011.
- [15] Yoshiki Kuramoto. Self-entrainment of a population of coupled non-linear oscillators. In *International symposium on mathematical problems in theoretical physics*, pages 420–422. Springer, 1975.
- [16] Yoshiki Kuramoto. *Chemical oscillations, waves, and turbulence*, volume 19. Springer Science & Business Media, 2012.
- [17] Ron Larson and Bruce H Edwards. *Multivariable calculus*. Cengage Learning, 2013.
- [18] Adilson E Motter, Seth A Myers, Marian Anghel, and Takashi Nishikawa. Spontaneous synchrony in power-grid networks. *Nature Physics*, 9(3):191, 2013.
- [19] Louis M Pecora and Thomas L Carroll. Master stability functions for synchronized coupled systems. *Physical review letters*, 80(10):2109, 1998.
- [20] Louis M Pecora, Francesco Sorrentino, Aaron M Hagerstrom, Thomas E Murphy, and Rajarshi Roy. Cluster synchronization and isolated desynchronization in complex networks with symmetries. *Nature communications*, 5:4079, 2014.

-
- [21] David G Schaeffer and Ian Stewart. *Singularities and groups in bifurcation theory*. Springer, 1985.
- [22] Francesco Sorrentino, Louis M Pecora, Aaron M Hagerstrom, Thomas E Murphy, and Rajarshi Roy. Complete characterization of the stability of cluster synchronization in complex dynamical networks. *Science advances*, 2(4):e1501737, 2016.
- [23] Benjamin Steinberg. *Representation theory of finite groups: an introductory approach*. Springer Science & Business Media, 2011.
- [24] Boris S Tsukerblat. *Group theory in chemistry and spectroscopy: a simple guide to advanced usage*. Courier Corporation, 2006.
- [25] Daniel A Wiley, Steven H Strogatz, and Michelle Girvan. The size of the sync basin. *Chaos: An Interdisciplinary Journal of Nonlinear Science*, 16(1):015103, 2006.
- [26] Kaihua Xi, Johan LA Dubbeldam, and Hai Xiang Lin. Synchronization of cyclic power grids: Equilibria and stability of the synchronous state. *Chaos: An Interdisciplinary Journal of Nonlinear Science*, 27(1):013109, 2017.